Radiative quenching of He^+ ions from mixtures with D_2 molecules at temperatures below 100 K. A theoretical study using 3D optical potential in a ro-vibrational adiabatic representation

Felicja Mrugała*

Institute of Physics, Faculty of Physics, Astronomy and Informatics, Nicolaus Copernicus University, Grudziadzka 5, 87-100 Torun, Poland

Abstract

In a recent study of radiative reactions in the $He^+(^2S) + H_2(X\,^1\Sigma_g^+; v{=}0, j)$ collisions at subthermal energies [F. Mrugała and W. P. Kraemer, J. Chem. Phys. **138**, 104315 (2005)], a model was developed that describes rigorously translational, vibrational, and rotational nuclear motions of the reactant system and approximately, through a negative-imaginary-valued optical potential, the global effect of spontaneous emission — the quenching of the He^+ ions. The model is applied here to describe the quenching in collisions with D_2 molecules. The collisions on the 3-dimensional complex molecular+optical potential surface are treated within the close-coupling approach. The coupled equations in the atom-diatom translational coordinate, previously formulated and solved in the standard diabatic basis, are transformed here to a ro-vibrational adiabatic representation. The transformed equations are solved with the help of the log-derivative propagation scheme combined with the Smooth-Variable-Discretization technique to account for the pertinent nonadiabatic couplings. Due to faster convergence with respect to the adiabatic basis size, the present implementation of the close-coupling to the He^++D_2 (H_2) collisions is about 10 times more efficient computationally. The calculations are carried out for the He^+ + ortho-D_2 and He^+ + para-D_2 systems in the energy ranges from 10^{-6} up to 44.6 meV above the respective lowest, $v{=}0\,j{=}0$ and $j{=}1$, thresholds. Above 1400 resonances in these ranges are found and characterized in terms of their energy positions and widths, dissociative and radiative. Most of the resonances show up as sharp peaks in the reaction yield functions (the characteristics equivalent to but more convenient than cross-sections). By averaging these functions with appropriate energy distributions, the rate constants for the quenching of the He^+ ions from mixtures with equilibrium and normal D_2 gases (k and $k_{\rm nrm}$) are determined as functions of temperature (T) in the range up 100 K. The values of $k\,(k_{\rm nrm})$, in the unit of 10^{-15} $\rm cm^3 s^{-1}$, are: 0.39 (0.41) in the $T{=}0$ limit, 49.7 (43.9) at the maximum near 20 K, and 33.6 (33.5) at 100 K. Using results of the previous study, effects of the H→D substitution on the reaction rate are resolved and demonstrated to be qualitatively different in ultracold ($T{<}0.1$ mK) and subthermal ($T{>}10$ K) ranges. In the first range, the rate constants k ($k_{\rm nrm}$) become smaller, by factors of 0.86 (0.57) at 0 K. In the subthermal range, the isotopic substitution enhances the rate constants by factors of 1.2−1.5 in the mixtures with normal population of ortho- and para- components and by somewhat smaller factors (maximally 1.37) — in the fully equilibrium mixtures. This enhancement is entirely due to a larger number of rotational Feshbach resonances contributing to the reaction in the heavier system.

Radiative reactions
in
He^++D_2 and **He^++H_2**

$$He^+(^2S) + a_2(X\,^1\Sigma_g^+; v{=}0, j) \xrightarrow{He^+ - a_2(A\,^2A')} h\nu +$$

a=D, H

$$+ \begin{cases} He\,a_2^+(X\,^2A') & \text{RA} \\ He - a_2^+(X\,^2A') \longrightarrow He(^1S) + a_2^+(X\,^2\Sigma_g^+; v', j') & \text{RCT} \\ [He + a_2^+](X\,^2A') \longrightarrow a(^2S) + He\,a^+(X\,^2\Sigma^+; v'', j'') & \text{iRaT} \end{cases}$$

RA — Radiative Association
+RCT — Radiative Charge Transfer
+iRaT — indirect Radiative atom Transfer
= trad — total radiative process or

RADIATIVE QUENCHING
of
$^4He^+$ IONS
from
MIXTURES with **D_2** or **H_2 MOLECULES**

Toruń, 2016

A. THEORY

The theory has been described in detail in papers on the radiative reactions in the He^++H_2 system, Refs. 1–3. Application to the He^++D_2 system does not require any essential modification. Still, some definitions and formulas need to be quoted in order to present comprehensibly the results of the application. Moreover, a refinement in the practical implementation of the theory has been achieved which seems worthy of a description here. More specifically, exploited in the present work is the 3D optical potential model of spontaneous emission in atom+diatom systems, proposed in Ref. 3. The model is implemented using close-coupling approximation in a ro-vibrational adiabatic representation.

The 'trad' (total radiative) reaction in the He^++D_2 gas mixture of temperature T is described by the rate equation

$$-\frac{d}{dt}n_{\mathrm{He}^+} = k(T)\, n_{\mathrm{D}_2}\, n_{\mathrm{He}^+} \tag{1}$$

in which n denotes the number density of the subscribed species and $k(T)$ is the rate constant (function). Collisions with ortho-D_2 and para-D_2 components (nuclear spin values I=0, 2 and I=1, respectively) make two separate contributions to the rate constant,

$$k(T) = \sum_{\mathrm{c=p(ara),o(rtho)}} k^{\mathrm{c}}(T) \tag{2}$$

and each contribution k^{c} is an infinite sum of terms coming from partial-wave resolution of stationary scattering states of the colliding pair He^++c-D_2,

$$k^{\mathrm{c}}(T) = \sum_J \sum_{p=1,-1} (2J{+}1)\, k^{\mathrm{c}}(T;J,p)\,. \tag{3}$$

J is the total angular momentum quantum number and p — the spectroscopic parity. The total angular momentum accounts for rotations of c-D_2 and for rotations of He^+ relative to c-D_2. The quantum numbers describing these rotations are denoted with j and l, where j may take only even (odd) values for c=o (p) and values of l allowed for given J and p are: $l_{\min}, l_{\min}{+}2, \ldots, l_{\max}$ with $l_{\min}{=}|J{-}j|{+}\frac{1-p}{2}$ and $l_{\max}{=}J{+}j{-}\frac{1-p}{2}$.

The partial rate constant $k^{\mathrm{c}}(T;J,p)$ is obtained through appropriate averaging,

$$k^{\mathrm{c}}(T;J,p) = \int dE\, P^{\mathrm{c}}(E,T)\, \frac{\partial}{\partial E} R^{\mathrm{c}}(E;J,p)\,, \tag{4}$$

of the energy differential rate function

$$\frac{\partial}{\partial E} R^{\mathrm{c}}(E;J,p) = \frac{1}{2\pi\hbar}\, p^{\mathrm{trad,\,c}}(E;J,p)$$

in which $p^{\mathrm{trad,\,c}}(E;J,p)$, called the partial reaction yield function[4], is the probability sum of all radiative transitions possible in the He^++c-D_2 collisions with definite J and p values at a given total energy E. The energy E is the sum of energy of relative translational motion and of vibration-rotation energy (ε_{vj}) of the c-D_2 subunit. Thus, the function $p^{\mathrm{trad,\,c}}(E;J,p)$ accounts for transitions from all the states $|E,J,p;v\,j\,l\rangle$ (with J and p fixed) which are related to open $v\,j$ channels in collisions at the energy E,

$$p^{\mathrm{trad,\,c}}(E;J,p){=}\sum_v \sum_{j(c)} p^{\mathrm{trad}}_{vj}(E;J,p)\,\Theta(E{-}\varepsilon_{vj}) \quad \text{with} \quad p^{\mathrm{trad}}_{vj}(E;J,p){=}\sum_l p^{\mathrm{trad}}_{vjl}(E;J,p)\,, \tag{5}$$

where $j(c)$ denotes values of definite parity, even (odd) for c=o (p), Θ is the Heaviside step function, and the sum $\sum_l$ is over every second value from the range $[l_{\min}(J,j,p), l_{\max}(J,j,p)]$.

The energy density of states of the colliding system is highly non-uniform; numerous quasi-bound states of the complex He^+−c-D_2 (rotational Feshbach or shape resonances) are formed. This is reflected in the energy dependence of the partial yield functions; they become sums of two distinct terms

$$p^{\mathrm{trad,c}}(E;J,p) = p^{\mathrm{trad,c}}_{\mathrm{bck}}(E;J,p) + \sum_n \frac{\Gamma_n^{\mathrm{trad},Jp}\,\Gamma_n^{Jp}}{(E-E_n^{\mathrm{res},Jp})^2 + (\Gamma_n^{\mathrm{trad},Jp}+\Gamma_n^{Jp})^2/4}\,. \tag{6}$$

The term $p^{\mathrm{trad,c}}_{\mathrm{bck}}(E;J,p)$, varying slowly with E, describes radiative transitions from 'flat' continuum, and the sum of Lorentz functions describes transitions from the resonances. The radiative transitions from a given resonance (n,J,p) are accounted for through the parameter (radiative width) $\Gamma_n^{\mathrm{trad,Jp}}$ and transitions back to the He^+ and D_2 fragments — through the dissociative width Γ_n^{Jp}.

Upon inserting Eqs. (4) and (5) into Eq. (3) and rearranging the involved summations and integration, the following concise formula is obtained for the rate constants functions $k^{\mathrm{c}}(T)$

$$k^{\mathrm{c}}(T) = \frac{1}{2\pi\hbar}\int dE\, P^{\mathrm{c}}(E,T)\, p^{\mathrm{trad,c}}(E)\,, \tag{7}$$

where $p^{\mathrm{trad,c}}(E)$ is the total radiative reaction yield[4] in the He^++c-D_2 collisions at the energy E,

$$p^{\mathrm{trad,c}}(E) = \sum_p \sum_J (2J{+}1)\, p^{\mathrm{trad,c}}(E;J,p) = \sum_v \sum_{j(c)} p^{\mathrm{trad}}_{vj}(E)\,. \tag{8}$$

$p^{\mathrm{trad}}_{vj}(E)$ defined by the second equality and Eq. (5) describes the part of the reaction yield which comes from the initial vj state of the D_2 reactants. Correspondingly, the rate constants $k^c(T)$ can be resolved into components $k^{\mathrm{c}}_{vj}(T)$ and $k^{\mathrm{c}}_{vj}(T;J,p)$ being the averages (7) of the yield functions $p^{\mathrm{trad,c}}_{vj}(E)$ and $p^{\mathrm{trad,c}}_{vj}(E;J,p)$, respectively.

The population factor $P^{\mathrm{c}}(E,T)$ in Eq. (4) and (7) appropriate for the He^++D_2 gas at thermal equilibrium is

$$P^{\mathrm{c}}(E,T) = \frac{g^{\mathrm{c}}}{Z(T)}\Big(\frac{2\pi\hbar^2}{\mu k_B T}\Big)^{3/2}\exp(-E/k_BT)\,, \tag{9}$$

where $Z(T){=}\sum\limits_{\mathrm{c}} g^{\mathrm{c}} Z_{\mathrm{c}}(T)$ with $g^{\mathrm{c}}{=}6\,(3)$ for c=o (p),

$$Z_{\mathrm{o}}(T) = \sum_v \sum_{j\ \mathrm{even}} (2j{+}1)\exp(-\varepsilon_{vj}/k_BT) \qquad \text{and} \qquad Z_{\mathrm{p}}(T) = \ldots \sum_{j\ \mathrm{odd}} \ldots\,,$$

μ is the reduced mass of the He^++D_2 system, and k_B is the Boltzmann constant.

Of interest is also the rate constant function $k(T)$ for the quenching of the He^+ ions from mixtures with 'normal' deuterium gas characterized by fixed $g^{\mathrm{o}}{:}g^{\mathrm{p}}$ (i.e. non-equilibrium) relative concentration of ortho- and para- components. For such mixtures, the averaging (4) should be done with the population factor

$$P^{\mathrm{c}}_{\mathrm{nrm}}(E,T) = \frac{g^{\mathrm{c}}}{g^{\mathrm{o}}{+}g^{\mathrm{p}}}\,{}_{\mathrm{c}}P(E,T)\,, \tag{10}$$

where ${}_{\mathrm{c}}P(E,T)$ describes mixtures with pure c-component of D_2 and differs from the factor of Eq. (9) by that $1/Z_{\mathrm{c}}(T)$ appears in place of $g^c/Z(T)$.

To distinguish between the different kinds of mixtures, the symbols $k^{\mathrm{c}}_{\mathrm{nrm}}$ and ${}_{\mathrm{c}}k$ are introduced for the rate constant obtained when the factor P^{c} in Eq. (4) is replaced with $P^{\mathrm{c}}_{\mathrm{nrm}}$ and ${}_{\mathrm{c}}P$, respectively.

3D OPTICAL POTENTIAL MODEL

The model serves the determination of the partial yield functions $p^{\rm trad}(E;J,p)$ (the index 'c' is hereafter omitted) and consists in using the Hamiltonian

$$^{\rm opt}H(\mathbf{r},\mathbf{R}) = H(\mathbf{r},\mathbf{R}) + {}^{\rm opt}V(r,R,\theta) \tag{11}$$

which describes rigorously the translational, vibrational, and rotational nuclear motions of the He^++D_2 system and approximately, through the optical potential $^{\rm opt}V$, the global effect of spontaneous emission, i.e. the quenching of the He^+ ions. $\mathbf{r}$ and $\mathbf{R}$ are the Jacobi vectors which join, respectively, the deuterons and the center-of-mass of the deuterons with the He nucleus, r and R denote the lengths of these vectors and θ — the angle between them. The reagent system moves on the potential energy surface (PES) of the first excited electronic state of $[HeHH]^+$, and the quenching process consists in transitions to the continuity of ro-vibro-translational states on the ground electronic state of $[HeHH]^+$. The PESes of the initial and final electronic states are denoted hereafter by $\overline{V}^A$ and $\overline{V}^X$, respectively. The radiative $A{\to}X$ transitions are mediated by electric-dipole vector $\mathbf{d}(\mathbf{r},\mathbf{R})$. This vector obviously enters the optical potential

$$^{\rm opt}V(r,R,\theta) = -\frac{\imath}{2}\,\frac{4}{3c^3\hbar^3}\,\mathbf{d}^2(r,R,\theta)\,[\Delta V(r,R,\theta)]^3\,. \tag{12}$$

The second essential constituent of this potential, due to which it becomes local, is the average, coordinate dependent energy of emitted photons, denoted here by $\Delta V(r,R,\theta)$. The state-to-state calculations of Ref. 3 on the RCT and RA reactions in the He^++H_2 system suggested the following prescription to model this quantity

$$\Delta V(r,R,\theta) = \overline{V}^A(r,R,\theta) - \overline{V}^A(r,R{\to}\infty) - \overline{V}^X(r,R,\theta){+}\Delta E\,, \tag{13}$$

where ΔE=74209 cm^{-1} is the separation between the thresholds He^++$D_2(v{=}0,j{=}0)$ and He+$D_2^+(v'{=}0,j'{=}0)$. The value of ΔE is smaller by 298 cm^{-1} than the value for He^++H_2 which accounts for the smaller difference between the zero-point energies of D_2 and D_2^+.

Let $\underset{N_{\rm o}\times N_{\rm o}}{{}^{\rm opt}\mathbf{S}^{Jp}}(E)$ denote the S-matrix which characterizes (the asymptotic behavior of) the partial scattering states of the Hamiltonian $^{\rm opt}H$ at energy E. Elements of the matrix, $[{}^{\rm opt}\mathbf{S}^{Jp}(E)]_{\alpha',\alpha}$, give probability amplitudes of transitions between open $\alpha{=}(vjl)$ states. The probabilities do not add to $N_{\rm o}$ i.e. $^{\rm opt}\mathbf{S}^{Jp}$ in not unitary, because of the presence of the optical potential. Thus, the required summarized radiative transition probability is

$$p^{\rm trad}(E;J,p) = {\rm Tr}\big[\mathbf{I} - ({}^{\rm opt}\mathbf{S}^{Jp})^\dagger\,{}^{\rm opt}\mathbf{S}^{Jp}(E)\big]\,. \tag{14}$$

Because of smallness of the optical potential, the distorted-wave (DW) approximation can be used

$${}^{\rm opt}\mathbf{S}^{Jp}(E) \approx \mathbf{S}^{Jp}(E) - 2\pi\imath\,\langle\mathbf{\Psi}^{(-)JMp}(E)|\,{}^{\rm opt}V\,|\mathbf{\Psi}^{(+)JMp}(E)\rangle\,. \tag{15}$$

Here $\underset{1\times N_{\rm o}}{\mathbf{\Psi}^{(\pm)JMp}}(E){:=}\big\{|E^{(\pm)}JMp,(vjl)_i\rangle, i{=}1,\ldots,N_{\rm o}\big\}$ is the vector of partial, energy-normalized scattering states of the molecular Hamiltonian H, the subscripts $(\pm)$ denote the $\underset{\rm in}{\rm out}$-going-wave type of the states, M is the quantum number of the total angular momentum projection on space-fixed z-axis, and $\mathbf{S}^{Jp}(E)$ is the related, unitary scattering matrix.
The resulting DW approximation to the function $p^{\rm trad}(E;J,p)$ is

$$p^{\rm trad,DW}(E;J,p) = 4\pi\imath\,{\rm Tr}\,\langle\mathbf{\Psi}^{(+)JMp}(E)|{}^{\rm opt}V\,|\mathbf{\Psi}^{(+)JMp}(E)\rangle\,. \tag{16}$$

As well-known[10,11], the DW approximation may become formally inapplicable at resonances. Molecular interactions responsible for dissociative decay of a resonance may become comparable

in strength or even (much) smaller than the interactions causing the radiative transitions. However, this fact can easily be circumvented in practice, as originally indicated in Ref. 10. It appears that accurate values of the resonance parameters ($E^{\rm res}$, Γ, $\Gamma^{\rm trad}$) can be extracted from profiles in $p^{\rm trad,DW}(E;J,p)$ even when the profiles themselves are evidently too high (an explicit demonstration is provided in Ref. 3). So, taking these parameters, the proper resonance profiles, i.e. the Lorentzians that appear in $p^{\rm trad}(E;J,p)$, Eq. (6), can be formed for the use in the temperature averaging, Eq. (4). If Lorentzian of a given resonance (n,Jp) is not too broad, the contribution to the partial rate constant $k^{\rm c}(T;J,p)$ can be approximated as[12]

$$k_{\rm res_n}(T;J,p) \approx \frac{1}{\hbar}\, P^{\rm c}(E_n^{\rm res},T)\, \Gamma_n^{{\rm trad},Jp}\, \frac{\Gamma_n^{Jp}}{\Gamma_n^{{\rm trad},Jp}+\Gamma_n^{Jp}}\,. \tag{17}$$

In the **Close-Coupling Body-Fixed diabatic representation**, the Hamiltonian ${}^{\rm opt}H(\mathbf{r},\mathbf{R})$ takes the form

$${}^{\rm opt}\mathbf{H}^{Jp}(R) = \mathbf{H}^{Jp}(R) - \tfrac{\imath}{2}\,{}^{\rm opt}\mathbf{W}^{Jp}(R) \qquad \text{with} \qquad \mathbf{H}^{Jp}(R) = -\tfrac{\hbar^2}{2\mu}\mathbf{I}\tfrac{d^2}{dR^2} + \mathbf{W}^{Jp}(R)\,, \tag{18}$$

where the bold-faced letters denote $N\times N$ matrices: $\mathbf{I}$ is the unit matrix, $\mathbf{W}^{Jp}(R)$ and ${}^{\rm opt}\mathbf{W}^{Jp}(R)$ are symmetric molecular and optical potential coupling matrices. Elements of the matrices are labeled by composite index $\beta=(v,j,\lambda)$ where λ denotes the absolute value of the quantum number of projection of the angular momentum $\mathbf{J}$ (and $\mathbf{j}$) on the axis Z aligned with the vector $\mathbf{R}$. Expressions for elements of the matrix $\mathbf{W}^{Jp}(R)$, originally given in Ref. 8, are listed in numerous papers. Here this matrix is constructed with application of the dimensionality reducing approximation which is described in Sec.IV of Ref. 1. Formula for elements of the matrix ${}^{\rm opt}\mathbf{W}^{Jp}(R)$ valid when the approximation $\mathbf{d}^2\approx d_Z^2$ is acceptable, was given in Ref. 3, Eqs. (31)-(33). Complete version of this formula, accounting for the second component of the dipole vector in the three-nuclei plane, is given in Appendix 1.

The respective representation of scattering functions $\mathbf{\Psi}^{(+)JMp}(E;\mathbf{r},\mathbf{R})$ is given by the matrix of radial functions $\underset{N\times N_{\rm o}}{\mathbf{F}^{(+)Jp}}(E;R)$ which satisfies the coupled equations

$$[E\mathbf{I} - \mathbf{H}^{Jp}(R)]\,\mathbf{F}^{(+)Jp}(E;R)=0 \tag{19}$$

and appropriate boundary conditions at R=0 and at R=R_∞ ($\to\infty$), namely, $\mathbf{F}^{(+)Jp}(E;0)$=0 and $\mathbf{U}^{Jp,T}\,\mathbf{F}^{(+)Jp}(E;R_\infty)\,\mathbf{U}^{Jp}$=$\mathbf{O}^{-\,Jp}(E;R_\infty)$−$\mathbf{O}^{+\,Jp}(E;R_\infty)\,\mathbf{S}^{Jp}(E)$ with $\mathbf{O}^{\pm\,Jp}$ built of the spherical Riccati-Hankel functions. $\mathbf{U}^{Jp}$ denotes transformation from the body-fixed to the space-fixed (SF) reference frame (details in Ref. 1).
Formula (16) becomes expressed in terms of integrals over R-coordinate

$$p^{\rm trad,DW}(E;J,p) = 2\pi\,{\rm Tr}\,\langle\mathbf{F}^{(+)Jp}(E)|\,{}^{\rm opt}\mathbf{W}^{Jp}|\,\mathbf{F}^{(+)Jp}(E)\rangle\,. \tag{20}$$

The CC-BF-diabatic representation is used for the following its features:

(i) it well displays the character of motion in the He^+-D_2 and He^+-H_2 complexes (cf. Figs. A3-A5, A7 in Ref. 3). The index $\beta=(v,j,\lambda)$ of the row of leading components of the radial function matrix $\mathbf{F}^{(+)Jp}(E;R)\,\mathbf{U}^{Jp}$ at $E\approx E_n^{{\rm res},Jp}$ gives three quantum numbers, denoted as v_r, b, and k, which characterize approximately the vibrational and rotational motion of the diatom within the complex in state (n,J,p). The fourth approximate quantum number, v_R, describes atom-diatom vibrations. Thus, the formal index n, enumerating only the quasi-bound states, can be replaced with the informative label $(v_r\,b\,k\,v_R)$.

(ii) it allows for the dimensionality reducing approximation mentioned at the beginning of this section (exclusion of components with λ-value larger than a specified $\lambda_{\rm max}$).

Close-Coupling Space-Fixed adiabatic representation

The representation is constructed with the help of orthogonal transformation $\mathbf{T}^{Jp}(R)$ which diagonalizes the coupling matrix $\mathbf{W}^{Jp}(R)$ of the Hamiltonian H in the CC-BF-diabatic representation,

$$[\mathbf{T}^{Jp}(R)]^T\,\mathbf{W}^{Jp}(R)\mathbf{T}^{Jp}(R) = \mathbf{e}^{Jp}(R)\,. \tag{21}$$

The resulting ro-vibrational adiabatic potentials, on the diagonal of $\mathbf{e}^{Jp}(R)$, are labeled by three numbers $\overline{v}$, $\overline{j}$, and $\overline{l}$ which correlate with the quantum numbers v, j, and l, respectively, since at large R's the diagonalization becomes equivalent to rotation of the body-fixed reference frame back to the space-fixed frame.

Obviously, non-adiabatic couplings

$$\mathbf{A}^{Jp}(R) = [\mathbf{T}^{Jp}(R)]^T\,\tfrac{d}{dR}\mathbf{T}^{Jp}(R) \qquad \text{and} \qquad \mathbf{B}^{Jp}(R) = [\mathbf{T}^{Jp}(R)]^T\,\tfrac{d^2}{dR^2}\mathbf{T}^{Jp}(R)$$

appear in the respective matrix form of H,

$${}_{\rm a}\mathbf{H}^{Jp}(R) = -\tfrac{\hbar^2}{2\mu}\left[\mathbf{I}\tfrac{d^2}{dR^2} + 2\mathbf{A}^{Jp}(R)\tfrac{d}{dR} + \mathbf{B}^{Jp}(R)\right] + \mathbf{e}^{Jp}(R)\,. \tag{22}$$

The reason for introducing this ro-vibrational adiabatic representation is the expectation that the dimension of the matrix ${}_{\rm a}\mathbf{H}^{Jp}(R)$ may substantially be reduced when solving the respective coupled equations for radial components of the scattering functions $\mathbf{\Psi}^{(+)JMp}(E;\mathbf{r},\mathbf{R})$,

$$\left[E\mathbf{I} - {}_{\rm a}\mathbf{H}^{Jp}(R)\right]_{M\times M}\mathbf{f}^{(+)Jp}(E;R){=}0\,, \tag{23}$$

and accurate values of the partial yield functions $p^{\rm trad,DW}(E;J,p)$ will be obtained as

$$p^{\rm trad,DW}(E;J,p) = 2\pi\,{\rm Tr}\,\langle\mathbf{f}^{(+)Jp}(E)|\,{}^{\rm opt}\mathbf{v}^{Jp}|\,\mathbf{f}^{(+)Jp}(E)\rangle \tag{24}$$

with

$${}^{\rm opt}\mathbf{v}^{Jp}(R){=}\underset{M\times N}{[\mathbf{T}^{Jp}(R)]^T}\;\underset{N\times N}{{}^{\rm opt}\mathbf{W}(R)}\;\underset{N\times M}{\mathbf{T}^{Jp}}(R)\,.$$

If not resorting to the DW approximation, one may expect to obtain accurate yield functions $p^{\rm trad}(E;J,p)$ from solutions of the equations with the truncated Hamiltonian matrix $\left[{}^{\rm opt}_{\rm a}\mathbf{H}^{Jp}(R)\right]_{M\times M}$,

$$\left\{\left[E\mathbf{I} - {}_{\rm a}\mathbf{H}^{Jp}(R)\right]_{M\times M} + \tfrac{\imath}{2}\,{}^{\rm opt}\mathbf{v}^{Jp}(R)\right\}{}^{\rm opt}\mathbf{f}^{(+)Jp}(E;R){=}0\,. \tag{25}$$

Obviously, having to solve smaller sets of (M) coupled equations in the adiabatic representation instead of the original (N) coupled equations in the diabatic representation would not yet guarantee any substantial computational savings. Sharp structures due to avoided-crossings of the adiabatic potentials occur in the non-adiabatic couplings, see Fig. A2, and very small step size would be needed to pass them through in the course of solving the coupled equations. However, one has now at choice the Smooth-Variable Discretization (SVD) technique[13,14]. This technique avoids the usual difficulties with strongly localized non-adiabatic couplings though requires somewhat bigger amount of information on input. Namely, it requires that overlapping integrals between the adiabatic basis functions at neighboring R-points of a grid covering the range $R_0(\approx 0) - R_\infty(\to\infty)$ be available. This information is available here in terms of the matrices

$$\underset{M\times M}{\mathcal{O}^{Jp}}(R;\overline{R}) = \underset{N\times M}{[\mathbf{T}^{Jp}(R)]^T}\;\underset{N\times M}{\mathbf{T}^{Jp}}(\overline{R})\,. \tag{26}$$

Appendix 1: CC-BF-diabatic representation of the 3D optical potential for spontaneous emission in atom+diatom systems

The potential is represented by skew-Hermitian matrix ${}^{\rm opt}\mathbf{V}(R)=\frac{i}{2}{}^{\rm opt}\mathbf{W}^{Jp}(R)$ whose elements are:

$$\left[{}^{\rm opt}\mathbf{W}^{Jp}(R)\right]_{\tilde\beta,\beta} = \delta_{\tilde\lambda,\lambda}\sum_{\Lambda=-1}^{1}\left[{}^{\rm opt}\mathbf{W}^{\lambda p}_{\Lambda}(R)\right]_{\tilde v\tilde j,vj} \tag{27}$$

$$\text{with}\qquad {}^{\rm opt}\mathbf{W}^{\lambda p}_{\Lambda}(R) = \frac{4}{3c^3\hbar^3}\left[\mathbf{d}^{\lambda p}_{\Lambda}(R)\right]^T\left[\mathbf{\Delta V}^{\lambda+\Lambda}(R)\right]^3\mathbf{d}^{\lambda p}_{\Lambda}(R)\,, \tag{28}$$

$$\text{where}\qquad \left[\mathbf{d}^{\lambda p}_{\Lambda}(R)\right]_{\tilde v\tilde j;\,vj} = f^{\lambda}_{\Lambda}(p)\sum_{L}\langle\tilde v\tilde j|D_{L|\Lambda|}(r,R)|vj\rangle_r\, g^{\lambda}_{L\Lambda}(\tilde j,j)\,, \tag{29}$$

$$g^{\lambda}_{L\Lambda}(\tilde j,j) = (-1)^L\left[\frac{(L+|\Lambda|)!}{(L-|\Lambda|)!}\right]^{1/2}C(j\,L\,\tilde j;\lambda\,\Lambda\,\lambda{+}\Lambda)\,C(\tilde j\,L\,j;000)\,, \tag{30}$$

$$\begin{aligned} f^{\lambda}_{0}(p) &= 1 \quad \text{except for} \quad f^{0}_{0}(-1){=}0\,,\\ f^{\lambda}_{\pm1}(p) &= \begin{cases} \frac{1+p}{2} & \text{for}\quad \lambda{=}0,\mp1\,,\\ \frac{1}{\sqrt{2}} & \text{for}\quad \lambda{\neq}0,\mp1\,, \end{cases} \end{aligned} \tag{31}$$

$$\text{and}\qquad \left[\Delta\mathbf{V}^{\lambda}(R)\right]_{\tilde v\tilde j;\,vj} = \sum_{L}\langle\tilde v\tilde j|\Delta V_L(r,R)|vj\rangle_r\, g^{\lambda}_{L0}(\tilde j,j)\,. \tag{32}$$

The functions $D_{L|\Lambda|}(r,R)$ for $|\Lambda|{=}0,1$ come from the expansions into the Legendre functions of the two components of the transition dipole vector in the three-nuclei plane,

$$d_Z(r,R,\theta){=}\sum_L D_{L0}(r,R)\,P_L(\cos\theta)\qquad\text{and}\qquad d_X(r,R,\theta){=}\sum_L D_{L1}(r,R)\,P^1_L(\cos\theta)\,,$$

and the functions $\Delta V_L(r,R)$ come from the Legendre polynomial expansion of the coordinate dependent average photon emission energy $\Delta V(r,R,\theta)$, Eq. (13). The symbol $C(\ldots;\ldots)$ denotes Clebsh-Gordan coefficient.

It is worthy of noting that elements of the matrix ${}^{\rm opt}\mathbf{W}^{Jp}(R)$ do not actually depend on the quantum number J.

$\mathbf{He^+}$+$\mathbf{D_2}$ versus $\mathbf{He^+}$+$\mathbf{H_2}$

Fig. A1. Hamiltonian matrices in CC-BF-diabatic representation

$$^{\rm opt}\mathbf{H}^{Jp}(R) = -\frac{\hbar^2}{2\mu}\mathbf{I}\frac{d^2}{dR^2} + \mathbf{V}^{Jp}(R)$$

$$\mathbf{V}^{Jp}(R) = \mathbf{W}^{Jp}(R) - \tfrac{i}{2}\,^{\rm opt}\mathbf{W}(R)$$

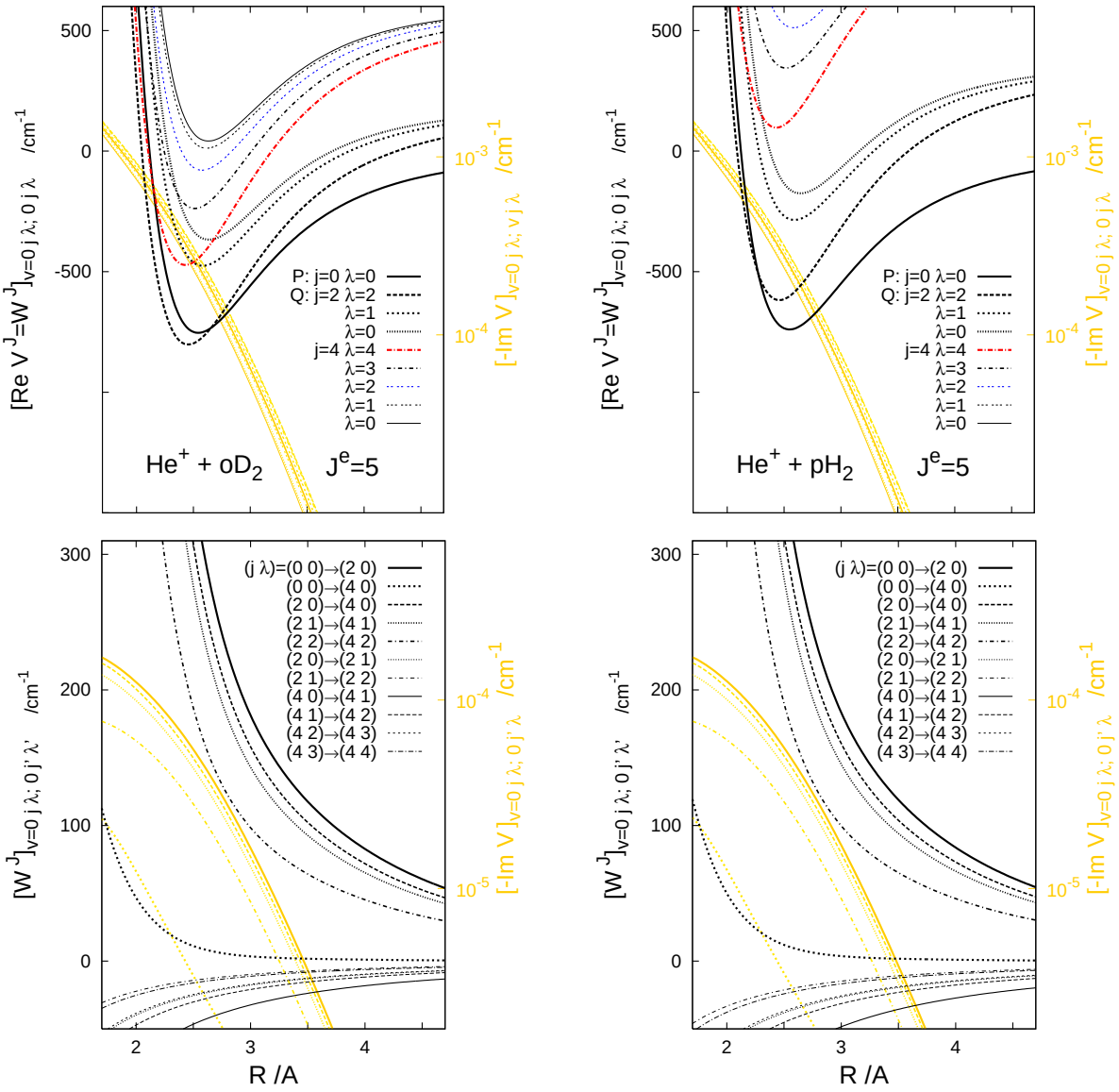

This figure illustrates: (i) the overall shape of diagonal and off-diagonal elements of the two coupling matrices $\mathbf{W}$ and $^{\rm opt}\mathbf{W}$ of the CC-BF-diabatic representation of the Hamiltonian $^{\rm opt}H$, and (ii) how the particular elements of the matrices that describe the He^++D_2 system differ from those describing the lighter (≈1.5 times) He^++H_2 system. Two features of the optical potential elements should be noted: (i) they all decline rapidly, the diagonal ones — by a factor of ∼70 within the short R-interval of 2 - 3.5 Å, and (ii) they hardly change upon the isotopic substitution.

$\mathbf{He}^+ + \mathbf{D}_2$ versus $\mathbf{He}^+ + \mathbf{H}_2$

Fig. A2. Hamiltonian matrices in CC-SF-adiabatic representation

$$ {}^{\mathrm{opt}}\mathbf{H}^{Jp}(R) = -\frac{\hbar^2}{2\mu}\left[\mathbf{I}\frac{d^2}{dR^2} + 2\mathbf{A}^{Jp}(R)\frac{d}{dR} + \mathbf{B}^{Jp}(R)\right] + \mathbf{V}^{Jp}(R) $$

$$ \mathbf{V}^{Jp}(R) = \mathbf{e}^{Jp}(R) - \tfrac{\imath}{2}\,{}^{\mathrm{opt}}\mathbf{v}^{Jp}(R) $$

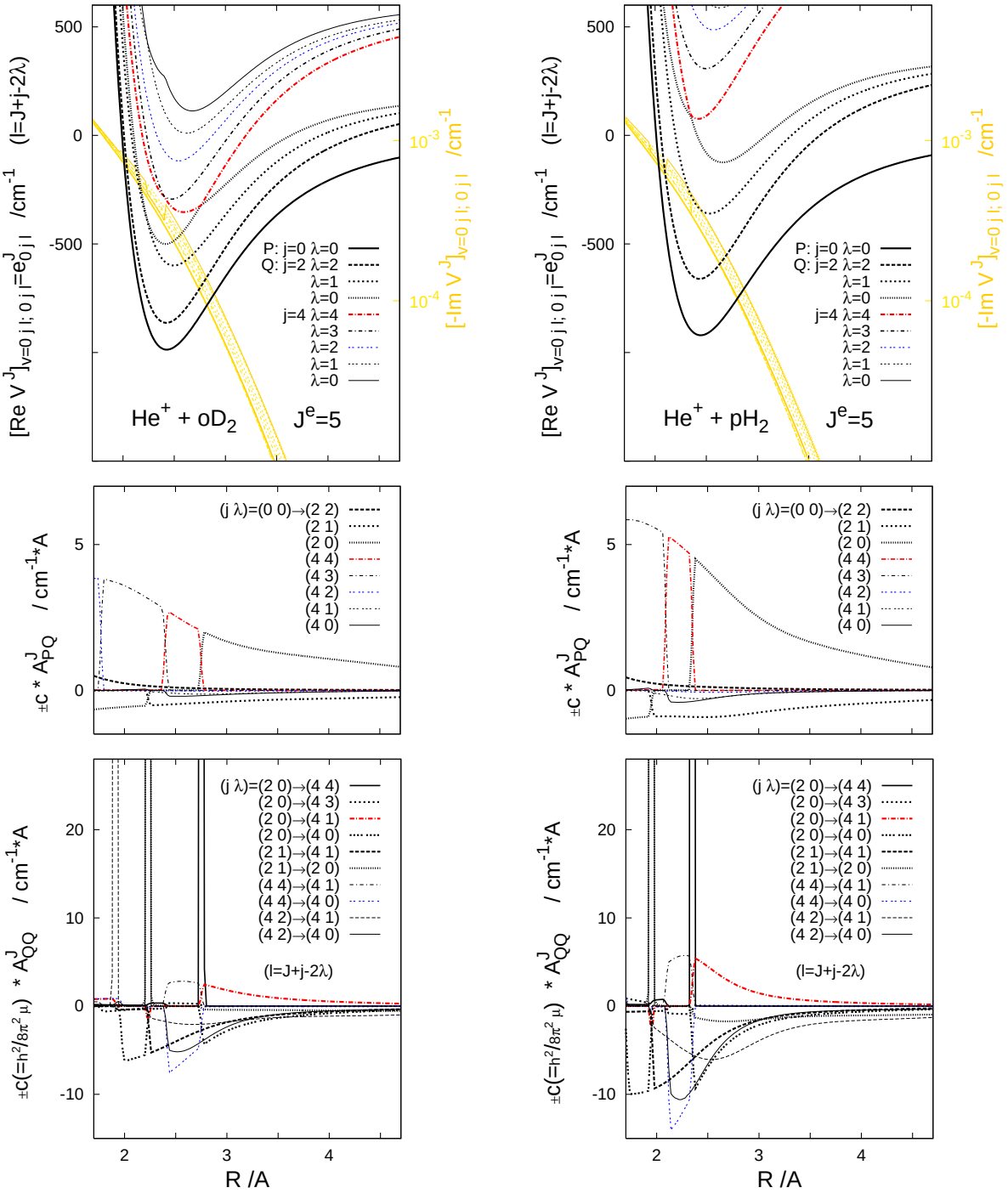

This figure should give a feeling of how discouraging the idea of using the CC-SF-adiabatic representation would be if the arising non-adiabatic couplings had to be explicitly dealt with.

B. CALCULATIONS

In the calculations on dynamics of the 'trad' reaction in the $He^+ + D_2$ collisions exactly the same electronic structure input was used as in the previous calculations[3] for the $He^+ + H_2$ system, namely, the PESes $\overline{V}^A(r, R, \theta)$ and $\overline{V}^X(r, R, \theta)$ and the transition dipole function $d_Z(r, R, \theta)$ from Ref. 5.
The following were the consecutive steps of the calculations:

1. The determination of positions ($E^{\rm res}$) and dissociative widths (Γ) of quasi-bound of the complexes $He^+ - o\text{-}D_2$ and $He^+ - p\text{-}D_2$ in the energy range up to $\sim$360 cm^{-1} above their lowest dissociation thresholds, v=0 j=0 (E=ε_{00}=0) and j=1 (E=ε_{01}=59.7 cm^{-1}), respectively. The life-time matrix analysis[15,16] was the main approach exploited. Altogether, about 1400 quasi-bound states have been found. The widths Γ of about 1280 of them are in the range $5\times10^{-8} - 2$ cm^{-1}.

2. The determination of radiative widths ($\Gamma^{\rm trad}$) of the quasi-bound states. The procedure applied was that described in Ref. 3 (Part C of Supplementary Material). Except for cases of very sharp resonances ($\Gamma \ll 0.05$ cm^{-1}), the procedure requires the determination of respective resonance profiles in the functions $p^{\rm trad}(E; Jp)$. The profiles were determined for above 540 resonances for which $\sim 0.05 < \Gamma < 2$ cm^{-1}.

3. The determination of background parts of the yield functions, $p^{\rm trad,c}_{\rm bck}(E; J, p)$. This meant in practice a subtraction of sharp resonance features from the functions $p^{\rm trad,c}(E; J, p)$ which were generated at grids of $\sim 60 - \sim 80$ energy points covering the range $10^{-8} - 360$ cm^{-1} above the respective lowest threshold. The functions $p^{\rm trad,c}_{\rm bck}(E; J, p)$ were determined for J^e=0−32 and J^f=1−32 (28) for c=p (o) (altogether 126 functions).

4. The integration of the total yield functions $p^{\rm trad,c}(E)$ multiplied by the appropriate populations factors to determine finally the rate constants $k^{\rm c}$ in the temperature range $1\mu - 100$K. Except for a few cases, mostly in the cold range, the integration over the peaks in the resonance parts of the yield functions, $p^{\rm trad,c}_{\rm res}(E)$, was done analytically.

Because of denser spectrum of resonances and larger number of partial waves contributing, the task of determining the rate constant functions for the $He^+ + D_2$ system required significantly larger computational work than in the $He^+ + H_2$ case. Of much help in completing this task was the fact that a more efficient method could be exploited. The method is presented below.

Smooth-Variable-Discretization log-derivative method for evaluation of free-free integrals

Precisely, the algorithm to be presented here generates two quantities which concern/involve the solution of the following boundary-value problem

$$\left[\mathbf{I}\tfrac{d^2}{dR^2}+2\mathbf{A}(R)\tfrac{d}{dR}+\mathbf{B}(R)+\mathbf{b}(E;R)\right]\mathbf{\Psi}(E;R)=0\mathbf{I}\,, \tag{33}$$

$$\mathbf{\Psi}(E;R_0{\approx}0){=}0\mathbf{I}\,,\qquad \mathbf{\Psi}(E;R_\infty){=}\mathbf{I}\,. \tag{34}$$

The quantities are:

$$\mathbf{L}(E;R_\infty){:=}[\tfrac{d}{dR}\mathbf{\Psi}(E;R_\infty)][\mathbf{\Psi}(E;R_\infty)]^{-1}{+}\mathbf{A}(R_\infty)$$

$$\text{and}\qquad \mathbf{J}(E;R_\infty):=\int_{R_0}^{R_\infty}\mathbf{\Psi}^T(E;R)\,\boldsymbol{\kappa}(R)\,\mathbf{\Psi}(E;R)\,dR\,. \tag{35}$$

All bold-faced symbols denote here $M{\times}M$ matrices. The matrices within the square brackets in Eq. (33) come from the operator $\left[E\mathbf{I}-{}_{\rm a}\mathbf{H}^{Jp}(R)\right]_{M\times M}$ of Eq. (23) multiplied by $\frac{2\mu}{\hbar^2}$. Thus, $\mathbf{b}(E;R){:=}\frac{2\mu}{\hbar^2}[E\mathbf{I}-\mathbf{e}(R)]$ is a diagonal matrix, and the non-adiabatic coupling matrices have the following properties: $\mathbf{A}^T{=}-\mathbf{A}$, and

$$\mathbf{B}{=}\tfrac{d}{dR}\mathbf{A}{+}\mathbf{A}^2{+}\mathbf{\Delta}\qquad\text{with}\qquad \mathbf{\Delta}{:=}-\tfrac{d}{dR}\mathbf{T}^T\underset{N\times M}{\tfrac{d}{dR}\mathbf{T}}{+}\mathbf{A}^T\mathbf{A}\,.$$

In the integral $\mathbf{J}$, the 'transition matrix' $\boldsymbol{\kappa}(R)$ is assumed to be symmetric, $\boldsymbol{\kappa}^T{=}\boldsymbol{\kappa}$.

The formulas of the algorithm are:

$$\mathbf{z}_0^{-1}=0\mathbf{I}\,,\qquad \mathbf{u}_0{=}\tfrac{h^2}{3}\boldsymbol{\kappa}_0\,, \tag{36}$$

$$\mathbf{u}_l=\mathcal{O}_{l-1,l}^T\,\mathbf{z}_{l-1}^{-1}\,\mathbf{u}_{l-1}\,\mathbf{z}_{l-1}^{-1}\mathcal{O}_{l-1,l}+\begin{cases}\frac{h^2}{48}\mathbf{q}_l\boldsymbol{\kappa}_l\mathbf{q}_l & \text{for}\quad l{=}1,3,\ldots,2L{-}1\,,\\ \frac{2h^2}{3}\boldsymbol{\kappa}_l & \text{for}\quad l{=}2,4,\ldots,2L\,,\end{cases} \tag{37}$$

$$\mathbf{z}_l=-\mathcal{O}_{l-1,l}^T\,\mathbf{z}_{l-1}^{-1}\,\mathcal{O}_{l-1,l}\qquad+\begin{cases}-6\mathbf{I}+\mathbf{q}_l & \text{for}\quad l{=}1,3,\ldots,2L{-}1\,,\\ 2\mathbf{I}-\frac{2h^2}{3}\mathbf{b}_l & \text{for}\quad l{=}2,4,\ldots,2L\,,\end{cases} \tag{38}$$

$$\mathbf{L}=(\mathbf{z}_{2L}{-}\mathbf{I}{+}\tfrac{h^2}{3}\mathbf{b}_{2L})/h\,, \tag{39}$$

$$\mathbf{J}=(\mathbf{u}_{2L}-\tfrac{h^2}{3}\boldsymbol{\kappa}_{2L})/h\,, \tag{40}$$

$$\text{where}\qquad \mathbf{q}_l=[\tfrac{1}{8}\mathbf{I}+\tfrac{h^2}{48}\mathbf{b}_l]^{-1}\,, \tag{41}$$

$$\mathbf{b}_l{=}\mathbf{b}(R_l)\,,\qquad \boldsymbol{\kappa}_l{=}\boldsymbol{\kappa}(R_l)\,,\qquad \mathcal{O}_{l-1,l}{=}\mathcal{O}(R_{l-1};R_l)\,,$$

$$R_l{=}R_0{+}lh\,,\quad\text{and}\quad R_{2L}{=}R_\infty\,.$$

The algorithm closely resembles the version of the log-derivative method[17] of Johnson which was proposed in Ref. 18 for equations in quasi-diabatic representations. The only differences are: (i) the overlaps $\mathcal{O}$ stand in place of the first-derivative-coupling-removing transformations and (ii) the term Δ of the coupling matrix $\mathbf{B}$ does not explicitly appear in the SVD version. Actually, the two (the SVD and the quasi-diabatic) algorithms become equivalent in the $M{=}N$ limit, meaning here the limit of completeness of the adiabatic basis, $\Delta{=}0$.

It is worthy of stressing at this point that the SVD algorithm is correct irrespective of degree of completeness of the adiabatic basis, for any $M \leq N$, i.e. when the absent term Δ may play a non-negligible role. [This not always is true for algorithms which exploit the popular diabatic-by-sector technique of dealing with non-adiabatic couplings, cf . Ref. 19]. The statement relies on the fact that formulas (36)-(41) lead, in the $h \to 0$ limit, to correct differential equations for the matrices $\mathbf{L}(E; R_\infty)$ and $\mathbf{J}(E; R_\infty)$ as functions of R_∞ (renamed here to R),

$$\tfrac{d}{dR}\mathbf{L}(E;R) = -\mathbf{b}(R) - \boldsymbol{\Delta}(R) - \mathbf{L}^2(E;R) + \mathbf{A}^T(R)\,\mathbf{L}(E;R) + \mathbf{L}(E;R)\,\mathbf{A}(R)\,, \tag{42}$$

$$\tfrac{d}{dR}\mathbf{J}(E;R) = \boldsymbol{\kappa}(R) + \big[\mathbf{A}^T(R) - \mathbf{L}(E;R)\big]\mathbf{J}(E;R) + \mathbf{J}(E;R)\big[\mathbf{A}(R) - \mathbf{L}(E;R)\big]\,. \tag{43}$$

Namely, the term Δ appears, as it should, in the equation for the matrix $\mathbf{L}$.

When the boundary R_∞ is placed sufficiently far away from the origin $R_0 \approx 0$, so that $\mathbf{A}(R_\infty) \approx 0$, the matrix $\mathbf{L}$ obtained from the algorithm becomes the ordinary log-derivative matrix which, in the standard way, can be converted to the scattering matrix $\mathbf{S}$. The integral $\mathbf{J}$, evaluated with the optical potential ${}^{\rm opt}\mathbf{v}$ inserted for $\boldsymbol{\kappa}$, will give then the integral occurring in Eq. (24) upon the following operation

$$\langle \mathbf{f}^{(+)}(E)|\,{}^{\rm opt}\mathbf{v}|\,\mathbf{f}^{(+)}(E)\rangle = [\ldots]^\dagger\,\mathbf{J}(E;R_\infty)\,[\mathbf{O}^-(E;R_\infty) - \mathbf{O}^+(E;R_\infty)\,\mathbf{S}(E)]\,. \tag{44}$$

Analogously, the integral $\mathbf{J}$ evaluated with $\boldsymbol{\kappa}=\mathbf{I}$ can be converted to the matrix $2\pi\hbar\langle \mathbf{f}^{(+)}|\,P_{[R_0,R_\infty]}|\,\mathbf{f}^{(+)}\rangle$ (with $P_{[R_0,R_\infty]}$ denoting projector on the indicated interval of R-coordinate) which is one of two essential constituent of the life-time matrix, cf. the description of the life-time analysis in Ref. 16 and of the sojourn-time analysis in Ref. 3 (Part A of Supplementary Material).

Formulas of the algorithm concerning the matrix $\mathbf{L}$ can also be used to calculate the probabilities $p^{\rm trad}$ from the coupled equations accounting 'exactly' for the optical potential, Eq. (25). Nothing but the replacement $\mathbf{b}_l \longrightarrow \mathbf{b}_l + \imath\frac{\mu}{\hbar^2}\,{}^{\rm opt}\mathbf{v}_l$ is needed to adapt the formulas to this purpose.

An illustration of performance of the SVD log-derivative algorithm in the determination of the probabilities $p^{\rm trad,DW}$ and of the resonance parameters $E^{\rm res}$, Γ, and $\Gamma^{\rm trad}$ is given in Fig. B1. The features exposed are:

- the convergence of the results with the SF-adiabatic basis size, how much truncated the basis may be compared to the size of the BF-diabatic basis used to its construction,
- the convergence with the step size, how it compares with the convergence of the 'diabatic' version of the algorithm[20]. [The 'diabatic' version can be recovered from formulas (36)-(41) by using $\mathbf{W}(R_l)$ instead of $\mathbf{e}(R_l)$ in the construction of $\mathbf{b}_l$, inserting ${}^{\rm opt}\mathbf{W}(R_l)$ instead of ${}^{\rm opt}\mathbf{v}(R_l)$ for $\boldsymbol{\kappa}_l$, and setting all $\mathcal{O}$'s to $\mathbf{I}$.]

In the performed calculations on the 'trad' reaction in the $He^+ + D_2$ collisions, the SF-adiabatic bases were truncated typically by factors slightly larger than two. Due to the possibility of using step sizes practically the same as in the diabatic algorithm the computations could be speeded up about ten times.

CC-SF-adiabatic versus CC-BF-diabatic representation

Fig. B1. Convergence properties of the SVD-log-derivative method

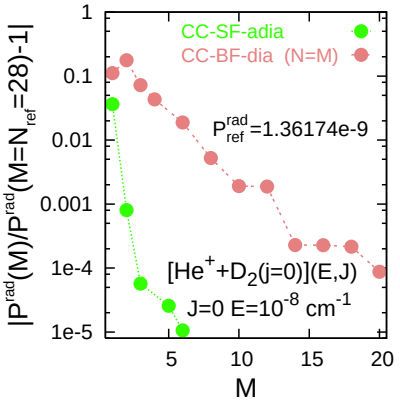

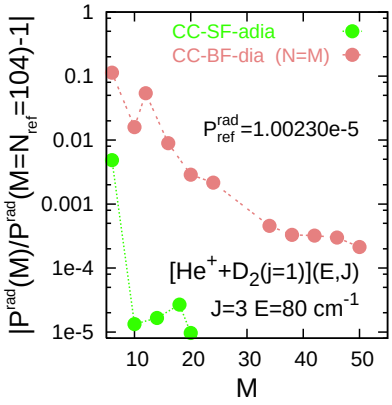

Probabilities $p^{\mathrm{trad,DW}}(E;J,p)$ for two exemplary E,J-values (p=1). Errors due to truncation of the SF-adiabatic basis versus errors due to decrease of the BF-diabatic basis size. The 'complete' adiabatic basis is constructed from N_{ref} BF-diabatic basis functions. The diabatic basis of a decreased size $N<N_{\mathrm{ref}}$ is obtained by eliminating functions which correspond to highest closed channels.

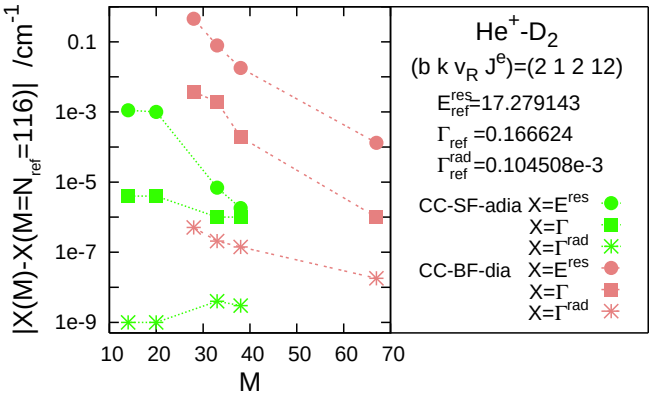

Parameters of exemplary non-sharp resonance extracted from respective profile in the function $p^{\mathrm{trad,DW}}(E;J^e)$. Errors due to the use in the calculations of the profile of truncated SF-adiabatic and BF-diabatic bases.

All 'SF-adia' results presented here and in the panels of first and third rows have been obtained using the same step size (h=0.01Å) as used in the calculations of 'BF-dia' results with the 'diabatic' version of the algorithm.

Parameters E^{res} and Γ of exemplary sharp resonance extracted from respective profile in the trace of the life-time matrix.
Convergence with the size of the SF-adiabatic and BF-diabatic bases.

Below: Convergence with the step size (h) in the SVD and in the diabatic log-derivative algorithms. 'exc' denotes result yielded by a given algorithm and a given size (M) of the respective basis when the step size h=0.01Å is used.

Generally, errors of results generated with the SVD algorithm behave the same as errors of the diabatic version, i.e. they scale like $C\times h^4$ with nearly the same scaling factor C. A departure from this behavior may occur if the adiabatic basis is truncated too drastically (here from N=132 to M=22).

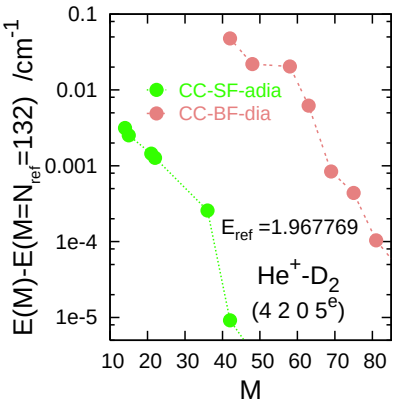

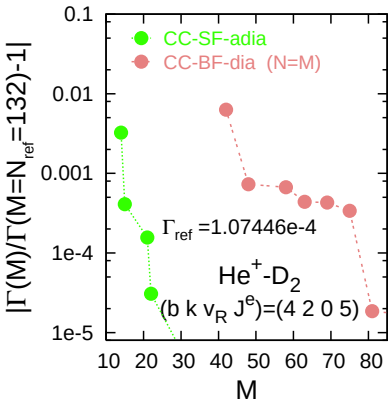

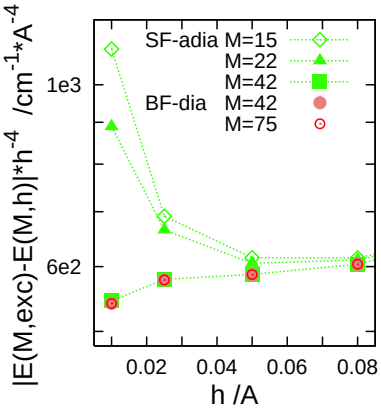

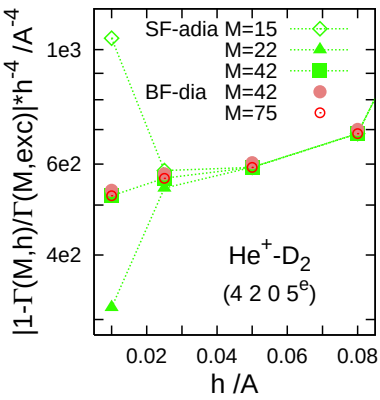

C. RESULTS

He^+-D_2 versus He^+-H_2 complex

FIGURES

C1. Energies of J=0 bound states. Location on PES of first excited electronic of $[HeHH]^+$.

C2. Structure of energy levels of bound and quasi-bound states associated with v=0 j=0 − 5 thresholds. J=k levels.

C3. Dissociative versus radiative widths of predissociating states (rotational Feshbach resonances).

C4. Radiative widths of rotational (J) levels in selected vibrational states $[v_r$=0 v_θ=$b-k$ $v_R]$ k

TABLES

I. $He^+-o\text{-}D_2$. Energies, dissociative and radiative widths of 'vibrational' (J=k) states below v=0 j=0, 2, 4 thresholds.

II. Same as in **I** for levels of $He^+-p\text{-}D_2$ below v=0 j=1, 3, 5 thresholds.

III. $He^+-o\text{-}D_2$. Energies, dissociative and radiative widths of rotational ($J\geq k$) states associated with v=0 j=2 threshold in the range from v=0 j=0 up to j=3 threshold (includes 280 resonances).

IV. Same as in **III** for states associated with v=0 j=4 threshold (includes 196 resonances).

V. Same as in **III** for states associated with v=0 j=0 (30 shape resonances).

VI. $He^+-p\text{-}D_2$. Energies, dissociative and radiative widths of rotational states associated with v=0 j=3 threshold in the range from v=0 j=1 up to j=3 threshold (543 resonances).

VII. Same as in **VI** for states associated with v=0 j=5 threshold (100 resonances).

VIII. Same as in **VI** for states associated with v=0 j=1 (75 shape resonances).

Radiative decay of He^+ from mixtures with D_2 and from mixtures with H_2

FIGURES

C5. Yield functions for the radiative reaction in collisions with c-D_2 and c-H_2 for c=o,p.

a.-c. Partial yield functions $p^{\mathrm{trad,c}}(E; J, p)$, i.e. probability sums of radiative transitions from partial (J=0−30) continuum states of the He^++c-D_2 systems, as functions of energy in the 10^{-5}—360 cm^{-1} range above the respective lowest threshold.

d.-e. Total yield functions $p^{\mathrm{trad,c}}(E)$. Resonance and background parts. Validity of capture model.

C6. Rate constants of radiative decay from mixtures with pure ortho- or para- D_2 or H_2.

a. Partial rate constants in low temperature range, T<1 K.

b. Feshbach resonance contributions to total rate constants at Ts up to 100 K.

C7. Rate constants of radiative decay from mixtures with equilibrium and normal H_2 and D_2 as functions of temperature in the 1μK – 100 K range.

a. Contributions of transitions involving ortho- and para-H_2(D_2).

b. Feshbach-resonance versus background and shape-resonance contributions.

c. D_2/H_2 isotope effects in cold and subthermal ranges.

TABLES

IX. Rate constants functions plotted in Fig. **C7a** at selected temperature values.

$\mathbf{He^+{-}D_2}$ versus $\mathbf{He^+{-}H_2}$

Fig. C1. Energies of bound J=0 states

Location on PES of $[HeH_2]^+(A\,^2A')$

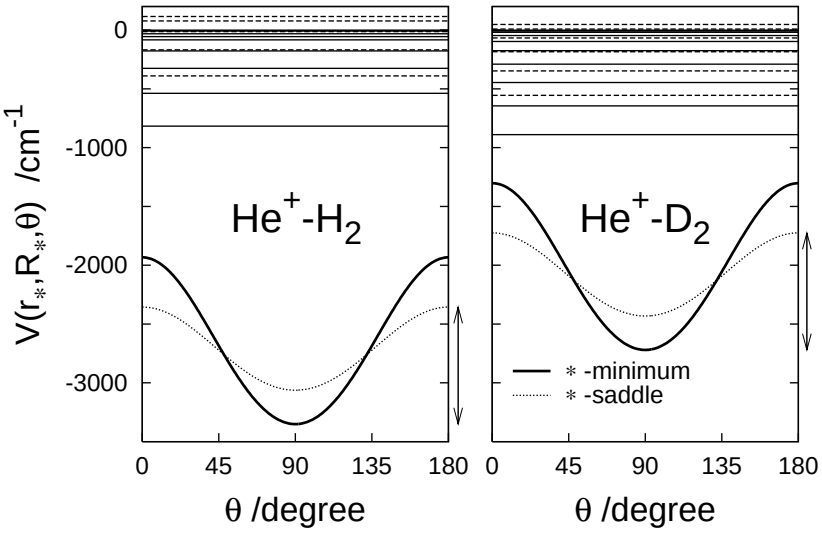

1D cuts of the PES of the first excited electronic state of the $[HeH_2]^+$ system[5] through the minimum, r^*=0.748$\mathring{A}$, R^*=2.3872$\mathring{A}$ (thick line), and the saddle point at θ=0, π: r^*=0.7421$\mathring{A}$, R^*=2.8484$\mathring{A}$. The double arrow shows the barrier to linearity, of 995 cm^{-1}. The thresholds $He^+{+}a_2(v{=}0\,j{=}0)$ for a=H and a=D (at which zero of the energy E is placed) lie, respectively, 3350.8 and 2730.0 cm^{-1} above the minimum of the PES. The energy levels of bound J=0 states of the complexes $He^+{-}H_2(I{=}0)$ and $He^+{-}D_2(I{=}0,2)$ are drawn with solid lines, of the complexes $He^+{-}H_2(I{=}1)$ and $He^+{-}D_2(I{=}1)$ — with dashed lines. The zero-point energies of $He^+{-}H_2$ and $He^+{-}D_2$ are 2533.7 and 1831.0 cm^{-1}, respectively.

Fig. C2. Energies of $b\,k\,v_R\,J{=}k\,p{=}1$ states associated with $\mathrm{He^+{+}a_2}(v{=}0,j)$ thresholds (a=D,H) for $j{=}0{-}5$ ($b{\sim}j$)

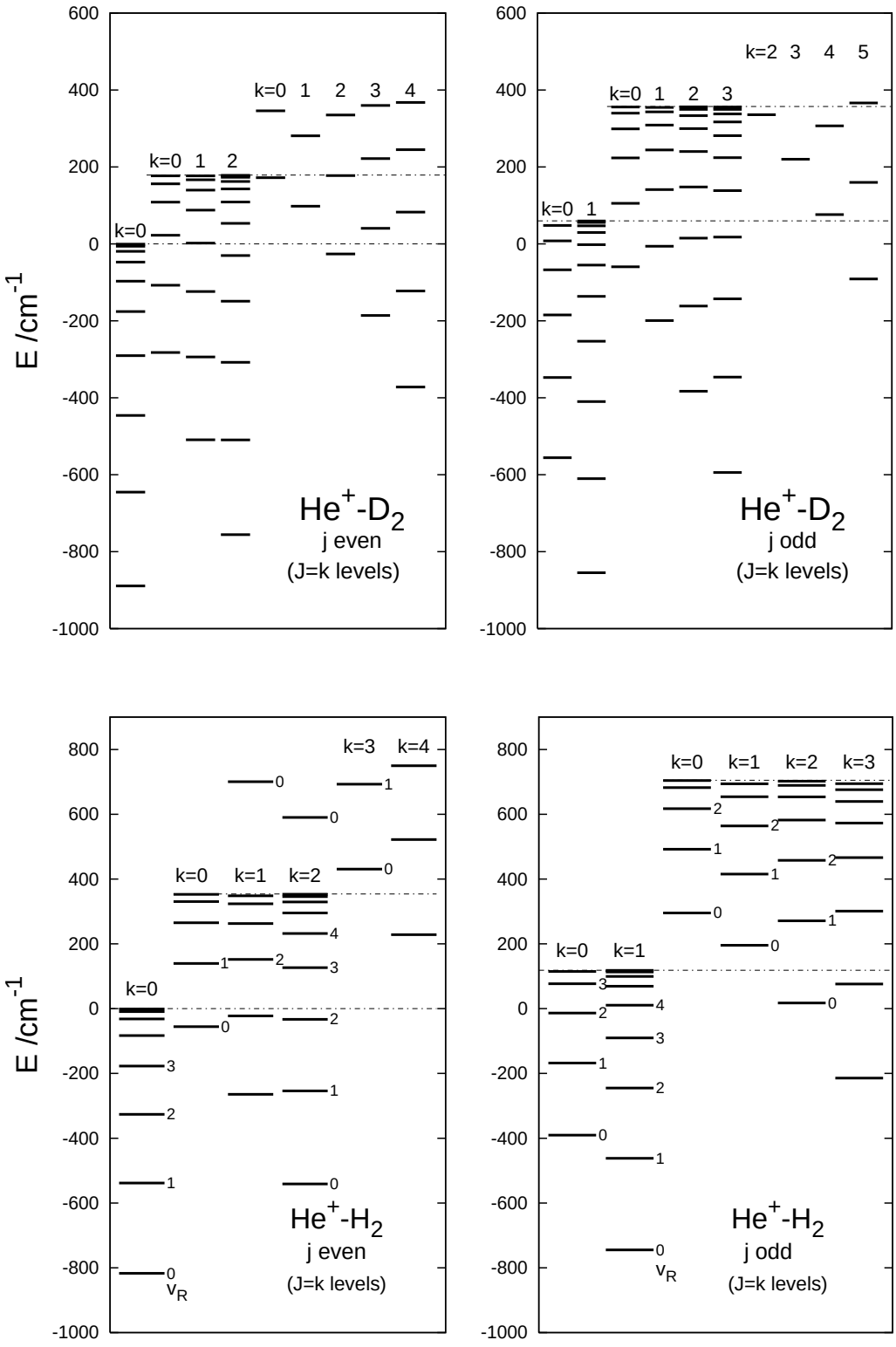

He^+-D_2 vs He^+-H_2

Fig. C3. Predissociating states associated with j=2, 4 thresholds
Dissociative and radiative widths

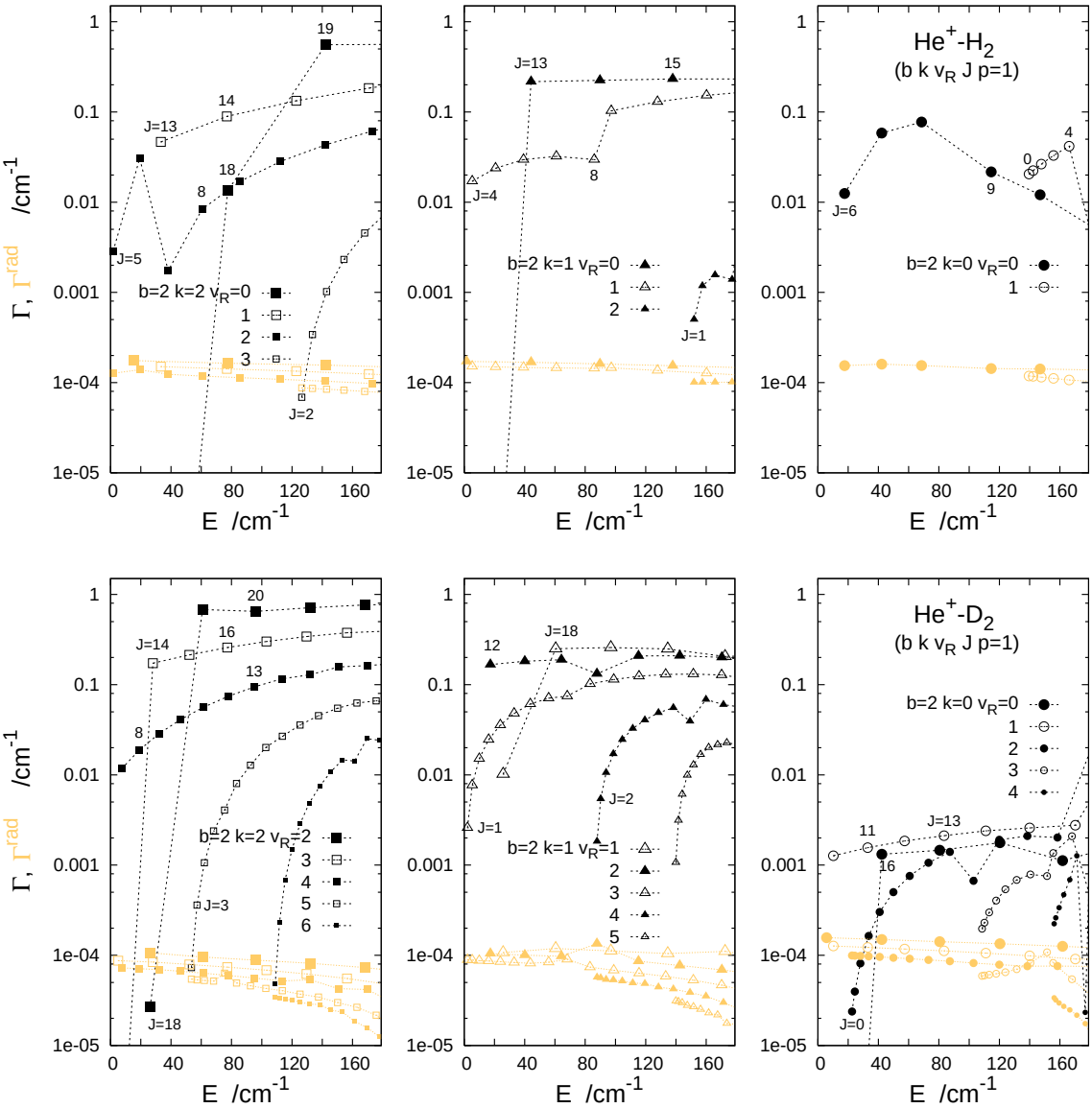

Shown are only states in the energy range from 0 to 178 cm^{-1} ($\approx\varepsilon_{02}$ of D_2) as they have the largest impact on the low temperature rate constants of the 'trad' reaction, especially in mixtures with equilibrium D_2 or H_2. In the specified range, there are 45 predissociating states of the He^+-H_2 complex, all shown in the three upper panels, and above 250 states of the He^+-D_2 complex, 202 of them are shown in the four lower panels. The widths Γ of low lying resonances may have a significant impact on the rate constant values when they are comparable to or incomparably smaller than the widths $\Gamma^{\rm trad}$, cf. Eq. (17). It is therefore worthy of noting that the lowest lying state of the He^+-D_2 complex, $(b\,k\,v_R\,J^p)=(4\,2\,0\,5^e)$, is characterized by the width ratio $\Gamma/(\Gamma^{\rm trad}+\Gamma)\approx0.33$, see Table IV. In the case of the lowest state of the He^+-H_2 complex, $(2\,2\,2\,5^e)$, this ratio is ≈0.96, see Table I in Ref. 3.

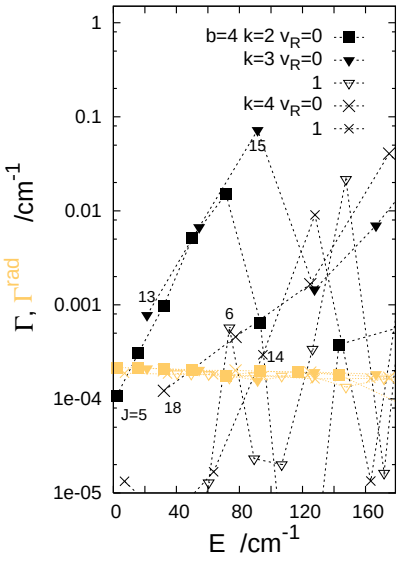

He^+-D_2 vs He^+-H_2

Fig. C4. Radiative widths of rotational (J) levels in selected vibrational states $[v_r{=}0\, v_\theta{=}b{-}k\, v_R]\, k$

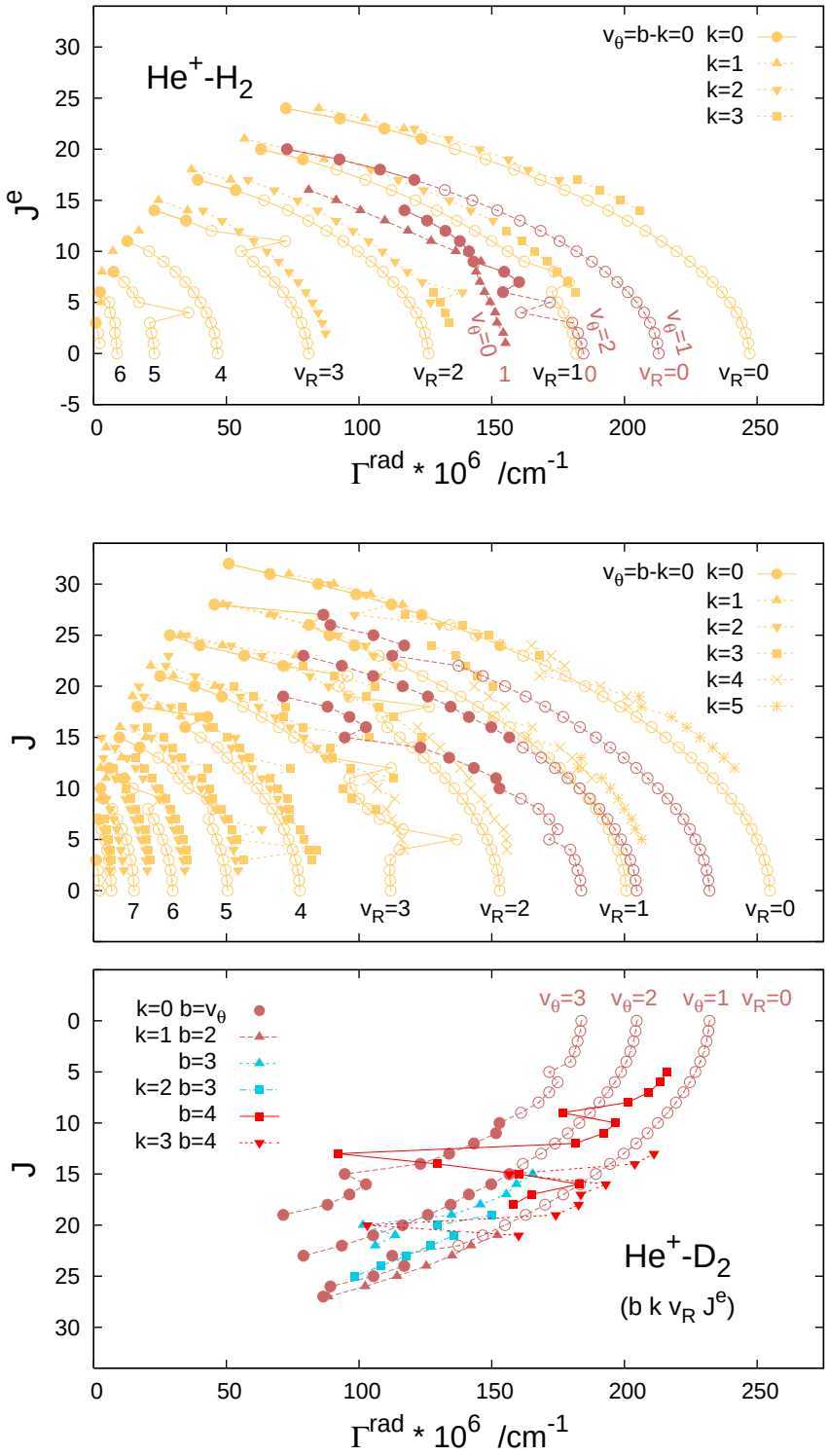

Shown are the widths $\Gamma^{\rm trad}$ of all quasi-bound J levels of the selected vibrational states of the $He^+{-}H_2$ and $He^+{-}D_2$ complexes which lie no higher than the threshold $\varepsilon_{02}(=354.03\ {\rm cm}^{-1})$ and $\varepsilon_{03}(=357.1\ {\rm cm}^{-1})$, respectively. In cases of states assigned with $k{=}0$, shown are also the widths $\Gamma^{\rm trad}$ of bound rotational levels (open circles).

The radiative widths of the states of the two complexes show qualitatively the same correlations with the quantum numbers assigned to the states.

As to quantitative differences, one should note first that disturbances due to state mixing are more numerous in the He^+-D_2 complex. Because of them, exploitation of simple fitting formulas in the analysis of the widths becomes problematic. In Ref. 3, the following formula was used to describe the J dependence of the widths of He^+-H_2,

$$\Gamma^{\rm rad}(J) \approx \Upsilon - \sum_{m=1}^{2} \gamma_m [J(J+1)-k^2]^m \,.$$

The parameters Υ, γ_1, and γ_2 obtained from fitting the formula to the calculated widths were reasonably smooth functions of the numbers v_R, v_θ, and k. Attempts to fit this formula to the widths of He^+-D_2 did not give parameters of similar quality, except for the largest parameter, Υ.

Figure next to this text provides a comparison of parameters Υ and γ_1 obtained for the widths $\Gamma^{\rm trad}$ of J levels in the states $[0\,0\,v_R]\,k{=}0$ of He^+-D_2 and He^+-H_2. The parameter Υ as function of the number v_R of the states of He^+-D_2 is slightly larger at $v_R{=}0$ and decreases less rapidly with v_R growing than the function $\Upsilon(v_R)$ for He^+-H_2. The values of the parameter γ_1 pertaining to He^+-D_2 are in turn smaller by a factor which is close (at the lowest v_R's, at least) to the reduced mass ratio $\mu_{\rm He^+-D_2}/\mu_{\rm He^+-H_2}$(=1.497).

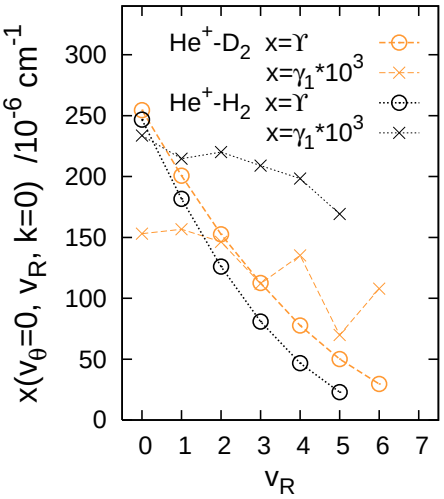

Fig. C4a. Radiative widths of lowest rotational levels ($J{=}k$) of groups k in different vibrational states $[v_r{=}0\,v_\theta{=}b{-}k\,v_R]$

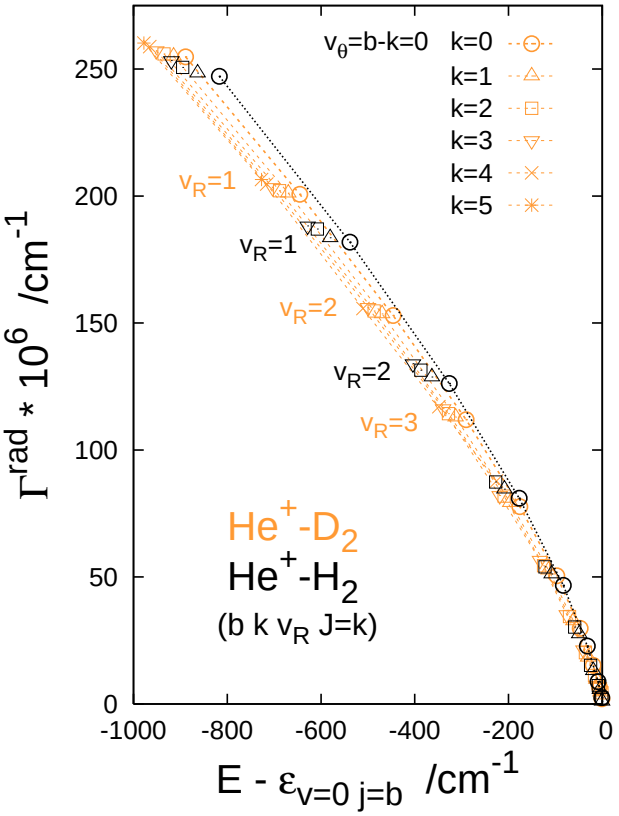

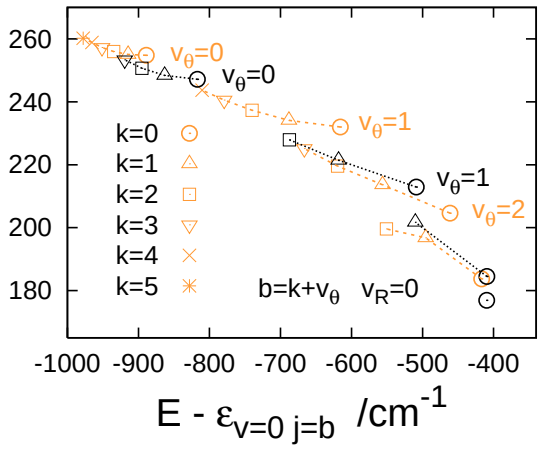

As abscissa values of the symbols in the figure shown are the binding energies of the (bound) ro-vibrational states assigned with $b{=}0,1$ or the 'quasi-binding' energies of the (quasi-bound) states with $b{>}1$.

Functions of states assigned with b and $J{=}k$, their largest radial components, are supported mainly by the potentials $W^{Jp}_{v=0\,j=b\,\lambda=k;0kk}(R)$. The shapes of these potentials for $He^+{+}D_2$ (the well depths) do not differ much from the shapes of the potentials for $He^+{+}H_2$, cf. Fig. A1. Therefore, the fact that a given state $[0\,v_\theta\,v_R]\,J{=}k$ has larger binding energy in He^+-D_2 means that function of this state is squeezed to a smaller interval of smaller R-values than the respective function for He^+-H_2. Together with the properties of the optical potential pointed out in the comment to Fiq. A1, this explains what is seen here: the widths $\Gamma^{\rm rad}(J{=}k){\approx}\Upsilon$ of the corresponding vibrational states of the two complexes lie nearly on the same smooth curve.

Radiative decay of He^+ ions from gas mixtures with D_2 or H_2 molecules

Fig. C5a. Partial yield functions $p^{\mathrm{trad,c}}(E;J,p)$

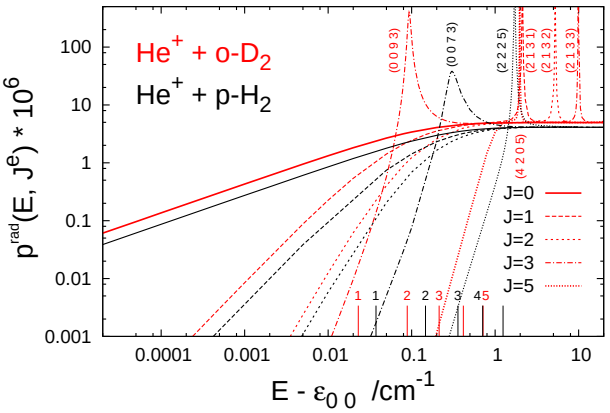

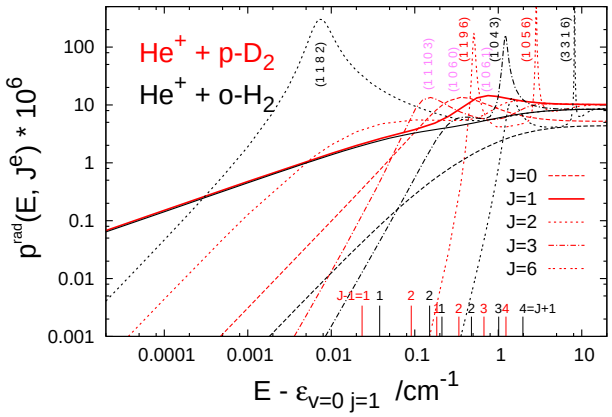

The functions are plotted here for several lowest J^e-value states of the He^++c-a_2 systems with a=D, H and c=ortho, para in the energy ranges from 10^{-5} to 20 cm^{-1} above the respective lowest threshold, j=0 (left panel) or j=1. In these ranges, only one channel, v=0 j with j=0 or j=1, is open in the He^++c-a_2 collisions; so,

$$p^{\mathrm{trad}}(E;J^p)=p^{\mathrm{trad}}_{0j}(E;J^p)\,,$$

cf. Eq. (5).

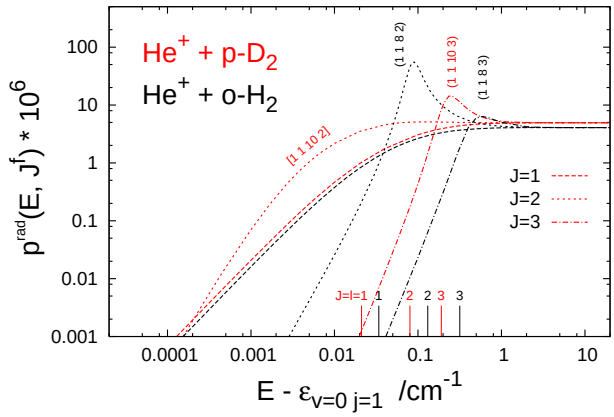

Exposed are: (see also Figs. B6-B7 in Ref. 3)

- Wigner's threshold law,

$$p^{\mathrm{trad}}_{0j}(E;J^p)\underset{E\ll E^{\mathrm{cbr}}_{l_{\min}}}{\sim}\mathcal{C}^{\mathrm{trad}}_{l_{\min}(J^p,j)}\times(E-\varepsilon_{0j})^{l_{\min}+\frac{1}{2}}\qquad\text{with}\quad l_{\min}(J^p,j)=|J-j|+\tfrac{1-p}{2}\,,\tag{45}$$

  where $E^{\mathrm{cbr}}_{l(J^p,j)}$ with $l\geq 1$ denotes the value of the adiabatic potential $e^{J^p}_{\overline{v}=0\overline{j}\overline{l}}(R)$ at the top of the centrifugal barrier in it. (The correlation: $\overline{j}\to j$ and $\overline{l}\to l$ for $R\to\infty$ is exploited hereafter). In the cases of $l_{\min}(J^e,j)$=0, the value $E^{\mathrm{cbr}}_{l_{\min}(J^e+1,j)}$ should be used in the above formula. The heights $E^{\mathrm{cbr}}_{l(J^p,j)}-\varepsilon_{0j}$ of the barriers for j=0, 1 and for several lowest Js are shown by the positions of the sticks on the lower x-axes of the panels. The barriers are obviously lower in the heavier system. The factors $\mathcal{C}^{\mathrm{trad}}_{l_{\min}}$ for He^++o-D_2 are seen to be larger than their counterparts for He^++p-H_2. Above the j=1 threshold, the relations become more complicated.

- the lowest lying resonances of the He^+-D_2 and He^+-H_2 complexes. The vertical labels are the quantum numbers of the resonances, $(b\,k\,v_R\,J)$. The label in square brackets (the lower panel) concerns a bound state. The near-threshold shape resonances and bound states have a significant impact on the values of the factors $\mathcal{C}^{\mathrm{trad}}_{l_{\min}(J^p,j)}$.

- the qualitative difference in the behavior of the functions $p^{\mathrm{trad}}_{0j}(E;J^p)$ in the E-ranges well-below and -above the respective centrifugal barrier tops. Functions for given j and different Js reach the same plateau above the barriers.

A reservation: The behavior of the functions $p^{\mathrm{trad}}_{0j}(E;J^p)$ presented here is only qualitatively correct at collision energies $E-\varepsilon_{0,j=0,1}$ below ~2 cm^{-1}. The long-range interactions which would become influential at these energies are suppressed in the PES used in the calculations[5]. On the other hand, due to this defect a more detailed analysis of the H⟶D substitution effects becomes possible. Namely, validity of expansion (47) for any $l_{\min}$ can be exploited.

. . . in the near-threshold regions

From formulas (24) and (44), the following expressions can be obtained for the factors $\mathcal{C}^{\rm trad}_{l_{\rm min}(J^p,j)}$,

$$\mathcal{C}^{\rm trad}_{l_{\rm min}(J^p,j)} = \Big(\frac{2\mu}{\hbar^2}\Big)^{l_{\rm min}+\frac{1}{2}} \frac{a^{\rm trad}_{l_{\rm min}}}{[(2l_{\rm min}+1)!!]^2} \qquad \text{with} \qquad a^{\rm trad}_{l_{\rm min}} = \frac{4\mu}{\hbar^2}\, b^{\rm trad}_{l_{\rm min}}$$

$$\text{and} \qquad b^{\rm trad}_{l_{\rm min}(J^p,j)} = \Big[1-\frac{a_{l_{\rm min}}}{R_\infty^{2l_{\rm min}+1}}\Big]^2 R_\infty^{2l_{\rm min}+2} J_{l_{\rm min}(J^p,j)}(\varepsilon_{0j};R_\infty)$$

$$= \lim_{R_\infty\to\infty} R_\infty^{2l_{\rm min}+2} J_{l_{\rm min}}(\varepsilon_{0j};R_\infty)\,, \tag{46}$$

where the factor $a_{l_{\rm min}}$ comes from the formula for near-threshold behavior of $v{=}0jl_{\rm min}$-diagonal element of the matrix $\mathbf{S}^{Jp}$

$$[\mathbf{S}^{Jp}(E)]_{0jl_{\rm min};0jl_{\rm min}} \approx 1 - 2\imath \frac{a_{l_{\rm min}}}{(2l_{\rm min}+1)!!(2l_{\rm min}-1)!!}\Big[\frac{2\mu}{\hbar^2}(E{-}\varepsilon_{0j})\Big]^{l_{\rm min}+\frac{1}{2}}, \tag{47}$$

and $J_{l_{\rm min}(J^p,j)}(\varepsilon_{0j};R_\infty)$ denotes the respective $\overline{v}{=}0\,\overline{j}\,\overline{l}_{\rm min}$-diagonal element of the matrix $\mathbf{J}(E;R_\infty)$ of the free-free integrals from the SVD-log-derivative method at $E{-}\varepsilon_{0j}{\to}0^+$. The existence of the limit written in Eq. (46) can be checked with the help of the differential equation (43), by integrating it analytically after the following simplifications: (i) only the single element $[\mathbf{J}(E;R)]_{0\overline{j}\,\overline{l}_{\rm min};0\overline{j}\,\overline{l}_{\rm min}}$ is retained, (ii) the optical potential term ($\boldsymbol{\kappa}$) is ignored as negligible at large R's, and (iii) the element $[\mathbf{L}(E;R)]_{0\overline{j}\,\overline{l}_{\rm min};0\overline{j}\,\overline{l}_{\rm min}}$ is approximated with $\frac{l_{\rm min}+1}{R}$ — the logarithmic derivative of the Riccati-Bessel function $j_{l_{\rm min}}(kR)$ in the $k{\to}0$ limit. The factor $a^{\rm trad}_{l_{\rm min}}$, having dimension of length$^{2l_{\rm min}+1}$, is the optical-potential counterpart of the factor $a_{l_{\rm min}}$ — the scattering length in the molecular potential when $l_{\rm min}{=}0$.

In table below, the factors $\mathcal{C}^{\rm trad}_{l_{\rm min}(J^p,j)}$ for $J^p{=}0{-}3$ above the $v{=}0\,j{=}0,1$ thresholds are listed together with the related factors $b^{\rm trad}_{l_{\rm min}}$, $a_{l_{\rm min}}$, and the centrifugal barrier heights $E^{\rm cbr}_{l_{\rm min}}{-}\varepsilon_{0j}$. Cases most strongly affected by near-threshold states of the $He^+{-}a_2$ complexes for a=D,H are marked with asterisk. The state which affects a given marked $\mathcal{C}^{\rm trad}_{l_{\rm min}(J^p,j)}$ has the label $(b\,k\,v_R\,J^p)$ with $b{=}j$, $k{=}\frac{J+j-l_{\rm min}+(1-p)/2}{2}$, $v_R{=}9\,(10)$ and $7\,(8)$ near the $j{=}0\,(1)$ threshold for a=D and a=H, respectively. It is a shape resonance (a virtual state) if $a_{l_{\rm min}>0}{\ll}0$ ($a_{l_{\rm min}=0}{\ll}0$) or a weakly bound state if $a_{l_{\rm min}}{\gg}0$. The sign and magnitude of entries in the '$a_{l_{\rm min}}$' columns are consistent with the fact that the sequence of states of the $He^+{-}D_2$ complex $(1\,1\,10\,J^p)$ for $J^{e,f}{=}1{-}3$ crosses the $j{=}1$ threshold just above $J^f{=}2$ while the sequence of states $(1\,1\,8\,J^p{=}1{-}3)$ of $He^+{-}H_2$ crosses this threshold between $J{=}1$ and $J{=}2$. Mainly because of this difference the ratio of the factor $C^{\rm trad}_{l_{\rm min}(J^p,1)}$ for $He^+{-}D_2$ to its counterpart for $He^+{-}H_2$, varies so widely between the different J^p cases, from 0.1 for $J^e{=}2$ to above 1500 for $J^f{=}2$.

	$He^+{+}D_2$				$He^+{+}H_2$			
$l_{\rm min}(J^p,j)$	$\mathcal{C}^{\rm trad}_{l_{\rm min}}$ ♮♯	$b^{\rm trad}_{l_{\rm min}}$ †	$a_{l_{\rm min}}$ ‡	$E^{\rm cbr}_{l_{\rm min}}{-}\varepsilon^{\sharp\flat}_{0j}$	$\mathcal{C}^{\rm trad}_{l_{\rm min}}$ ♮♯[a]	$b^{\rm trad}_{l_{\rm min}}$ †	$a_{l_{\rm min}}$ ‡	$E^{\rm cbr}_{l_{\rm min}}{-}\varepsilon^{\sharp\flat}_{0j}$
$0\,(0\ ,0)$	$1.36\,(-5)$	$51.0\,(-10)$	$+21.6$		$8.65\,(-6)$	$59.3\,(-10)$	$+21.3$	
$1\,(1^e,0)$	$2.73\,(-4)$	$27.6\,(-6)$	$+12.7\,(3)$	0.023	$1.16\,(-4)$	$32.2\,(-6)$	$+13.0\,(3)$	0.037
$2\,(2^e,0)$	$1.44\,(-3)$	$10.9\,(-2)$	$+19.3\,(6)$	0.089	$6.56\,(-4)$	$20.4\,(-2)$	$+26.4\,(6)$	0.147
$3\,(3^e,0)$	$*5.86\,(-3)$	$65.3\,(+1)$	$-81.7\,(9)$	0.214	$1.44\,(-4)$	98.7	$-31.5\,(9)$	0.359
$1\,(0\ ,1)$	$9.78\,(-5)$	$98.8\,(-7)$	-60.3	0.184	$1.31\,(-5)$	$36.2\,(-7)$	$+30.9\,(4)$	0.212
$0\,(1^e,1)$	$1.51\,(-5)$	$56.4\,(-10)$	$+33.6$		$1.43\,(-5)$	$97.9\,(-10)$	$+33.2$	
$1\,(2^e,1)$	$4.44\,(-3)$	$44.9\,(-5)$	$+10.4\,(4)$	0.023	$*4.52\,(-2)$	$12.5\,(-3)$	$-42.6\,(4)$	0.038
$2\,(3^e,1)$	$1.26\,(-3)$	$95.3\,(-3)$	$-35.2\,(6)$	0.091	$1.49\,(-4)$	$46.3\,(-3)$	$-18.4\,(6)$	0.151
$1\,(1^f,1)$	$6.88\,(-4)$	$69.5\,(-6)$	$+44.7\,(3)$	0.021	$5.29\,(-4)$	$14.6\,(-5)$	$+57.0\,(3)$	0.034
$2\,(2^f,1)$	$*3.68$	$27.9\,(+1)$	$+22.4\,(8)$	0.080	$*2.19\,(-3)$	$68.1\,(-2)$	$-95.8\,(6)$	0.131
$3\,(3^f,1)$	$8.73\,(-4)$	97.2	$-50.9\,(9)$	0.190	$6.94\,(-5)$	47.5	$-29.1\,(9)$	0.317

♮ in units of $E^{-(l_{\rm min}+\frac{1}{2})}$. ♯ E in cm^{-1}. † in bohr$^{(2l_{\rm min}+3)}{\times}$hartree. ‡ in bohr$^{(2l_{\rm min}+1)}$.

♭ $\varepsilon_{00}{=}0$, $\varepsilon_{01}{=}59.74$ and 118.37 cm^{-1} for D_2 and H_2, respectively. [a] these values are slightly more accurate than those given in Ref. 3 (Fig. B6).

Fig. C5b. . . . above the centrifugal barriers

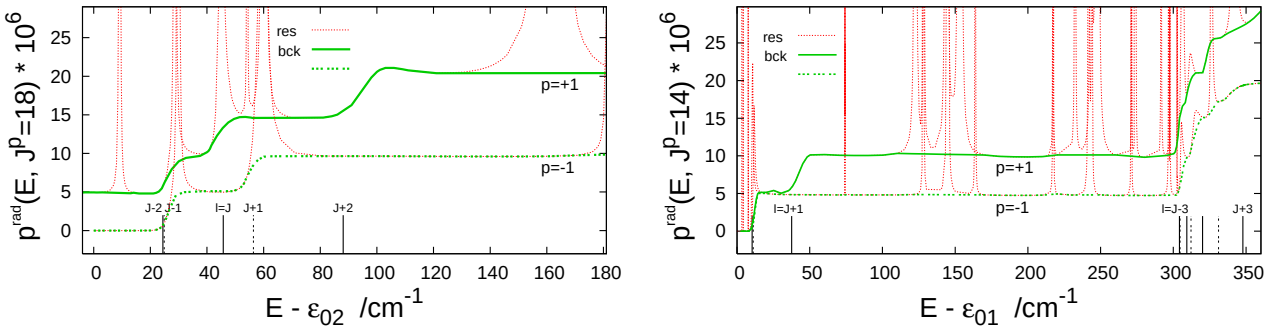

Exemplary functions $p^{\mathrm{trad,c}}(E;J^p)$ for He^++c-D_2 for c=o (left panel) and c=p in the energy ranges extending above the first excited threshold, j=2 and j=3, respectively. Demonstrated are:

- the resolutions of the functions into the resonance and background parts,
- the behavior of the background parts

$$p^{\mathrm{trad,c}}_{\mathrm{bck}}(E;J^p)=\sum_{j(c)} p^{\mathrm{trad(bck)}}_{0j}(E;J^p)\,\Theta(E-\varepsilon_{0j})\,.$$

Clearly seen are j+1 different plateaus in the functions $p^{\mathrm{trad(bck)}}_{0j}(E,J^e)$ and j plateaus in the functions $p^{\mathrm{trad(bck)}}_{0j}(E,J^f)$ for j=1−3, evidently associated with the contributing l-components, cf. Eq. (5). The background can approximately be described with the formula

$$p^{\mathrm{trad,c}}_{\mathrm{bck}}(E;J^p)\approx \overline{p}^{\mathrm{trad}}\sum_{j(c)}\sum_{\lambda=\frac{1-p}{2}}^{\mathrm{min(j,J)}}\Theta(E-E^{\mathrm{cbr}}_{l(J^p,j,\lambda)})\,, \tag{48}$$

where $l(J^p,j,\lambda)=J+j+\frac{1-p}{2}-2\lambda$ and $\overline{p}^{\mathrm{trad}}\approx 5\times10^{-6}$. (Though λ serves here only enumerating the l's allowed for given J, j, and p, it actually is the angular momentum projection quantum number of the BF-diabatic representation, see Fig. A2.)

Fig. C5c. . . . background parts

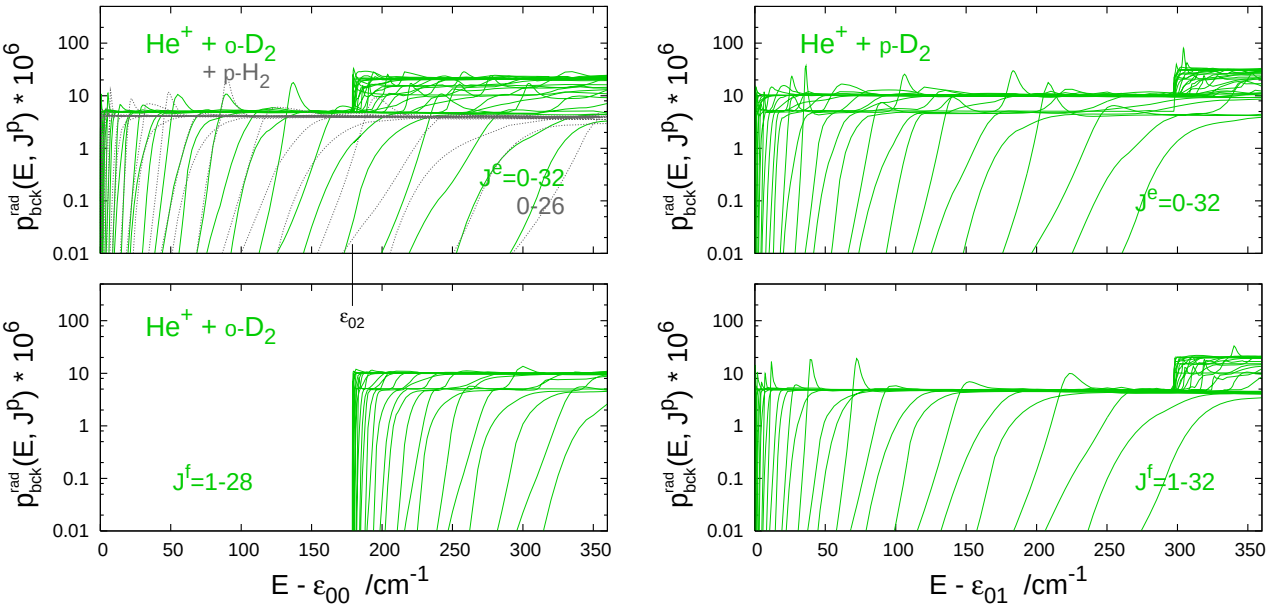

Plotted here are all functions $p^{\mathrm{trad,c}}_{\mathrm{bck}}(E;J^p)$ determined for $He^+ + c{-}D_2$ in the present calculations and functions for He^++p-H_2 from Ref. 3. Some wider resonance profiles near the centrifugal barrier tops are left in the background parts. This was considered appropriate for assuring accuracy in the thermal averaging, Eq. (4).

Fig. C5d. Total yield functions $p^{\mathrm{trad,c}}(E)$

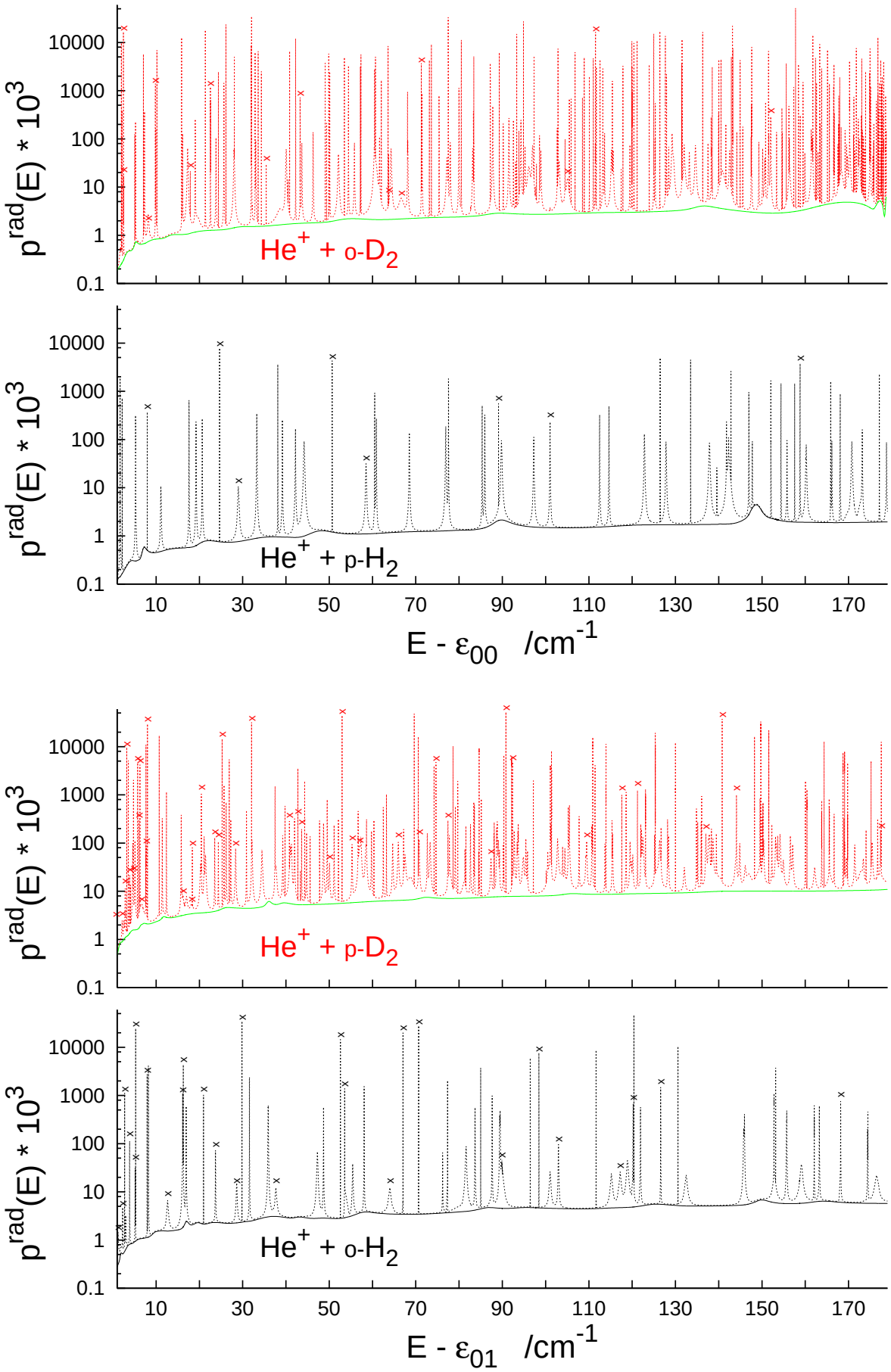

The functions are shown here only in halves of the energy ranges scanned in the calculations. The crosses mark peaks due to sharp shape resonances.

Fig. C5e. . . . background parts

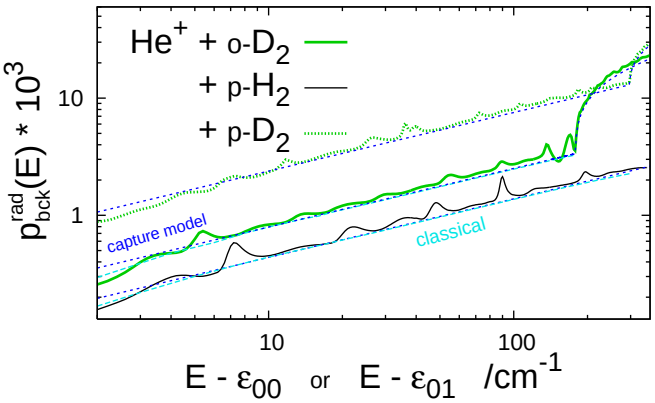

The functions $p^{\rm trad,c}_{\rm bck}(E)$ plotted with the green and black lines are obtained by summing up, according to Eq. (8), the partial functions $p^{\rm trad,c}_{\rm bck}(E,J^p)$ shown in Fig. C5c. The light-blue lines represent the classical counterparts of the functions $p^{\rm trad,o}_{\rm bck}(E)$ for He^++o-D_2 and $p^{\rm trad,p}_{\rm bck}(E)$ for He^++p-H_2 in the E-ranges below the ε_{02} threshold, at 179 and 354 $\rm cm^{-1}$, respectively, above ε_{00}=0. They are obtained as

$$p^{\rm trad}_{\rm class}(E) = \frac{2\mu E}{\hbar^2\pi}\,\sigma^{\rm trad}_{\rm class}(E)$$

from the classical cross-sections for the 'trad' reaction in the two systems,

$$\sigma^{\rm trad}_{\rm class}(E) = 2\pi \int_0^{b_{\rm max}(E)} b db\, p^{\rm trad}_{\rm class}(E,b) \qquad \text{with} \qquad p^{\rm trad}_{\rm class}(E,b) = 2\int_{R_{\rm trn}}^{\infty} \frac{A(R)\,dR}{\left\{2[E-Eb^2/R^2-V(R)]/\mu\right\}^{1/2}}$$

and the matrix elements $[\mathbf{W}^{J=0}(R)]_{000;000}$ and $\frac{1}{\hbar}[^{\rm opt}\mathbf{W}(R)]_{000;000}$ inserted for $V(R)$ and $A(R)$, respectively. b is the impact parameter and $R_{\rm trn}$ is the turning point in the effective potential $V_{\rm eff}(R;E,b)$=$V(R)$+Eb^2/R^2 at the energy E. $b_{\rm max}(E)$ is the value of b for which the second turning point appears at a given E at the top of barrier in $V_{\rm eff}$. The probabilities $p^{\rm trad}_{\rm class}(E,b)$ for b>$b_{\rm max}$, depending on the values of $A(R)$ at R's outside the third turning point, are assumed totally negligible. For b<$b_{\rm max}(E)$ in turn,

$$p^{\rm trad}_{\rm class}(E,b) \approx \overline{p}^{\rm trad} \qquad \text{and} \qquad p^{\rm trad}_{\rm class}(E) \approx \overline{p}^{\rm trad}\,\frac{2\mu E}{\hbar^2\pi}\,\sigma^{\rm cpt}(E)\,, \tag{49}$$

where $\sigma^{\rm cpt}$ is the capture cross-section[22],

$$\sigma^{\rm cpt}(E) := \pi\, b^2_{\rm max}(E) \approx \frac{\zeta}{\sqrt{E}}\,. \tag{50}$$

As an extension of this capture model to energies E>ε_{0j} for j>0, one gets the function,

$$p^{\rm trad,c}_{\rm cpt}(E) = \xi \sum_{j(c)} (2j+1)\,\sqrt{E-\varepsilon_{0j}}\,\Theta(E-\varepsilon_{0j}) \qquad \text{with} \qquad \xi=\overline{p}^{\rm trad}\,\frac{2\mu}{\hbar^2\pi}\zeta\,. \tag{51}$$

This function is plotted with the blue dotted line for each He^++c-a_2 system shown in the figure. The values of the parameters involved are collected in table below.

	He^++D_2	He^++H_2	$\frac{He^+ + D_2}{He^+ + H_2}$
ζ ♭	10.46	10.47	≈1
$\overline{p}^{\rm trad}$	4.82 (−6)	3.95 (−6)	$\approx\left(\frac{\mu_{He^+ + D_2}}{\mu_{He^+ + H_2}}\right)^{\frac{1}{2}}$
ξ ♮	1.18 (−1)	6.47 (−2)	$\approx\left(\frac{\mu_{He^+ + D_2}}{\mu_{He^+ + H_2}}\right)^{\frac{3}{2}}$

♭in bohr$^2\times$ hartree$^{1/2}$, ♮ in hartree$^{-1/2}$

More details on application of the capture model

In order to justify the approximation $p^{\rm trad,c}_{\rm bck}(E)\approx p^{\rm trad,c}_{\rm cpt}(E)$ one starts with inserting Eq. (48) into Eq. (5) and, assuming large number of Js contributing, one replaces

$$\sum_J (2J+1) \sum_{\lambda=\frac{1-p}{2}}^{\min(j,J)} \Theta(E-E^{\rm cbr}_{l(J^p,j,\lambda)}) \qquad \text{with} \qquad \sum_{\lambda=\frac{1-p}{2}}^{j} \int_0^{l_{\max}(E,j,\lambda,p)} dl\,(2l+1)\,.$$

Next, in analogy to Eq. (49), one introduces the capture cross-sections $\sigma^{\rm cpt}_{j\lambda p}$,

$$\int_0^{l_{\max}(E,j,\lambda,p)} dl\,(2l+1) = \frac{2\mu}{\pi\hbar^2}\,(E-\varepsilon_{0j})\,\sigma^{\rm cpt}_{j\lambda p}(E-\varepsilon_{0j})\,,$$

getting the following expression

$$p^{\rm trad,c}_{\rm bck}(E) \approx \overline{p}^{\rm trad}\,\frac{2\mu}{\pi\hbar^2} \sum_{j(c)} \Theta(E-\varepsilon_{0j})\,(E-\varepsilon_{0j}) \left[\sum_{p=\pm1} \sum_{\lambda=\frac{1-p}{2}}^{j} \sigma^{\rm cpt}_{j\lambda p}(E-\varepsilon_{0j})\right]. \qquad (52)$$

The cross-sections $\sigma^{\rm cpt}_{j\lambda p}(E-\varepsilon_{0j})$ are obtained as functions of the kinetic energy in the $v{=}0\,j$ channel by interpolating between values at $E{=}E^{\rm cbr}_{l(J^p,j,\lambda)}$ for l's corresponding to fixed numbers j, λ, and p, and changing J, which are defined by the equality

$$\frac{\hbar^2}{2\mu}\,\frac{l(J^p,j,\lambda)[l(J^p,j,\lambda)+1]}{[R^{\rm cbr}_{l(J^p,j,\lambda)}]^2} = \frac{1}{\pi}\,\frac{(E^{\rm cbr}_{l(J^p,j,\lambda)}-\varepsilon_{0j})\times\sigma^{\rm cpt}_{j\lambda p}(E^{\rm cbr}_{l(J^p,j,\lambda)}-\varepsilon_{0j})}{[R^{\rm cbr}_{l(J^p,j,\lambda)}]^2}\,.$$

As previously, $R^{\rm cbr}_{l(J^p,j,\lambda)}$ and $E^{\rm cbr}_{l(J^p,j,\lambda)}$ denote coordinates of the top point of the centrifugal barrier in the adiabatic potential $e^{J^p}_{\overline{v}=0\overline{j}\overline{l}}(R)$ with $\overline{l}{=}J{+}\overline{j}{+}\frac{1-p}{2}{-}2\lambda$. In the case of $j{=}0$ channel, however, the barrier top points in the diabatic potentials $[\mathbf{W}^J(R)]_{000;000}$ are used. The cross-section $\sigma^{\rm cpt}_{001}(E-\varepsilon_{00})$ obtained in this way appears practically indistinguishable from $\sigma^{\rm cpt}(E)$ determined from the classical effective potentials. An inspection of the cross-sections $\sigma^{\rm cpt}_{j\lambda p}(E-\varepsilon_{0j})$ for $j{=}0,1,2$ channels plotted in the figure below provides a rationale for the final step of the derivation, i.e. for converting rhs of Eq. (52) to the form (51).

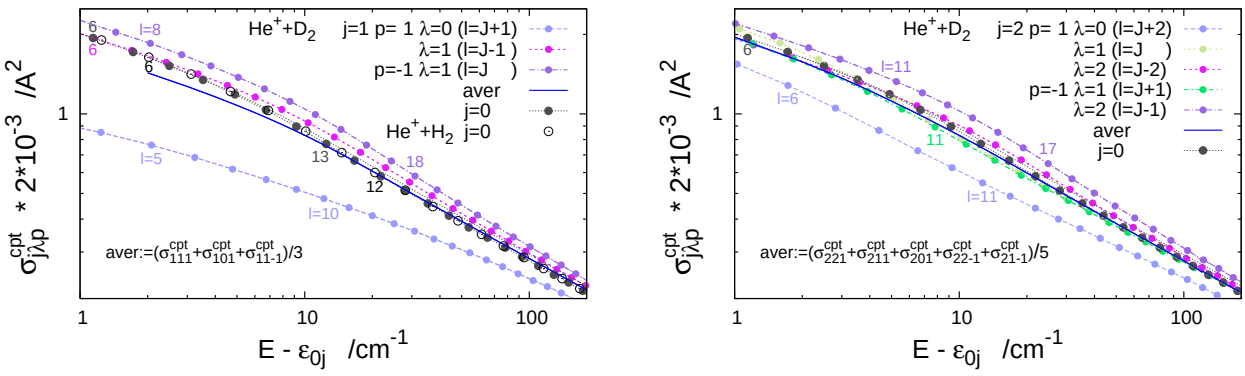

The relevant observations are:

$$\sum_{p=\pm1} \sum_{\lambda=\frac{1-p}{2}}^{j} \sigma^{\rm cpt}_{j\lambda p}(E-\varepsilon_{0j}) \;\approx\; (2j+1)\,\sigma^{\rm cpt}_{001}(E-\varepsilon_{0j})\,,$$

$$\sigma^{\rm cpt}_{001}(E-\varepsilon_{0j}) \;\approx\; \zeta\times(E-\varepsilon_{0j})^{-1/2}\,.$$

Actually, the latter relation is well satisfied at energies $(E-\varepsilon_{0j})>\sim 7\,{\rm cm}^{-1}$. Deviations from linearity of the lines in the plots are visible at smaller energies. They reflect the inaccuracy of the asymptotic part of the PES used in the calculations (see the comment below Fig. C5a). The cross-sections $\sigma^{\rm cpt}_{001}$ for $He^+{+}H_2$ (the open circles in the left panel) come from Fig. B7a of Ref. 3. The factor in the label of that figure is incorrect. It should be as here: $2*10^{-3}$.

Radiative decay of He^+ ions from gas mixtures with pure ortho- or para- D_2 or H_2

Fig. C6a. Partial rate constant functions ${}_{\rm c}k_{0j}(T, J^p)$ in low temperature range, T<1 K

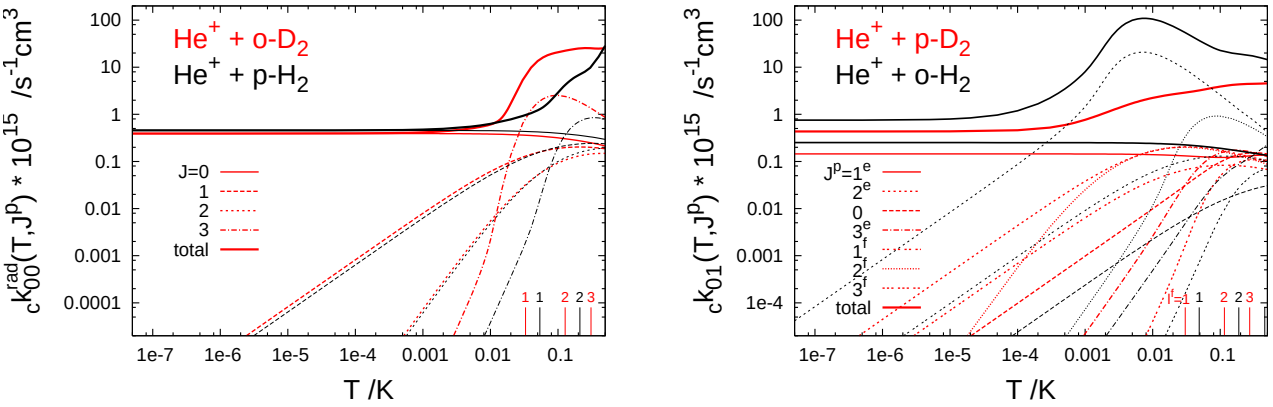

The functions plotted, ${}_{\rm c}k_{0j}(T, J^p)$ for j=0, 1 and c=p,o, have been obtained from the probability (yield) functions $p^{\rm trad}_{0j}(E; J^p)$ shown in Fig. C5a as

$$ {}_{\rm c}k_{0j}(T, J^p) = \frac{1}{2\pi\hbar}\int dE\, {}_{\rm c}P(E,T)\, p^{\rm trad}_{0j}(E; J^p)\, \Theta(E{-}\varepsilon_{0j}) $$

with the population factor ${}_{\rm c}P(E,T)$ defined below Eq. (10). Exposed is the threshold behavior,

$$ {}_{\rm c}k_{0j}(T, J^p) \underset{T\ll(E^{\rm cbr}_{l_{\rm min}}-\varepsilon_{0j})/k_B}{\sim} \frac{1}{2j{+}1}\, \mathcal{K}^{\rm trad}_{l_{\rm min}(J^p,j)}\, (k_BT)^{l_{\rm min}}\,, \qquad (53) $$

where $$ \mathcal{K}^{\rm trad}_{l_{\rm min}(J^p,j)} = \frac{4\pi}{\hbar}\left(\frac{\mu}{\hbar^2}\right)^{l_{\rm min}} \frac{b^{\rm trad}_{l_{\rm min}}}{(2l_{\rm min}{+}1)!!}\,. $$

The values of $(E^{\rm cbr}_{l_{\rm min}(J^p,j)}{-}\varepsilon_{0j})/k_B$ are shown by the sticks on the T axes for all Js shown in the left panel (j=0) and for J^f's shown in the right panel.

. . . and 'total' rate constants ${}_{\rm c}k_{0j}(T)$

$$ {}_{\rm c}k_{0j}(T) = \sum_p \sum_J (2J{+}1)\, {}_{\rm c}k_{0j}(T, J^p) $$

At k_BT well-below the respective first excited threshold, these rates become truly total, i.e.,

$$ {}_{\rm c}k_{00}(T) \underset{T\ll\frac{\varepsilon_{02}}{k_B}}{\approx} {}_{\rm c}k(T){=}\sum_{j{\rm even}} {}_{\rm c}k_{0j}(T) \qquad \text{and} \qquad {}_{\rm c}k_{01}(T) \underset{T\ll\frac{\varepsilon_{03}-\varepsilon_{01}}{k_B}}{\approx} {}_{\rm c}k(T){=}\sum_{j{\rm odd}} {}_{\rm c}k_{0j}(T) $$

for c=o (p) and c=p (o) of He^++c-a_2 with a=D (H), respectively. At T=0, only one partial rate ${}_{\rm c}k_{0j}(T, J^p)$, with J^e=j, contributes to ${}_{\rm c}k_{0j}(T)$,

$$ {}_{\rm c}k_{0j}(T{=}0) = \mathcal{K}^{\rm trad}_{0(j,j)} = \frac{4\pi}{\hbar} b^{\rm trad}_{0(j,j)}\,. \qquad (54) $$

The values of ${}_{\rm c}k_{00}(0)$ and ${}_{\rm c}k_{01}(0)$ for the mixtures with c-D_2 and c-H_2 are compared in table below.

He^++c-D_2		He^++c-H_2	
${}_{\rm o}k_{00}(0){=}{}_{\rm o}k(0)^\flat$	${}_{\rm p}k_{01}(0){=}{}_{\rm p}k(0)$	${}_{\rm p}k_{00}(0){=}{}_{\rm p}k(0)$	${}_{\rm o}k_{01}(0){=}{}_{\rm o}k(0)$
3.923	4.343	4.565	7.534

$^\flat$ all entries in 10^{-16} $\rm cm^3s^{-1}$.

Fig. C6b. Rate constants ${}_c k(T)$ at $T \leq 100$ K

Feshbach resonance contributions...

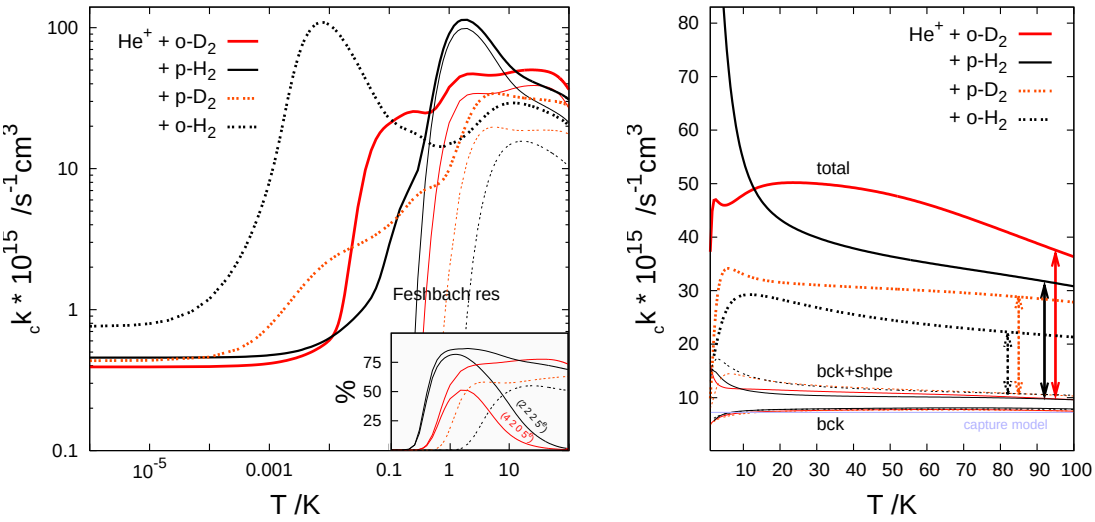

In the left panel, the Feshbach resonance contributions are shown with the tiny lines. The red lines, solid and broken, represent contributions of 463 (b=4 and b=2 p=1) and 770 (b=3, 5) resonances to the rates ${}_o k(T)$ and ${}_p k(T)$, respectively, for the mixtures with o-D_2 and p-D_2, the black solid and broken lines — contributions of 165 (b=2) and 144 (b=3) resonances to the rates ${}_p k(T)$ and ${}_o k(T)$, respectively, for He^++c-H_2 mixtures with c=p,o. In the inset, these contributions are shown in per cent. Additionally shown are the largest individual Feshbach resonance contributions to the function ${}_o k(T)$ for He^++o-D_2 and ${}_p k(T)$ for He^+−p-H_2, brought by the $(b\,k\,v_R\,J^p)$=$(4\,2\,0\,5^e)$ and the $(2\,2\,2\,5^e)$ resonance, respectively. An explanation why the latter is so much larger than the former is given in Table IV and Fig. C3.
In the right panel, the Feshbach resonance contributions to the rate constants functions for the four He^++c-a_2 mixtures, with a=D,H and c=o,p, are shown as differences between the 'total' and 'bck+shpe' curves indicated by the vertical double arrows.

shape resonance contributions

These contributions dominate in the low temperature range, ∼1 mK — ∼0.2 K. A couple of resonances of this kind, shown in Fig. C5a, lie closer to the respective lowest threshold than any Feshbach resonance. In particular, the large peak in the function ${}_o k(T)$ for the He^++o-H_2 mixture at ∼0.008 K is entirely due to the $(1\,1\,8\,2^e)$ resonance. The rapid growth of the function ${}_o k(T)$ for the He^++o-D_2 mixture, starting at ∼0.01 K, and the broad maximum at ∼0.2 K are due to the $(0\,0\,9\,3^e)$ resonance. However, the increase of the function ${}_p k(T)$ for He^++p-D_2 starting at ∼1 mK and the broad feature at ∼10 mK are not resonance effects; they should be attributed to the weakly bound state $(1\,1\,10\,2^f)$, see the analysis below Fig. C5a. At higher temperatures, certainly above 10 K, the contributions of shape resonances (of 80, 65, 14, and 47 such resonances formed with o-D_2, p-D_2, p-H_2, and o-H_2, respectively) become overwhelmed by the Feshbach resonance contributions. Above 20 K, they become also smaller than the background contributions.

continuum state (background) contributions

At very low temperatures, T<10^{-5} K, the functions ${}_c k_{\rm bck}(T)$ are constant and equal to the respective values of ${}_c k(0)$ listed in the table on the previous page. At Ts above 10 K these functions become constant again but here their values are nearly the same, no matter whether they concern the mixture with o-D_2, p-D_2, p-H_2, or o-H_2. This feature is a consequence of validity of the capture model. Indeed, upon averaging of the yield functions of Eq. (51) with the population factors ${}_c P(E,T)$ one gets

$$ {}_c k_{\rm bck}(T) \approx k_{\rm cpt}^{\rm trad} = \frac{\pi\hbar^2}{\sqrt{2}}\,\frac{\xi}{\mu^{3/2}}\,. \qquad (55) $$

The values of $k_{\rm cpt}^{\rm trad}$ that result from this formula for the quenching reaction in the mixtures with D_2 and with H_2 differ as little as 7.23 and 7.29×10^{-15} $\rm cm^3 s^{-1}$.

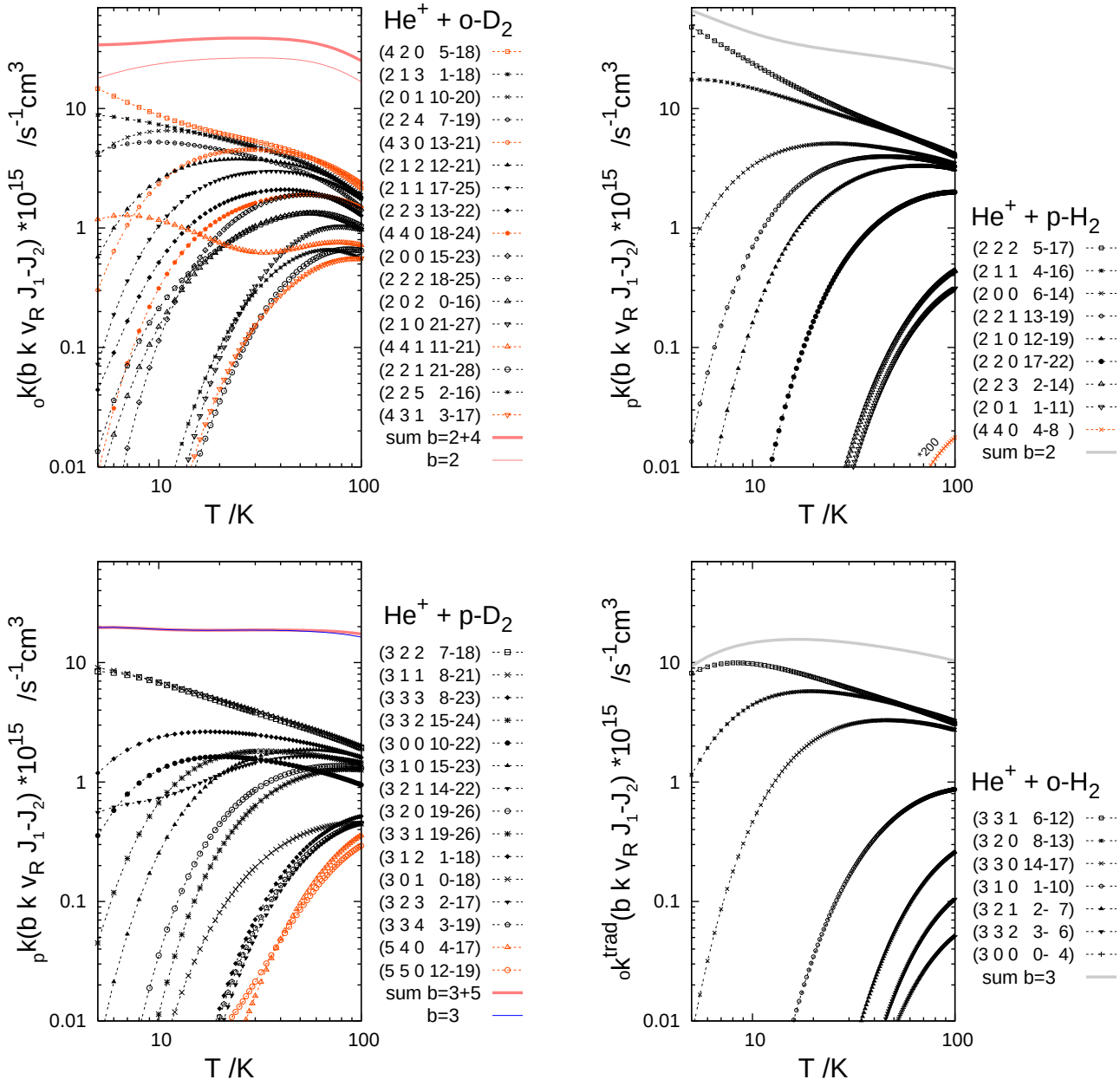

Here, the Feshbach resonance contributions to the functions ${}_ck(T)$ are shown separately from the 'bck+shpe' contributions. Apart from the total values of ${}_ck_{\mathrm{res(Fesh)}}(T)$ (thick solid lines) shown are also parts brought by resonances belonging to different groups $(b\,k\,v_R)$. The following facts should be noted:

(i) About one third of the entire 'res(Fesh)' contribution in the He^++o-D_2 system comes from b=4 resonances, especially from their (4 2 0) and (4 3 0) groups. In the He^++p-D_2 system, resonances from two b=5 groups, (5 4 0) and (5 5 0), might be expected important considering their positions relative to the v=0 j=1 threshold, cf. Fig. C2, and their relatively large widths Γ^{trad}, cf. Tables VI-VII. However, the widths Γ of these resonances are so small that the factors $\Gamma/(\Gamma^{\mathrm{trad}}+\Gamma)$ standing in Eq. (17) make their actual contributions almost negligible.

(ii) The b=4 and b=5 resonances in the He^++H_2 system can totally be ignored as contributors to the 'trad' reaction rates at temperatures below 100 K. Indeed, no b=5 resonance and only five b=4 resonances of this system lie in the relevant energy ranges, i.e. closer than ∼350 cm^{-1} to the respective, v=0 j=1 or j=0, threshold. The lowest b=4 resonance occurs at ∼220 cm^{-1}. Moreover, all the five resonances can dissociate only through j=4→0 transitions. Their widths Γ are more than two orders of magnitude smaller than widths of the resonances (b=2) decaying via Δj=2 transitions. Consequently, the factors $\Gamma/(\Gamma^{\mathrm{trad}}+\Gamma)$ to insert into Eq. (17) are merely $\sim 10^{-3} - 10^{-5}$.

Radiative decay of He^+ ions from mixtures with equilibrium and normal D_2 or H_2

Rate constants in temperature range 10^{-6}–100 K

Fig. C7a. Contributions of collisions with ortho- and para-D_2 (-H_2)

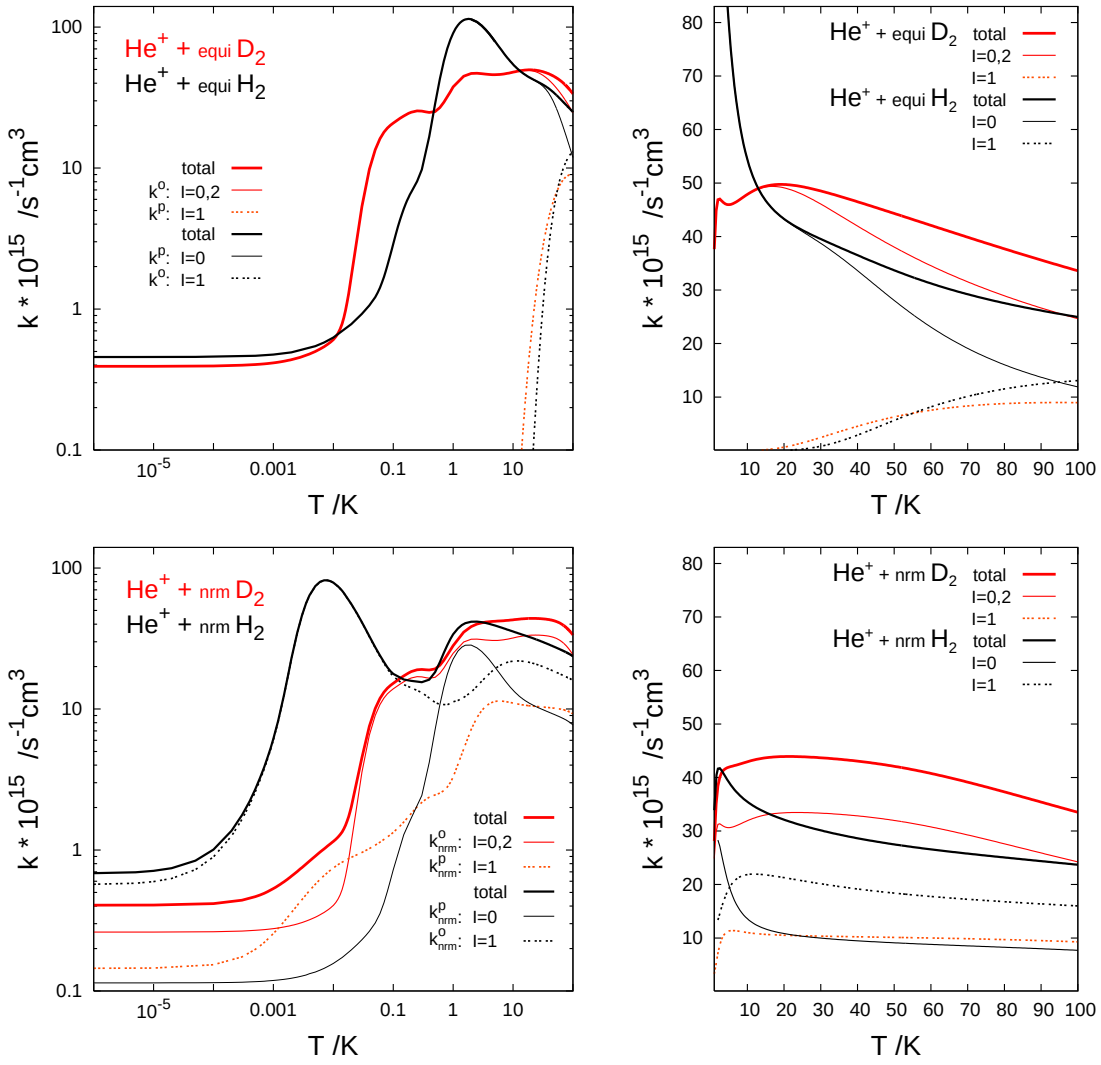

The relations between the functions $k(T)$, $k^{\rm c}(T)$, $k_{\rm nrm}(T)$, $k^{\rm c}_{\rm nrm}(T)$, and ${}_{\rm c}k(T)$ for c=o,p are:

$$k(T) \approx k^{\rm o}(T) \approx {}_{\rm o}k(T) \quad \text{at} \quad T{<}10\,{\rm K} \quad \text{for } {\rm He}^+ + {\rm D}_2\,,$$
$$k(T) \approx k^{\rm p}(T) \approx {}_{\rm p}k(T) \quad \text{at} \quad T{<}20\,{\rm K} \quad \text{for } {\rm He}^+ + {\rm H}_2\,,$$
$$\text{and} \qquad k^{\rm c}_{\rm nrm}(T) = \tfrac{g^{\rm c}}{g^{\rm p}+g^{\rm o}}\,{}_{\rm c}k(T) \quad \text{at any } T\,.$$

The values at T=0 in unit of 10^{-16} cm^{3}s^{-1}:

	$k(0)$	$k^{\rm o}_{\rm nrm}(0)$	$k^{\rm p}_{\rm nrm}(0)$
$He^+ + D_2$	3.923	2.615	1.448
$He^+ + H_2$	4.565	5.650	1.141

The ratios $k^{I=1}_{\rm bck}/k_{\rm bck}$ are nearly identical with the populations of I=1 components in the respective free D_2 or H_2 gas (green lines). The evidently lower 'tot' values of the ratios come mostly from differences in the numbers (divided by $2j$+1) of the Feshbach resonances which are formed above the v=0j=1 and the j=0 thresholds (in the ranges up to ~360 cm^{-1}).

. . . the impact of resonances

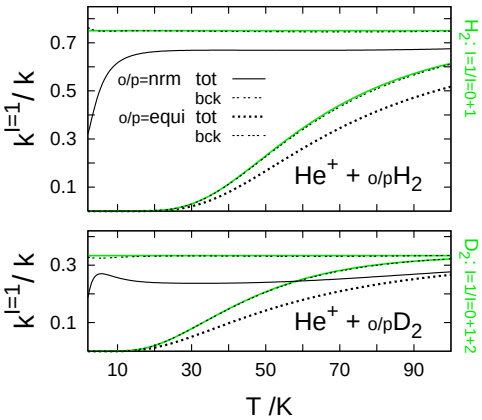

Fig. C7b. Resonance and background contributions

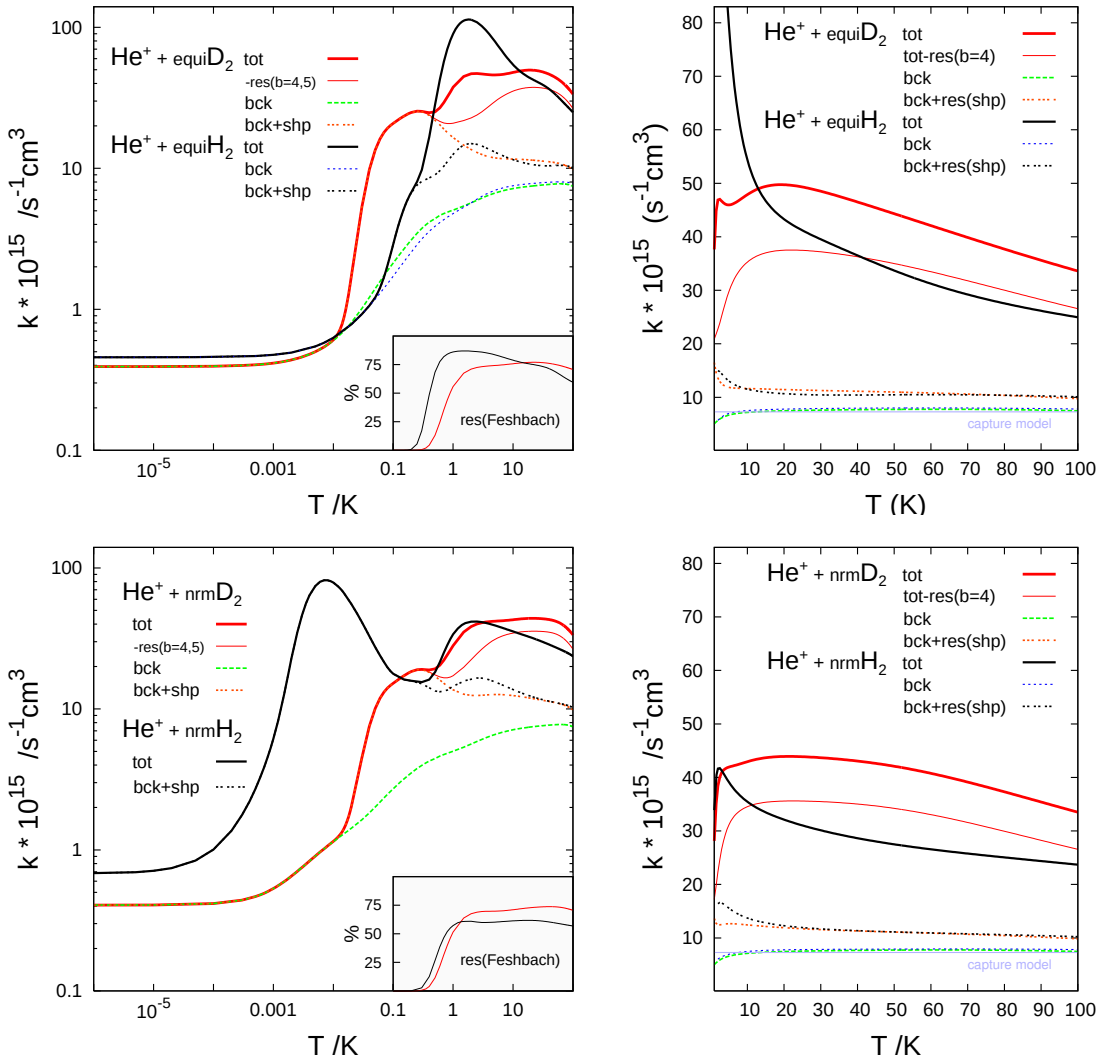

Fig. C7c. D/H isotope effect

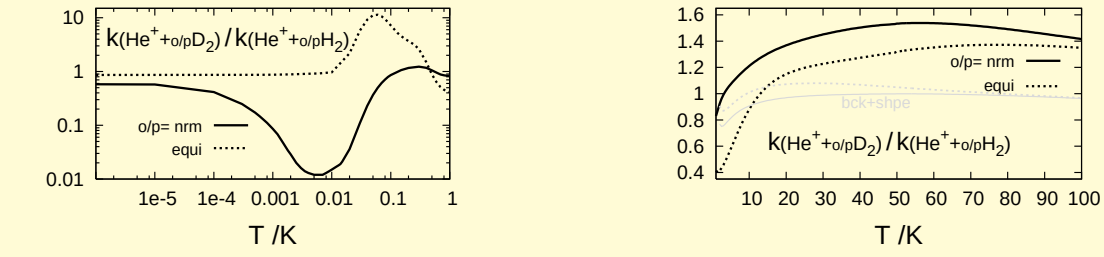

Referring to the scheme on page 1, one may conclude that of the two routes along which the 'trad' reaction can proceed at its initial stage, i.e. at the stage of the He^+ and H_2 (D_2) reactants approaching each other on the PES of the first excited electronic state of the $[HeHH]^+$ system, the route via complex formation is definitely more important than the direct (non-resonant) collision route. Of the two mechanisms of formation of the complexes which are possible (at subthermal energies) within the adopted collision model, the inverse rotational predissociation is definitely more important than the tunneling through centrifugal barriers. These conclusions are based on inspection of the second (and final) 'trad' reaction stage at which the He^+ and H_2 (D_2) reactants are close together and the radiative transitions take place out of their resonance and continuum states down to the ground electronic state of the $[HeHH]^+$ system. More concretely, the findings are:

- The radiative transitions which originate from the rotational Feshbach resonances have the decisive impact on the reaction rate. They contribute as much as 85 % to the rate constants of the reaction in the mixture with equilibrium H_2 at temperatures near 1K and as much as $70-75$ % in the mixtures with pure para-H_2 or pure ortho-D_2 at temperatures from about 10 K up to 100 K. No much smaller are the Feshbach resonance contributions to the reaction rates in the mixtures with equilibrium or normal D_2. More visibly smaller they are only in the mixtures with normal H_2, though still at the level of 60%, cf. the insets in the left panels of Fig. C6b and C7b.

- The shape resonances, as initial states of the radiative transitions, take the rate determining role in the cold range, between ∼0.5 mK and ∼0.5 K, simply because there is no Feshbach resonance to compete with them. In the subthermal range, their contribution drops below 10%.

- The effect of the $H_2 \rightarrow D_2$ substitution on the 'trad' reaction rate is qualitatively different in the cold and subthermal ranges, as shown in the two panels of Fig. C7c.

  In the first range, especially in its ultracold subrange, $T<\sim 0.1$ mK, the rate of the reaction becomes smaller after the substitution. In the $T=0$ limit, the coefficients $k(He^+ + o/pD_2)$ compare with the coefficients $k(He^+ + o/pH_2)$ like 0.39:0.46 and 0.41:0.71 (in unit of 10^{-15} cm^3s^{-1}) for o/p=equi and o/p=nrm, respectively. The latter relation is already affected by the lowest lying resonance of He^++o-H_2, labeled as $(1\,1\,8\,2^e)$. At somewhat higher Ts, around 7 mK, this resonance makes the relation look like 1:82, cf. Table IX. Just above this temperature, the near threshold shape resonances of He^++o-D_2 become operative, cf. Fig. C5a. They locally reverse the isotope substitution effect on the rate coefficient for the mixture with equilibrium H_2. Namely, around $T=0.05$ K, they enhance the coefficient $k(He^+ + \text{equi}\, D_2)$ so that it becomes above 10 times bigger than its counterpart for equi-H_2. Around $2-3$ K, the two lowest lying Feshbach resonances, $(2\,2\,2\,5^e)$ of $He^+ - H_2$ and $(4\,3\,0\,5^e)$ of $He^+ - D_2$, come into play. Because of unfavorable relation between the radiative and dissociative widths, the impact of the latter resonance on the rate coefficient $k(He^+ + \text{equi}\, D_2)$ is much weaker than the impact of the former resonance on the rate coefficient $k(He^+ + \text{equi}\, H_2)$. Therefore the ratio of these coefficients drops again below unity, down to 0.4.

  In the temperature range $\sim 10 < T \leq 100$ K, the $H_2 \rightarrow D_2$ substitution only enhances the 'trad' reaction rates, by factors of $\sim 1.2-1.5$ in the mixtures with o/p=normal and by somewhat smaller factors (maximally 1.37) – in the fully equilibrium mixtures. This effect is entirely due to the (nearly 4 times) bigger number of the rotational Feshbach resonances involved into the reaction in the heavier system. Indeed, as demonstrated by the gray curves in the right panel of Fig. C7c, a weak reverse effect would occur, i.e. the factors $k(He^+ + o/p\, D_2)/k(He^+ + o/p\, H_2)$ would be slightly smaller than unity if only the shape resonances were taken into account. Of the Feshbach resonances, the $b=4$ resonances of the $He^+ - D_2$ complex have an especially big part in the isotope effect in the subthermal range; compare the 'tot' and 'tot-res(b=4)' curves in Fig. C7b. This is because counterparts of these resonances in the $He^+ - H_2$ complex contribute practically nothing to the rate constants at Ts below 100 K.

TABLE I: $He^+-ortho\text{-}D_2$. Positions (E) and widths, dissociative (Γ) and radiative (Γ^{rad}), of 'vibrational' levels ($b\,k\,v_R$ J=k p) below the v=0 j=0, 2, 4 thresholds. The positions of the levels are relative to the v=0 j=0 threshold. The positions of the j>0 thresholds[a] are shown in lines marked with ε. All data are in cm^{-1}, the values of Γ^{rad} are multiplied by 10^6.

			p=1			p=−1		
b	k	v_R	E	Γ	Γ^{rad}	$E-E(p=1)$	Γ	$\Gamma^{rad}-\Gamma^{rad}(p=1)$
0	0	0	−889.03	0	254.8			
		1	−645.11	0	200.7			
		2	−446.07	0	153.0			
		3	−290.58	0	111.9			
		4	−175.81	0	77.7			
		5	−96.88	0	50.5			
		6	−47.16	0	29.8			
		7	−19.39	0	15.2			
		8	−6.09	0	6.7			
		9	−0.79	0	2.1			
2	2	0	−755.91	0	256.0	0.00	0	0.0
		1	−509.52	0	202.1	0.00	0	0.0
		2	−307.73	0	154.8	0.00	0	0.0
		3	−149.02	0	114.3	0.00	0	0.0
		4	−30.32	0	81.8	0.00	0	0.0
		5	53.50	7.3 (−5)	54.4	0.00	0	0.0
		6	108.91	4.8 (−5)	34.4	0.00	0	0.0
		7	142.93	2.1 (−5)	20.2	0.00	0	0.0
		8	162.38	1.8 (−5)	11.3	0.00	0	0.0
		9	173.05	1.1 (−5)	6.1	0.00	0	0.0
		10	178.13	1.1 (−5)	4.4	0.00	0	0.2
2	1	0	−509.25	0	234.1	0.14	0	0.0
		1	−294.02	0	178.8	0.16	0	0.1
		2	−123.94	0	130.4	0.14	0	0.0
		3	2.12	2.6 (−3)	89.1	0.14	0	0.1
		4	87.79	1.8 (−3)	57.1	0.13	0	−0.1
		5	139.96	1.1 (−3)	31.2	0.12	0	0.0
		6	166.70	4.7 (−4)	13.8	0.10	0	−0.1
		7	176.84	1.7 (−4)	6.0	0.12	0	−1.9
2	0	0	−282.42	0	204.6			
		1	−107.43	0	148.6			
		2	22.57	2.4 (−5)	99.4			
		3	108.52	2.0 (−4)	59.2			
		4	156.21	2.2 (−4)	33.8			
		5	176.79	5.8 (−5)	23.9			
ε			178.96					

TABLE I: continued

4	4	0	−372.08	0	258.9	0.00	0	0.0
		1	−122.43	0	204.7	0.00	0	0.1
		2	82.68	3.1 (−9)	155.7	0.00	0	1.9
		3	244.86	4.7 (−4)	117.0	0.00	4.7 (−4)	−0.1
		4	367.71	8.7 (−3)	87.8	0.00	8.6 (−3)	0.1
4	3	0	−186.00	0	240.6	0.00	0	0.0
		1	40.49	6.6 (−8)	185.8	0.00	0	0.0
		2	221.87	7.6 (−3)	135.5	0.00	7.8 (−3)	2.4
		3	359.81	8.7 (−3)	97.8	0.00	8.5 (−3)	0.0
4	2	0	−26.16	0	219.6	0.01	0	0.0
		1	177.44	6.0 (−5)	132.6	−0.10	0	0.7
		2	335.01	4.2 (−2)	117.5	0.01	3.8 (−2)	0.1
4	1	0	97.89	4.1 (−7)	196.8	1.15		1.3
		1	280.92	2.8 (−1)	143.8	0.90	1.2 (−1)	0.0
4	0	0	172.27	9.7 (−6)	147.9			
		1	343.13	2.1 (+0)	123.0			
ε			593.35					

[a]Shown are the threshold positions which result from the asymptotic part of the used PES for the $[HeHH]^+$ system[5]. In comparison with exact data for D_2[7], the positions $\varepsilon_{v=0\,2}$ and $\varepsilon_{v=0\,3}$ are too low by 0.11 and 0.36 cm^{-1}, respectively.

TABLE II: He^+-para-D_2. Positions (E) and widths, dissociative (Γ) and radiative (Γ^{rad}), of 'vibrational' levels (b=$j\,k\,v_R$ J=k p) below the v=0 j=1, 3, 5 thresholds[a]. The level positions are relative to the v=0 j=0 threshold. The positions of the j>0 thresholds[b] are shown in lines marked with ε. All data are in cm^{-1}, the values of Γ^{rad} are multiplied by 10^6.

			p=1			p=−1		
b	k	v_R	E	Γ	Γ^{rad}	$E-E(p=1)$	Γ	$\Gamma^{rad}-\Gamma^{rad}(p=1)$
1	1	0	−854.85	0	255.1	0.08	0	0.0
		1	−610.06	0	201.1	0.08	0	0.0
		2	−409.96	0	153.6	0.07	0	0.0
		3	−253.10	0	113.0	0.05	0	0.0
		4	−136.46	0	79.3	0.04	0	0.0
		5	−54.97	0	52.7	0.03	0	0.0
		6	−1.96	0	32.7	0.03	0	0.0
		7	29.69	0	18.4	0.02	0	0.0
		8	47.03	0	9.7	0.01	0	0.0
		9	55.95	0	4.7	0.01	0	0.0
		10	59.53	0	1.1	0.01	0	0.0
1	0	0	−555.89	0	232.0			
		1	−347.36	0	175.8			
		2	−184.58	0	125.6			
		3	−67.20	0	82.4			
		4	7.98	0	47.3			
		5	47.85	0	20.9			
ε			59.74					
3	3	0	−594.32	0	257.3	0.00	0	0.0
		1	−346.23	0	203.4	0.00	0	0.0
		2	−142.71	0	156.1	0.00	0	0.0
		3	17.67	0	116.3	0.00	0	0.0
		4	138.35	4.4 (−5)	82.1	0.00	4.4 (−5)	0.2
		5	224.10	4.2 (−5)	56.6	0.00	4.2 (−5)	0.1
		6	281.35	3.4 (−5)	35.2	0.00	3.4 (−5)	0.5
		7	317.03	2.4 (−5)	21.4	0.00	2.4 (−5)	0.0
		8	337.89	1.4 (−5)	12.2	0.00	1.4 (−5)	0.0
		9	349.68	1.6 (−5)	6.7	0.00	1.6 (−5)	0.0
		10	355.65	3.8 (−4)	2.9	0.00	1.4 (−5)	−0.1
3	2	0	−383.03	0	237.3	0.00	0	0.0
		1	−161.53	0	182.2	0.00	0	0.2
		2	14.86	0	134.5	0.00	0	0.1
		3	147.81	1.2 (−2)	94.7	0.06	7.2 (−3)	0.6
		4	240.22	2.1 (−3)	61.6	0.00	2.1 (−3)	0.0
		5	299.60	1.4 (−3)	36.9	0.03	1.6 (−3)	−0.1
		6	333.27	9.4 (−4)	26.8	0.01	9.4 (−4)	−0.3
		7	349.58	3.9 (−4)	8.3	0.01	4.1 (−4)	0.0
		8	356.07	9.4 (−5)	2.8	−0.04	4.7 (−4)	0.3

TABLE II: continued

3	1	0	−199.27	0	213.6	0.34	0	0.0
		1	−6.17	0	158.0	0.29	0	0.0
		2	141.10	1.9 (−2)	97.4	0.22	5.9 (−3)	11.7
		3	244.34	1.6 (−2)	70.4	0.13	6.0 (−3)	−0.3
		4	308.82	1.1 (−2)	40.2	−0.05	4.5 (−3)	−0.3
		5	343.20	4.5 (−3)	19.2	−0.51	2.3 (−3)	−1.1
		6	354.81	1.3 (−3)	5.3	0.57	6.3 (−4)	−0.5
3	0	0	−59.64	0	183.7			
		1	105.33	3.7 (−3)	129.4			
		2	223.52	7.0 (−4)	84.5			
		3	298.99	8.5 (−7)	49.1			
		4	339.91	8.7 (−5)	23.4			
		5	355.65	4.6 (−5)	5.6			
ε			357.10					
5	5	0	−91.20	0	260.2	0.00	0	0.7
		1	159.88	4.2 (−8)	206.5	0.00	1.3 (−8)	0.1
5	4	0	76.27	2.3 (−9)	243.7	0.00	2.8 (−9)	0.0
		1	306.77	3.8 (−5)	187.9	0.00	1.0 (−4)	−1.5
5	3	0	220.14	1.1 (−5)	225.1	0.00	5.9 (−6)	0.0
5	2	0	335.74	2.6 (−4)	199.6	0.06	1.1 (−8)	0.4
ε			886.66					

[a] b=5 levels lying above the ε_{03} threshold are not shown.
[b] The values of ε_{0j} for j=1, 3, and 5 are too small by 0.04, 0.21, and 0.55 cm^{-1}, respectively, cf. Ref. 7.

TABLE III: He^+-ortho-D_2. Positions (E, in cm^{-1}), dissociative widths (Γ, in cm^{-1}), and radiative widths (Γ^{rad}, in 10^{-6} cm^{-1}) of rotational states associated with the v=0 j=2 threshold (b=2) in the energy range from 0 (=ε_{00}) up to 357($\approx\varepsilon_{03}$) cm^{-1}.

	b=2 k v_R J p											
	p=1			p=−1			p=1			p=−1		
J	E	Γ	Γ^{rad}	ΔE (f-e)	Γ	$\Delta\Gamma^{rad}$ (f-e)	E	Γ	Γ^{rad}	ΔE (f-e)	Γ	$\Delta\Gamma^{rad}$ (f-e)
	k=2 v_R=0											
25	40.21	4 (−15)[a]	144.8	0.81	0	2.5						
26	97.32	3.4 (−6)	130.2	1.76	0	7.5						
27	161.53	2.0 (−1)	98.3	−3.39	0	29.0						
28	218.50	1.2	111.6	−0.55	4 (−18)	4.6						
29	278.28	1.7	102.6	−0.09	2.3 (−8)	1.5						
30	338.22	1.7	89.2	0.18	4.0 (−4)	1.4						
	k=2 v_R=1						k=1 v_R=0					
21	5.78	9 (−25)	107.0	−2.52	0	20.5	32.22	9 (−10)	152.1	26.53	0	−3.9
22	49.05	2.4 (−6)	113.7	−0.73	0	6.0	79.98	2.2 (−2)	142.2	28.62	0	−2.9
23	94.30	8.2 (−2)	105.4	0.12	0	6.0	129.23	2.1 (−1)	135.0	30.49	0	−5.4
24	140.90	1.1	102.5	0.42	0	−0.2	179.53	1.8 (−1)	125.3	32.36	7 (−15)	−6.1
25	188.26	1.3	92.1	0.46	2 (−26)	0.2	230.69	1.6 (−1)	114.3	34.14	9.9 (−6)	−6.5
26	235.66	1.3	81.0	0.59	1.6 (−8)	0.4	282.42	1.3 (−1)	102.3	35.76	2.0 (−3)	−7.3
27	282.51	1.3	68.0	0.78	1.7 (−3)	0.6	334.22	1.5 (−1)	88.4	37.05	6.9 (−2)	−9.5
28	327.43	1.6	50.3	1.13	4.5 (−1)	1.1						
	k=2 v_R=2						k=1 v_R=1					
17							25.68	1.0 (−2)	107.1	17.63	0	15.8
18	26.14	2.7 (−5)	106.7	0.29	0	2.2	60.47	2.5 (−1)	119.1	19.78	0	−3.3
19	60.83	6.8 (−1)	95.8	0.26	0	0.4	96.99	2.6 (−1)	111.8	21.44	0	−3.8
20	96.12	6.5 (−1)	88.5	0.35	0	0.1	134.62	2.5 (−1)	104.5	23.02	0	−4.9
21	132.05	7.1 (−1)	81.5	0.43	0	−0.8	172.47	2.0 (−1)	110.6	25.16	5 (−12)	−20.3
22	168.33	7.6 (−1)	73.0	0.52	0	−0.8	211.79	2.2 (−1)	85.4	26.24	2.3 (−3)	−5.6
23	204.54	7.9 (−1)	63.4	0.64	1 (−10)	−0.7	250.86	1.8 (−1)	73.2	26.41	7.0 (−2)	36.5
24	240.00	7.6 (−1)	51.8	0.80	1.7 (−3)	−0.6	289.15	3.1 (−1)	58.0	27.64	8.0 (−1)	−8.0
25	273.16	1.4	34.8	1.07	7.2 (−1)	0.6						
	k=0 v_R=0											
15	5.73	1 (−13)	156.6									
16	42.24	1.3 (−3)	149.8									
17	80.51	1.5 (−3)	141.4									
18	120.40	1.8 (−3)	134.5									
19	161.76	1.1 (−3)	125.9									
20	204.41	1.7 (−3)	116.4									
21	248.10	5.2 (−3)	105.3									
22	292.56	1.4 (−2)	93.5									
23	337.13	1.1 (−1)	79.0									

TABLE III: continued

	k=2 v_R=3						k=1 v_R=2					
12							17.28	1.7 (−1)	104.5	9.55	0	−1.4
13	5.07	1.0 (−7)	87.2	0.02	0	1.5	40.06	1.8 (−1)	100.3	10.88	0	−2.0
14	28.01	1.7 (−1)	84.1	0.12	0	0.0	64.28	1.9 (−1)	97.6	12.15	0	−4.4
15	52.13	2.1 (−1)	79.2	0.16	0	0.0	87.78	1.3 (−1)	134.3	15.43	0	−45.7
16	77.21	2.6 (−1)	74.0	0.20	0	0.0	115.23	2.1 (−1)	86.1	16.38	0	16.5
17	103.09	3.0 (−1)	68.4	0.26	0	0.0	142.53	2.1 (−1)	77.0	16.20	0	2.5
18	129.56	3.4 (−1)	62.2	0.32	0	0.0	170.35	2.0 (−1)	69.0	17.67	4 (−11)	−3.0
19	156.34	3.8 (−1)	55.3	0.40	0	0.0	198.41	1.8 (−1)	59.7	18.82	6.3 (−5)	−3.9
20	183.05	3.9 (−1)	47.6	0.49	7 (−20)	0.1	226.14	1.6 (−1)	48.7	19.51	1.0 (−1)	−5.9
21	209.09	3.8 (−1)	38.3	0.61	1.8 (−4)	0.1	252.29	9.8 (−1)	33.5	19.62	2.8	−5.5
22	233.17	8.7 (−1)	27.2	0.76	5.6 (−1)	−0.3						
	k=2 v_R=4						k=0 v_R=1					
7	7.32	11.7 (−3)	72.5	0.01	0	1.6						
8	19.05	18.9 (−3)	71.1	0.02	0	0.7						
9	32.06	28.6 (−3)	69.3	0.03	0	0.0						
10	46.28	41.1 (−3)	66.5	0.04	0	0.0	10.18	126.9 (−5)[b]	126.8			
11	61.62	56.4 (−3)	63.3	0.06	0	0.0	32.88	156.3 (−5)	122.5			
12	77.98	74.4 (−3)	59.8	0.08	0	0.0	57.32	185.0 (−5)	117.5			
13	95.24	94.6 (−3)	56.0	0.11	0	0.0	83.41	212.2 (−5)	112.0			
14	113.26	1.2 (−1)	51.9	0.15	0	0.0	111.03	239.5 (−5)	105.8			
15	132.01	1.3 (−1)	53.5	0.18	0	−0.6	140.03	258.1 (−5)	98.7			
16	150.65	1.6 (−1)	42.7	0.24	0	0.1	170.24	277.1 (−5)	90.8			
17	169.74	1.6 (−1)	41.8	0.35	0	3.5	201.53	19.6 (−3)	90.0			
18	188.14	1.7 (−1)	29.1	0.39	1.4 (−8)	0.2	233.17	14.7 (−3)	71.8			
19	205.30	2.6 (−1)	19.0	0.49	1.1 (−1)	0.1	264.99	1.1 (−1)	61.0			
	k=1 v_R=3						k=0 v_R=2					
0							22.57	23.8 (−6)	99.4			
1[c]	2.12	25.8 (−4)	89.1	0.14	0	0.1	24.41	39.7 (−6)	99.1			
2	5.25	76.9 (−4)	88.3	0.41	0	0.3	28.08	81.4 (−6)	98.4			
3	9.92	15.1 (−3)	87.1	0.81	0	0.4	33.57	164.2 (−6)	97.3			
4	16.12	24.6 (−3)	86.4	1.33	0	−0.2	40.85	301.9 (−6)	95.9			
5	23.83	35.7 (−3)	84.9	1.96	0	−0.3	49.90	501.1 (−6)	94.0			
6	33.02	48.1 (−3)	83.1	2.70	0	−0.4	60.68	758.6 (−6)	91.5			
7	43.67	61.0 (−3)	81.5	3.54	0	−0.7	73.14	106.2 (−5)	89.0			
8	55.82	70.8 (−3)	84.0	4.40	0	−3.7	87.22	140.1 (−5)	86.0			
9	68.15	74.7 (−3)	90.2	7.08	0	21.2	102.86	670.3 (−6)	82.0			
10	83.15	1.0 (−1)	73.9	6.34	0	3.4	119.97	190.9 (−5)	78.8			
11	98.90	1.1 (−1)	68.2	7.55	0	−0.3	138.50	209.8 (−5)	75.7			
12	115.62	1.2 (−1)	63.4	8.70	0	−1.1	158.43	20.2 (−4)	76.0			
13	133.21	1.3 (−1)	58.4	9.84	0	−1.5	195.25	8.7 (−2)	75.0			
14	151.49	1.3 (−1)	52.9	10.94	0	−1.9	217.42	9.4 (−2)	53.0			
15	170.22	1.3 (−1)	46.6	11.96	7.4 (−4)	−2.3						
16	189.05	1.2 (−1)	39.3	12.78	6.5 (−4)	−3.4						
17	207.34	1.4 (−1)	30.1	13.05	4.7 (−1)	−5.5						

TABLE III: continued

	k=2 v_R=5						k=1 v_R=4					
1							87.79	18.3 (−4)	57.1	0.13	0	−0.1
2	53.50	73.1 (−6)	54.4	0.00	0	0.0	90.22	54.2 (−4)	56.1	0.38	0	−0.1
3	57.18	36.0 (−5)	53.4	0.00	0	0.3	93.83	10.6 (−3)	53.9	0.75	0	0.9
4	62.05	10.5 (−4)	52.7	0.00	0	0.0	98.60	17.1 (−3)	53.3	1.23	0	0.0
5	68.09	23.9 (−4)	51.8	0.00	0	0.0	104.50	24.6 (−3)	51.8	1.82	0	−0.2
6	75.38	40.7 (−4)	63.3	0.01	0	0.0	111.48	32.7 (−3)	49.3	2.49	0	0.3
7	83.33	80.2 (−4)	49.3	0.01	0	0.3	119.48	40.5 (−3)	48.5	3.25	0	−1.3
8	92.56	12.8 (−3)	45.9	0.02	0	0.4	128.45	48.8 (−3)	44.4	4.05	0	0.1
9	102.68	20.1 (−3)	42.9	0.03	0	0.9	138.30	55.5 (−3)	42.2	4.90	0	−0.9
10	113.63	26.8 (−3)	40.5	0.05	0	0.5	149.28	39.3 (−3)	38.7	5.41	0	0.5
11	125.29	35.7 (−3)	37.1	0.07	0	0.9	159.90	68.4 (−3)	35.2	6.56	0	1.5
12	137.52	45.3 (−3)	34.5	0.09	0	0.2	171.46	60.0 (−3)	29.9	7.40	0	−1.2
13	150.16	54.8 (−3)	29.9	0.12	0	1.0	183.05	56.3 (−3)	24.8	8.02	4.3 (−3)	−2.5
14	162.97	62.6 (−3)	26.5	0.17	0	0.2	193.58	1.4 (−1)	32.4	8.62	1.1	−17.4
15	175.63	66.2 (−3)	21.7	0.21	0	0.2						
16	187.63	61.1 (−3)	15.5	0.27	1.1 (−4)	0.3						

	k=0 v_R=3		
0	108.52	196.5 (−6)	59.2
1	110.10	230.1 (−6)	59.8
2	113.23	298.9 (−6)	60.9
3	117.86	403.8 (−6)	62.5
4	123.94	53.9 (−5)	65.0
5	131.47	68.4 (−5)	70.2
6	140.54	78.7 (−5)	82.1
7	151.52	757.3 (−6)	108.2
8	155.61	13.6 (−4)	82.2
9	167.97	20.9 (−4)	54.3
10	180.61	41.7 (−4)	36.0
11	192.93	3.4 (−2)	29.5
12	204.68	9.5 (−1)	19.6

	k=2 v_R=6						k=1 v_R=5					
1							139.96	10.7 (−4)	31.2	0.12	0	0.0
2	108.91	47.8 (−6)	34.4	0.00	0	0.0	141.66	31.4 (−4)	30.7	0.36	0	0.0
3	111.72	233.7 (−6)	33.7	0.00	0	0.3	144.17	61.0 (−4)	29.8	0.69	0	−0.8
4	115.43	68.2 (−5)	32.6	0.00	0	0.2	147.48	99.2 (−4)	27.8	1.14	0	0.7
5	119.98	14.9 (−4)	31.8	0.00	0	−0.2	151.56	1.3 (−2)	26.9	1.64	0	0.1
6	125.35	28.8 (−4)	30.3	0.01	0	0.0	156.32	1.7 (−2)	25.2	2.23	0	0.3
7	131.45	48.8 (−4)	28.7	0.01	0	0.0	161.68	2.0 (−2)	23.0	2.78	0	0.2
8	138.25	74.3 (−4)	28.6	0.02	0	0.0	167.55	2.2 (−2)	21.8	3.38	0	−2.1
9	145.55	1.1 (−2)	24.7	0.03	0	0.1	173.67	2.3 (−2)	17.6	3.99	0	−1.6
10	153.38	1.5 (−2)	23.5	0.05	0	0.0	179.71	2.2 (−2)	17.2	4.54	9.5 (−3)	−6.5
11	161.38	1.4 (−2)	18.6	0.06	0	1.3	185.48	2.6 (−1)	7.2	4.46	1.3	−1.9
12	169.56	2.5 (−2)	15.8	0.10	0	0.6						
13	177.55	2.4 (−2)	12.6	0.14	0	0.1						
14	184.88	2.4 (−2)	8.1	0.19	2.2 (−3)	0.1						

TABLE III: continued

	k=2 v_R=7						k=0 v_R=4		
0							156.21	22.4 (−5)	33.8
1							157.33	25.9 (−5)	32.0
2	142.93	21.4 (−6)	20.2	0.00	0	0.0	159.50	33.7 (−5)	29.6
3	144.96	84.5 (−6)	19.6	0.01	0	0.8	162.60	47.0 (−5)	27.2
4	147.62	39.5 (−6)	19.4	−0.01	0	−0.6	166.56	68.8 (−5)	24.8
5	150.85	13.4 (−4)	17.9	0.01	0	0.0	171.24	12.7 (−4)	21.7
6	154.62	19.7 (−4)	16.7	0.01	0	0.0	176.79	23.3 (−6)	17.5
7	158.84	30.1 (−4)	15.3	0.01	0	0.0	182.33	3.2 (−2)	10.9
8	163.43	44.4 (−4)	13.8	0.02	0	−0.1	187.75	7.9 (−1)	9.4
9	168.29	59.2 (−4)	12.0	0.04	0	0.0			
10	173.21	71.2 (−4)	12.4	0.06	0	0.2			
11	178.12	79.0 (−4)	8.2	0.09	0	0.0			
13	186.08	9.2 (−1)	3.6	0.13	9.4 (−1)	−1.0			
	k=1 v_R=6						k=0 v_R=5		
1	166.70	47.4 (−5)	13.8	0.10	0	−0.1			
2	167.72	13.5 (−4)	13.4	0.30	0	−0.1	177.62	1.3 (−6)	16.4
3	169.21	24.8 (−4)	12.6	0.58	0	−0.2	179.21	9.7 (−4)	5.8
4	171.14	36.3 (−4)	11.5	0.92	0	−0.3			
5	173.47	42.5 (−4)	10.3	1.26	0	−0.7			
6	175.79	61.7 (−4)	10.0	1.85	0	−2.7			
7	178.55	5.0 (−3)	5.9	2.05	4.9 (−3)	−1.4			
8	181.07	1.1 (−1)	2.8	2.01	6.8 (−1)	−0.8			
	k=2 v_R=8								
2	162.38	17.6 (−6)	11.3	0.00	0	0.0			
3	163.77	83.0 (−6)	10.8	0.00	0	0.0			
4	165.58	24.5 (−5)	10.2	0.00	0	0.0			
5	167.75	51.9 (−5)	9.5	0.00	0	0.0			
6	170.24	9.4 (−4)	8.6	0.01	0	0.0			
7	172.97	1.5 (−3)	7.5	0.02	0	0.1			
8	175.84	2.1 (−3)	6.3	0.03	0	0.0			
9	178.69	2.6 (−3)	4.9	0.06	0	0.1			
10	181.23	1.1 (−1)	2.8	0.13	5.7 (−2)	−0.2			
	k=1 v_R=7						k=0 v_R=6		
0							176.79	58.1 (−6)	23.9
1	176.84	1.7 (−4)	6.0	0.12	0	−1.9	177.78	13.4 (−6)	51.7
2	180.71	3.2 (−1)	2.3	−1.33	1.5 (−2)	−0.4			
	k=2 v_R=9								
2	173.05	10.7 (−6)	6.1	0.00	0	0.0			
3	173.95	51.1 (−6)	5.6	0.00	0	0.0			
4	175.09	14.2 (−5)	5.1	0.00	0	0.0			
5	176.43	31.7 (−5)	4.4	0.01	0	0.0			
6	177.88	6.0 (−4)	3.6	0.04	0	0.3			
7	179.31	4.5 (−3)	2.5	0.04	7.6 (−4)	0.0			
	k=2 v_R=10								
2	178.13	3.4 (−6)	4.4	0.00	0	0.2			
3	178.55	6.6 (−5)	1.8	0.02	0	0.2			

[a]The widths $\Gamma \ll 10^{-9}$ cm^{-1} were determined with the help of the Siegert quantization method[?] .

[b]The widths Γ are shown with more figures in cases when they are comparable to the width $\Gamma^{\rm rad}$, i.e. when $0.1 \lesssim \Gamma/\Gamma^{\rm rad} \lesssim 10$.

[c]With red color are marked the b=2 resonances which are shown in Fig. C5, in the upper left panel.

TABLE IV: He^+-ortho-D_2. Energies (E, in cm^{-1}), dissociative widths (Γ, in cm^{-1}), and radiative widths (Γ^{rad}, in 10^{-6} cm^{-1}) of rotational states associated with the v=0 j=4 threshold (b=4) in the range $0-357$ cm^{-1}.

	b=4 k v_R J p											
	p=1			p=−1			p=1			p=−1		
J	E	Γ	Γ^{rad}	ΔE (f-e)	Γ	$\Delta\Gamma^{rad}$ (f-e)	E	Γ	Γ^{rad}	ΔE (f-e)	Γ	$\Delta\Gamma^{rad}$ (f-e)
	k=4 v_R=0											
18	32.06	122.1 (−6)	201.6	0.05	0	−0.7						
19	77.51	455.6 (−6)	200.8	0.04	0	0.1						
20	124.98	166.3 (−5)	190.9	0.10	0	4.0						
21	174.99	40.6 (−3)	167.9	−0.54	0	20.1						
22	225.57	49.0 (−4)	177.5	−0.11	263.8 (−6)	1.0						
23	278.43	1.8 (−1)	172.3	0.87	1.2 (−1)	−44.1						
24	332.70	3.1 (−1)	165.0	0.11	2.4 (−1)	−0.8						
	k=4 v_R=1						k=3 v_R=0					
11	7.07	13.3 (−6)	187.6	0.01	0	−0.1						
12	34.31	4.9 (−6)	184.2	0.01	0	−0.1						
13	63.60	16.8 (−6)	180.2	0.01	0	0.0	21.37	780.1 (−6)	211.1	0.18	0	0.5
14	94.88	295.0 (−6)	175.7	0.01	0	0.0	54.44	670.8 (−5)	203.9	0.38	0	2.9
15	127.95	90.3 (−4)	163.2	0.02	0	2.3	91.52	7.2 (−2)	156.6	−1.39	0	43.8
16	163.35	13.4 (−6)	165.3	0.02	0	0.1	127.67	146.6 (−5)	193.0	−0.77	0	−18.7
17	200.16	1.4 (−1)	149.9	0.07	2.3 (−1)	−8.7	166.63	698.2 (−5)	183.5	0.97	0	−8.3
18	238.97	2.0 (−1)	155.1	−0.02	3.0 (−1)	2.5	207.62	5.0 (−2)	182.7	1.20	5.4 (−2)	−3.6
19	279.28	2.7 (−1)	149.0	0.02	2.6 (−1)	1.1	250.29	5.2 (−1)	174.1	1.48	2.9 (−1)	3.9
20	321.14	3.6 (−1)	143.4	0.05	3.2 (−1)	0.2	292.59	1.1	103.1	4.18	4.2 (−1)	67.4
21							341.29	1.6	160.1	1.94	4.2 (−1)	2.4
	k=4 v_R=2						k=3 v_R=1					
3							40.49	6.6 (−8)	185.8	0.00	0	0.0
4	82.68	3.1 (−9)	155.7	0.00	0	1.9	49.40	1.1 (−6)	184.5	0.00	0	0.0
5	93.07	1.1 (−7)	155.4	0.00	0	0.8	60.49	12.9 (−6)	182.5	0.00	0	0.0
6	105.49	2.0 (−6)	154.4	0.00	0	0.1	73.61	572.4 (−6)	167.4	0.00	0	0.1
7	119.93	507.0 (−6)	151.0	−0.01	0	1.4	89.29	23.2 (−6)	177.1	0.00	0	0.0
8	136.31	100.4 (−6)	148.3	0.00	0	0.0	106.80	20.1 (−6)	175.6	0.01	0	0.1
9	154.69	2.5 (−7)	146.1	0.00	0	1.3	126.40	338.8 (−6)	172.4	0.02	0	0.3
10	174.97	14.5 (−6)	142.1	0.00	0	−0.1	147.59	21.7 (−3)	134.0	0.40	0	32.6
11	197.06	4.3 (−2)	141.5	0.00	4.3 (−2)	0.0	171.78	16.3 (−6)	163.9	0.15	0	−2.4
12	220.98	6.5 (−2)	138.1	0.00	6.3 (−2)	0.0	197.30	2.4 (−1)	161.0	0.12	2.6 (−1)	3.8
13	246.67	9.5 (−2)	134.4	0.01	8.9 (−2)	0.0	224.83	4.5 (−1)	157.4	0.15	2.7 (−1)	0.3
14	274.05	1.4 (−1)	130.5	0.01	1.2 (−1)	0.0	254.05	5.6 (−1)	152.7	0.26	3.2 (−1)	0.4
15	303.07	1.9 (−1)	126.3	0.02	1.7 (−1)	0.1	285.19	8.2 (−1)	143.8	0.20	3.6 (−1)	3.8
16	333.68	2.8 (−1)	122.1	0.04	2.4 (−1)	0.1	317.48	8.8 (−1)	141.4	0.61	3.9 (−1)	0.3
17							351.40	1.1	134.6	0.89	4.0 (−1)	0.4
	k=4 v_R=3											
4	244.86	473.3 (−6)	117.0	0.00	472.5 (−6)	−0.1						
5	253.88	188.2 (−5)	115.9	0.00	187.4 (−5)	0.0						
6	264.65	490.6 (−5)	114.3	0.00	486.2 (−5)	0.0						
7	277.16	10.6 (−3)	112.3	0.00	10.4 (−3)	0.0						
8	291.37	20.6 (−3)	110.3	0.00	19.9 (−3)	0.0						
9	307.29	36.7 (−3)	113.4	0.00	34.6 (−3)	0.0						
10	324.78	68.1 (−3)	106.8	0.01	61.7 (−3)	0.0						
11	343.96	1.2 (−1)	104.6	0.02	1.0 (−1)	0.1						

TABLE IV: continued

	k=2 v_R=0						k=1 v_R=0					
1							97.89	4.1 (−7)	196.8	1.15	0	1.3
2							101.03	5.4 (−9)	194.0	3.37	0	3.7
3							105.89	4.8 (−6)	189.8	6.54	0	6.6
4							112.58	30.3 (−6)	183.7	10.53	0	11.6
5	1.97[a]	107.4 (−6)	215.9	0.22	0	0.1	121.15	146.1 (−6)	173.6	15.26	0	19.8
6	15.89	308.3 (−6)	213.4	0.45	0	0.3	131.52	315.3 (−6)	156.9	20.77	0	33.5
7	32.00	980.6 (−6)	209.2	0.81	0	1.5	143.28	717.8 (−6)	124.3	27.47	0	63.3
8	50.12	512.9 (−5)	201.2	1.41	0	4.3	165.13	106.9 (−5)	140.8	26.53	20.2 (−3)	42.0
9	71.46	15.0 (−3)	176.6	0.49	0	−8.6	181.76	276.8 (−6)	158.6	33.23	13.0 (−3)	22.2
10	93.33	648.1 (−6)	196.7	3.36	0	−1.8	200.80	3.3	173.0	39.88	688.9 (−5)	3.6
11	117.45	4.2 (−8)	192.1	4.74	0	4.1	224.26	2.7	175.7	44.38	243.0 (−5)	−3.4
12	143.19	379.3 (−6)	181.5	6.82	0	11.2	249.46	2.6	171.7	49.30	446.2 (−6)	−4.6
13	180.20	566.5 (−6)	92.1	−0.19	7.4 (−6)	95.2	277.03	2.5	166.6	53.87	250.4 (−5)	−5.5
14	205.64	50.4 (−3)	129.3	6.68	1.9 (−1)	53.7	306.92	2.3	162.1	57.90	11.7 (−3)	−8.6
15	234.90	1.3	160.1	11.70	2.0 (−1)	17.8	339.09	2.0	156.2	61.02	33.3 (−3)	−11.6
16	268.60	4.0	182.9	14.29	1.8 (−1)	−11.1						
17	303.65	4.2	164.9	17.42	1.6 (−1)	0.2						
18	340.32	4.6	158.1	20.72	1.2 (−1)	−0.4						
	k=2 v_R=1						k=1 v_R=1					
1							280.92	2.8 (−1)	143.8	0.90	1.2 (−1)	0.0
2	177.44	59.8 (−6)	132.6	−0.10	0	0.7	283.88	5.7 (−1)	142.8	2.64	1.1 (−1)	0.2
3	183.65	6.8 (−2)	164.2	0.03	5.4 (−2)	0.0	288.44	9.6 (−1)	141.7	5.13	1.0 (−1)	−0.4
4	191.96	1.2 (−1)	162.8	0.09	8.3 (−2)	0.0	294.68	1.4	140.2	8.21	8.5 (−2)	0.0
5	202.29	2.1 (−1)	161.0	0.22	1.2 (−1)	0.0	302.72	1.8	138.2	11.75	7.0 (−2)	−0.1
6	214.59	3.4 (−1)	158.9	0.43	1.5 (−1)	0.0	312.64	2.2	136.0	15.62	5.4 (−2)	−11.0
7	228.82	5.2 (−1)	156.4	0.77	1.9 (−1)	0.0	324.52	2.6	133.5	19.67	3.7 (−2)	−4.6
8	244.92	7.6 (−1)	153.4	1.26	2.2 (−1)	0.2	338.43	2.8	130.8	23.75	3.6 (−2)	−2.3
9	262.83	1.1	150.2	1.96	2.4 (−1)	0.2	354.45	3.0	127.8	27.65	9.1 (−3)	−3.2
10	282.47	1.5	146.5	2.89	2.6 (−1)	−0.3						
11	303.78	1.9	142.4	4.09	2.7 (−1)	0.4						
12	326.69	2.4	137.8	5.60	2.6 (−1)	0.7						
13	351.10	3.0	132.8	7.48	2.4 (−1)	1.0						
	k=1 v_R=2											
2	335.01	4.2 (−2)	117.5	0.01	3.8 (−2)	0.1						
3	340.34	8.4 (−2)	116.4	0.03	6.4 (−2)	0.0						
4	347.39	1.5 (−1)	115.0	0.10	9.5 (−2)	0.0						
	k=0 v_R=0						k=0 v_R=1					
0	172.27	9.7 (−6)	147.9				343.13	2.1	123.0			
1	174.87	40.7 (−6)	113.5				345.90	1.9	122.7			
2	177.13	42.0 (−5)	36.0				351.39	1.7	122.0			
3	191.88	1.2	174.3									
4	204.32	1.0	174.1									
5	219.53	7.8 (−1)	172.1									
6	237.39	5.7 (−1)	169.9									
7	257.75	3.7 (−1)	167.0									
8	280.50	2.2 (−1)	160.7									
9	305.46	8.9 (−2)	159.4									
10	332.47	2.0 (−2)	154.7									

[a]The resonance closest to the v=0 j=0 threshold among all Feshbach resonances (b>0) of He^+−o-D_2. Because of the width Γ being above two times smaller than the width Γ^{trad}, the contribution of this resonance to the rate constant function $k(T)$ is only one third of what it would be if the relation $\Gamma \gg \Gamma^{trad}$ were true, cf. Eq. (17).

TABLE V: $He^+-ortho\text{-}D_2$. Energies (E, in cm^{-1}), dissociative widths (Γ, in cm^{-1}), and radiative widths (Γ^{rad}, in 10^{-6} cm^{-1}) of shape resonances $b{=}0\,k{=}0\,v_R\,J$.

v_R	J	E	Γ	Γ^{rad}	v_R	J	E	Γ	Γ^{rad}
0	27	37.82	2 (−19)	123.6	3	19	17.89	5.9 (−9)	48.3
	28	97.63	1.8 (−9)	112.2		20	43.27	85.8 (−6)	38.0
	29	157.76	48.1 (−6)	98.9		21	66.65	1.2	25.0
	30	217.63	20.7 (−3)	84.6	4	16	5.84	1 (−11)	34.5
	31	276.09	83.9 (−2)	66.4		17	22.55	49.6 (−4)	42.9
	32	332.37	6.5	50.9		18	38.59	1.5	16.5
1	24	16.26	1 (−21)	98.3	5	14	9.82	14.0 (−4)	17.3
	25	63.71	1.9 (−8)	88.8		15	19.56	1.1	9.7
	26	111.53	88.2 (−5)	81.2	6	11	2.45	3.6 (−6)	11.6
	27	152.01	66.7 (−3)	86.8		12	8.18	2.9 (−1)	5.9
	28	197.82	3.2	45.5	7	9	2.48	1.6 (−2)	3.6
2	22	35.43	1.1 (−8)	71.4		10	5.39	9.1 (−1)	2.6
	23	71.28	27.7 (−4)	56.7	8	6	0.38	3.0 (−4)	2.9
	24	105.06	63.9 (−2)	40.0		7	1.74	3.0 (−1)	1.5
	25	135.93	6.8	28.7	9	3	0.09	8.9 (−3)	0.9

The resonance marked with red color lies closer to the respective lowest threshold (here $v{=}0\,j{=}0$) than any other resonance of He^+-D_2, see Fig. C5.

TABLE VI: He^+-para-D_2. Energies (E, in cm^{-1}), dissociative widths (Γ, in cm^{-1}), and radiative widths (Γ^{rad}, in 10^{-6} cm^{-1}) of rotational states associated with the v=0 j=3 threshold (b=3 k v_R J p) in the range 59.745 ($=\varepsilon_{01}$) − 357 ($\approx\varepsilon_{03}$) cm^{-1}.

	b=3 k v_R J p											
	p=1			p=−1			p=1			p=−1		
J	E	Γ	Γ^{rad}	ΔE (f-e)	Γ	$\Delta\Gamma^{rad}$ (f-e)	E	Γ	Γ^{rad}	ΔE (f-e)	Γ	$\Delta\Gamma^{rad}$ (f-e)
	k=3 v_R=0											
23	74.96	2 (−19)	167.8	0.51	2 (−20)	0.5						
24	129.37	1.9 (−4)	152.9	0.95	1.6 (−5)	6.1						
25	186.09	3.0 (−1)	149.1	0.93	4.3 (−1)	−2.2						
26	243.17	4.4 (−1)	138.9	1.29	4.0 (−1)	2.7						
27	300.49	5.7 (−1)	117.3	2.58	4.2 (−1)	14.6						
	k=3 v_R = 1						k=2 v_R = 0					
19	73.35	5 (−11)	152.5	0.22	2 (−11)	6.1	65.78	4 (−18)	150.1	0.43	7 (−19)	6.0
20	117.07	2.5 (−1)	150.4	1.18	3.1 (−1)	9.5	108.43	8.4 (−2)	129.4	0.84	2.9 (−2)	12.9
21	162.53	2.3 (−1)	144.7	2.68	2.2 (−1)	9.1	152.49	1.4 (−1)	135.8	0.86	1.6 (−1)	−1.3
22	209.09	1.7	140.3	4.82	1.9 (−1)	6.4	197.59	1.9 (−1)	126.9	0.84	2.2 (−1)	−1.5
23	258.68	3.2	136.6	5.43	1.7 (−1)	1.9	243.66	2.6 (−1)	117.8	0.79	2.7 (−1)	−1.2
24	309.02	3.6	127.1	6.57	1.4 (−1)	2.3	290.48	2.8 (−1)	108.3	0.79	3.1 (−1)	−0.8
25							337.84	3.1 (−1)	98.3	0.82	3.4 (−1)	−0.6
	k=3 v_R=2						k=2 v_R=1					
14							63.87	1.3 (−8)	139.3	3.54	1.8 (−5)	16.3
15	85.93	2.2 (−2)	123.5	−0.49	9.1 (−3)	−4.1	94.21	2.5 (−1)	122.6	7.52	6.2 (−2)	33.8
16							128.53	1.5	133.6	10.35	3.3 (−2)	8.1
17	148.83	1.6 (−1)	113.1	−0.25	6.2 (−2)	−0.2	163.15	1.9	130.7	15.19	1.8 (−2)	20.0
18	182.20	1.7 (−1)	107.4	−0.30	9.2 (−2)	−1.0	199.43	2.2	125.7	20.36	1.1 (−2)	19.0
19	216.83	2.0 (−1)	102.9	−0.53	1.2 (−1)	−3.2	237.16	2.5	119.6	25.83	6.5 (−3)	16.8
20	253.20	2.2 (−1)	106.0	−1.59	1.5 (−1)	−13.3	276.20	2.7	113.1	31.54	3.8 (−3)	15.9
21	286.39	1.0 (−1)	90.7	1.26	1.8 (−1)	−5.6	316.46	2.8	106.2	37.39	2.1 (−3)	13.7
22	323.27	1.6 (−1)	78.7	0.87	2.0 (−1)	−1.7						
	k=1 v_R=0											
15	63.17	3 (−12)	165.4	28.73	1.6 (−1)	−20.8						
16	97.23	1.4 (−2)	159.3	28.47	1.9 (−1)	−21.2						
17	133.05	2.2 (−1)	155.5	27.82	2.0 (−1)	−24.1						
18	170.52	9.1 (−2)	145.7	26.88	2.1 (−1)	−21.0						
19	209.29	2.6 (−2)	134.8	25.90	2.0 (−1)	−17.6						
20	248.59	6.0 (−3)	101.5	25.55	1.9 (−1)	7.9						
21	292.88	2.0 (−1)	113.6	21.19	1.8 (−1)	−12.5						
22	334.71	3.3 (−1)	106.1	20.01	1.6 (−1)	−14.2						
	k=3 v_R=3						k=2 v_R=2					
7							64.37	6.7 (−2)	108.2	0.49	5.8 (−2)	−2.4
8	71.16	2.2 (−2)	106.4	−0.71	1.1 (−4)	13.9	80.05	2.5 (−1)	124.4	0.81	6.8 (−2)	2.7
9	87.00	2.4 (−2)	97.2	−0.35	1.3 (−3)	10.0	97.46	3.5 (−1)	122.2	1.56	7.0 (−2)	4.9
10	104.51	5.0 (−2)	93.9	−0.44	4.3 (−3)	8.6	116.67	4.9 (−1)	119.7	2.84	6.2 (−2)	5.6
11	122.24	1.9 (−2)	112.9	0.73	8.8 (−3)	−13.7	137.67	6.4 (−1)	117.2	4.71	4.8 (−2)	7.9
12	143.16	1.4 (−2)	97.0	0.14	1.5 (−2)	−3.1	160.51	8.0 (−1)	115.3	6.97	3.5 (−2)	6.3
13	165.01	3.9 (−2)	89.8	−0.02	2.3 (−2)	1.5	185.41	9.0 (−1)	117.5	9.20	2.5 (−2)	−0.1
14	188.14	8.1 (−2)	89.1	−0.21	3.4 (−2)	−3.0	213.08	7.3 (−1)	119.7	10.47	1.8 (−2)	−4.3
15	210.14	1.3 (−1)	103.7	1.88	4.6 (−2)	−21.8	244.45	3.7 (−1)	122.7	9.69	1.2 (−2)	−12.9
16	236.47	3.4 (−2)	78.8	0.67	6.0 (−2)	−4.1	279.14	1.5 (−1)	121.0	7.05	8.5 (−3)	−17.8
17	262.68	5.2 (−2)	71.5	0.46	7.4 (−2)	1.2	316.23	5.0 (−2)	102.3	3.29	5.5 (−3)	−10.0
18	289.15	7.2 (−2)	72.1	0.37	8.8 (−2)	0.8	355.14	1.3 (−2)	107.5	−1.26	1.2 (−3)	−20.0
19	316.34	9.0 (−2)	60.2	0.40	1.0 (−1)	−0.2						
20	343.52	1.0 (−1)	52.7	0.43	1.1 (−1)	−0.2						

TABLE VI: continued

	k=1 v_R=1						k=0 v_R=0					
8	63.32	1.6 (−3)	142.7	8.81	7.3 (−3)	−16.1						
9	81.17	2.3 (−1)	142.0	9.45	2.1 (−2)	−10.5						
10	101.03	1.5 (−1)	136.4	9.84	4.5 (−2)	−14.2	75.55	3.4 (−2)	152.9			
11	124.42	1.2 (−1)	121.2	7.99	7.4 (−2)	−2.0	100.78	2.4 (−1)	151.6			
12	148.42	6.7 (−2)	123.0	6.77	1.0 (−1)	−10.0	127.27	3.1 (−1)	143.3			
13	175.23	8.9 (−2)	120.5	4.02	1.2 (−1)	−13.2	154.57	3.5 (−1)	133.9			
14	203.70	4.3 (−1)	116.3	0.90	1.4 (−1)	−14.7	182.36	3.0 (−1)	123.1			
15	232.52	1.0	104.2	−1.34	1.5 (−1)	−8.4	213.02	2.0 (−1)	94.6			
16	261.61	1.5	96.0	−2.73	1.6 (−1)	−6.2	241.05	2.2 (−1)	102.6			
17	291.42	1.8	89.4	−3.87	1.6 (−1)	−6.2	270.80	1.4 (−1)	96.4			
18	322.09	1.9	83.1	−5.07	1.5 (−1)	−6.9	301.30	1.0 (−1)	88.1			
19	353.55	1.9	76.2	−6.52	1.4 (−1)	−7.6	332.17	1.5 (−1)	71.4			
	k=3 v_R=4						k=2 v_R=3					
2							147.81	1.2 (−2)	94.7	0.06	7.2 (−3)	0.6
3	138.35	4.4 (−5)	82.1	0.00	4.4 (−5)	0.2	153.16	3.7 (−2)	95.0	0.27	1.5 (−2)	2.3
4	144.39	1.8 (−4)	81.2	0.00	1.9 (−4)	0.2	160.24	7.6 (−2)	96.0	0.71	2.1 (−2)	2.1
5	151.89	4.9 (−4)	79.3	0.00	5.0 (−4)	−8.6	169.03	1.3 (−1)	96.0	1.37	2.3 (−2)	2.1
6	160.83	1.1 (−3)	77.9	0.00	1.1 (−3)	0.3	179.54	2.0 (−1)	94.9	2.19	2.3 (−2)	3.2
7	171.16	2.1 (−3)	73.9	0.00	2.1 (−3)	2.0	191.80	2.7 (−1)	96.0	3.10	2.2 (−2)	0.9
8	182.85	5.0 (−3)	73.6	−0.01	3.6 (−3)	−5.2	205.88	3.3 (−1)	94.7	3.94	2.0 (−2)	−0.7
9	195.68	2.2 (−2)	72.9	0.11	5.8 (−3)	−1.2	221.92	3.5 (−1)	94.6	4.49	1.8 (−2)	−3.4
10	209.93	9.3 (−3)	69.5	0.06	8.8 (−3)	−0.3	240.08	3.0 (−1)	94.1	4.51	1.5 (−2)	−6.1
11	225.26	1.2 (−2)	66.4	0.06	1.3 (−2)	−0.2	260.50	2.2 (−1)	92.8	3.75	1.3 (−2)	−9.5
12	241.79	1.4 (−2)	74.2	0.07	1.5 (−2)	0.5	283.11	1.3 (−1)	90.2	2.15	1.0 (−2)	−11.0
13	258.87	2.2 (−2)	58.8	0.08	2.4 (−2)	−0.4	307.69	6.3 (−2)	85.1	−0.22	7.6 (−3)	−11.6
14	276.99	2.9 (−2)	54.9	0.10	3.1 (−2)	−0.1	333.90	2.1 (−2)	68.8	−3.21	4.9 (−3)	−1.2
15	295.74	3.5 (−2)	50.2	0.13	3.8 (−2)	0.0						
16	314.92	4.2 (−2)	45.3	0.16	4.6 (−2)	−0.5						
17	334.30	4.9 (−2)	39.6	0.19	5.2 (−2)	−0.3						
18	353.50	5.2 (−2)	33.5	0.24	5.9 (−2)	0.3						
	k=1 v_R=2						k=0 v_R=1					
0							105.33	3.7 (−3)	129.4			
1	141.10	1.9 (−2)	97.4	0.22	5.9 (−3)	11.7	107.52	5.0 (−3)	124.2			
2	144.29	3.6 (−2)	106.8	0.60	2.4 (−3)	0.7	111.87	8.1 (−3)	128.1			
3	149.10	5.3 (−2)	103.1	1.01	6.4 (−5)	0.7	118.36	1.4 (−2)	126.3			
4	155.56	6.5 (−2)	102.3	1.35	1.6 (−3)	−2.8	126.93	2.5 (−2)	121.7			
5	163.67	6.7 (−2)	99.0	1.58	7.8 (−3)	−9.9	137.51	4.3 (−2)	118.1			
6	173.46	5.8 (−2)	97.7	1.64	1.7 (−2)	−5.8	149.99	7.1 (−2)	117.0			
7	184.92	4.3 (−2)	93.5	1.51	2.9 (−2)	−5.1	164.19	1.1 (−1)	115.5			
8	198.06	3.6 (−2)	89.7	1.14	4.2 (−2)	−4.9	179.88	1.7 (−1)	110.4			
9	212.86	7.1 (−2)	87.3	0.51	5.6 (−2)	−6.9	196.93	2.1 (−1)	102.3			
10	229.25	1.9 (−1)	83.4	−0.39	6.8 (−2)	−9.5	214.68	2.7 (−1)	97.6			
11	247.06	3.9 (−1)	79.6	−1.47	8.0 (−2)	−5.0	233.16	2.7 (−1)	90.5			
12	266.10	6.3 (−1)	75.8	−2.63	9.0 (−2)	−5.3	252.24	2.3 (−1)	83.3			
13	286.24	8.6 (−1)	72.0	−3.84	9.7 (−2)	−5.5	271.94	1.6 (−1)	64.5			
14	307.34	1.0	63.2	−5.86	7.8 (−2)	37.6	292.26	1.1 (−1)	40.2			
15	329.27	1.1	55.0	−6.83	1.0 (−1)	0.9	312.94	7.4 (−2)	62.4			
16	351.49	1.1	55.7	−8.15	9.7 (−2)	−6.8	334.07	9.1 (−2)	57.8			
17							355.16	1.3 (−1)	46.0			
	k=3 v_R=5						k=2 v_R=4					
2							240.22	2.1 (−3)	61.6	0.00	2.1 (−3)	0.0
3	224.10	4.2 (−5)	56.6	0.00	4.2 (−5)	0.1	244.02	5.5 (−3)	60.8	0.01	5.3 (−3)	−0.1
4	228.81	2.1 (−4)	84.0	0.00	2.0 (−4)	−0.4	249.12	1.1 (−2)	58.9	−0.02	9.6 (−3)	−0.5
5	234.94	5.0 (−4)	53.9	0.00	5.0 (−4)	0.1	255.58	2.1 (−2)	59.3	−0.16	1.5 (−2)	−0.9
6	242.09	1.0 (−3)	52.2	0.00	1.0 (−3)	0.0	263.51	4.6 (−2)	57.9	−0.53	2.1 (−2)	−7.9
7	250.30	1.9 (−3)	50.5	0.00	1.9 (−3)	0.0	273.17	9.0 (−2)	74.1	−1.09	2.0 (−2)	22.7
8	259.52	3.2 (−3)	48.1	0.01	3.2 (−3)	0.4	283.58	2.1 (−1)	62.6	−2.27	3.6 (−2)	−9.1
9	269.68	4.9 (−3)	44.7	0.01	4.9 (−3)	1.4	308.70	4.3 (−1)	51.8	−4.83	4.9 (−2)	−6.1

TABLE VI: continued

10	280.71	7.1 (−3)	43.6	0.02	7.2 (−3)	0.0	322.44	5.2 (−1)	47.6	−6.08	5.4 (−2)	−5.6
11	292.49	9.7 (−3)	40.7	0.02	9.9 (−3)	0.0	336.77	5.7 (−1)	42.9	−7.30	5.6 (−2)	−5.5
12	304.97	1.2 (−2)	42.9	0.03	1.3 (−2)	−0.3	351.49	5.8 (−1)	37.0	−8.51	5.5 (−2)	−5.6
13	317.75	1.6 (−2)	33.0	0.05	1.7 (−2)	1.1						
14	330.93	1.9 (−2)	29.9	0.07	2.1 (−2)	−0.8						
15	344.16	2.2 (−2)	26.4	0.10	2.3 (−2)	0.0						
16	356.98	2.4 (−2)	20.1	0.13	2.5 (−2)	−0.7						
	k=1 v_R=3						k=0 v_R=2					
0							223.52	7.0 (−4)	84.5			
1	244.34	1.6 (−2)	70.4	0.13	6.0 (−3)	−0.3	225.26	1.8 (−3)	83.9			
2	247.38	3.6 (−2)	69.7	0.37	6.8 (−3)	−0.7	228.71	5.2 (−3)	82.9			
3	251.92	7.5 (−2)	66.7	0.67	7.6 (−3)	1.5	233.79	1.3 (−2)	81.0			
4	258.05	8.9 (−2)	68.4	0.92	8.3 (−3)	−2.8	240.39	2.9 (−2)	76.2			
5	265.74	1.1 (−1)	67.6	1.07	8.8 (−3)	−2.8	248.30	5.4 (−2)	75.0			
6	275.07	1.2 (−1)	66.6	1.00	9.0 (−3)	−4.3	257.25	8.3 (−2)	70.8			
7	286.09	1.1 (−1)	65.7	0.57	8.7 (−3)	−5.7	266.91	9.6 (−2)	65.1			
8	298.85	8.4 (−2)	64.8	−0.31	7.9 (−3)	−6.6	277.15	9.1 (−2)	59.1			
9	313.39	4.8 (−2)	69.9	−1.49	5.4 (−3)	11.1	288.04	7.7 (−2)	54.5			
10	328.32	2.7 (−2)	76.7	−3.18	5.7 (−3)	−22.8	299.63	6.2 (−2)	50.0			
11	345.48	7.3 (−3)	53.6	−5.49	4.2 (−3)	−8.3	311.90	5.0 (−2)	45.4			
12							324.74	4.3 (−2)	37.8			
13							337.99	4.5 (−2)	35.9			
14							351.40	6.8 (−2)	30.2			
	k=3 v_R=6						k=2 v_R=5					
2							299.60	1.4 (−3)	36.9	0.03	1.6 (−3)	−0.1
3	281.35	3.4 (−5)	35.2	0.00	3.4 (−5)	0.5	302.37	3.3 (−3)	36.2	0.10	4.0 (−3)	−0.2
4	285.08	1.4 (−4)	34.8	0.00	1.4 (−4)	0.1	306.00	5.6 (−3)	36.3	0.24	6.9 (−3)	1.0
5	289.68	3.7 (−4)	33.8	0.00	3.6 (−4)	0.0	310.46	8.6 (−3)	31.4	0.45	1.0 (−2)	2.1
6	295.10	7.6 (−4)	32.4	0.00	7.6 (−4)	0.0	315.68	1.2 (−2)	32.5	0.72	1.4 (−2)	−0.7
7	301.28	1.4 (−3)	30.9	0.00	1.4 (−3)	0.0	321.63	1.5 (−2)	26.6	1.04	1.8 (−2)	3.2
8	308.16	2.2 (−3)	28.9	0.00	2.2 (−3)	0.2	328.22	1.7 (−2)	28.1	1.40	2.1 (−2)	−0.7
9	315.66	3.4 (−3)	27.0	0.01	3.4 (−3)	0.0	335.35	1.9 (−2)	25.7	1.78	2.4 (−2)	−0.8
10	323.64	4.7 (−3)	24.6	0.01	4.8 (−3)	0.1	342.89	2.0 (−2)	21.8	2.16	2.4 (−2)	0.2
11	332.00	6.3 (−3)	22.0	0.02	6.3 (−3)	0.0	350.67	2.3 (−2)	18.8	2.31	2.6 (−2)	4.7
12	340.56	8.2 (−3)	19.0	0.03	8.1 (−3)	0.0						
13	349.11	8.3 (−3)	15.7	0.06	1.0 (−2)	0.1						
	k=1 v_R=4						k=0 v_R=3					
0							298.99	8.5 (−7)	49.1			
1	308.82	1.1 (−2)	40.2	−0.05	4.5 (−3)	−0.3	300.17	8.6 (−4)	48.4			
2	311.36	2.2 (−2)	40.3	−0.17	4.6 (−3)	−1.0	302.49	5.3 (−3)	46.5			
3	315.20	3.1 (−2)	39.9	−0.44	4.7 (−3)	−1.6	305.92	1.7 (−2)	44.5			
4	320.36	3.5 (−2)	39.5	−0.91	4.8 (−3)	−2.7	310.35	4.0 (−2)	42.0			
5	326.82	3.5 (−2)	39.1	−1.63	4.7 (−3)	−4.1	315.69	7.4 (−2)	39.9			
6	334.50	2.3 (−2)	32.1	−2.63	4.3 (−3)	1.0	321.86	1.1 (−1)	36.6			
7	343.23	1.1 (−2)	37.6	−3.85	3.8 (−3)	−7.8	328.82	1.7 (−1)	31.7			
8	352.90	1.5 (−3)	27.8	−5.35	2.8 (−3)	−1.4	336.38	1.9 (−1)	28.7			
9							344.50	2.2 (−1)	27.0			
10							353.01	2.3 (−1)	23.4			
	k=3 v_R=7						k=2 v_R=6					
2							333.27	9.4 (−4)	26.8	0.01	9.4 (−4)	−0.3
3	317.03	2.4 (−5)	21.4	0.00	2.4 (−5)	0.0	335.24	2.1 (−3)	19.2	0.04	2.3 (−3)	0.0
4	319.75	9.0 (−5)	20.6	0.00	1.2 (−4)	0.0	337.72	3.5 (−3)	17.6	0.11	3.8 (−3)	0.0
5	323.08	2.4 (−4)	19.9	0.00	2.3 (−4)	0.0	340.67	4.8 (−3)	16.2	0.23	5.5 (−3)	0.0
6	326.93	5.0 (−4)	19.4	0.00	4.9 (−4)	0.0	344.05	6.1 (−3)	14.7	0.40	7.0 (−3)	−0.1
7	331.32	9.3 (−4)	17.3	0.00	8.7 (−4)	0.0	347.78	7.2 (−3)	14.5	0.62	8.4 (−3)	−0.9
8	336.10	3.1 (−3)	15.7	0.01	1.4 (−3)	0.0	351.49	7.3 (−3)	12.8	1.06	9.1 (−3)	−2.1
9	341.20	1.9 (−3)	13.9	0.01	2.2 (−3)	0.0	355.53	7.8 (−3)	8.4	1.37	1.0 (−2)	2.1
10	346.50	2.6 (−3)	12.1	0.02	3.8 (−3)	0.1						
11	351.82	3.9 (−3)	10.0	0.01	1.4 (−3)	0.1						
12	356.94	2.4 (−3)	7.5	0.04	2.6 (−3)	0.0						

TABLE VI: continued

	k=1 v_R=5						k=0 v_R=4					
0							339.91	8.7 (−5)	23.4			
1	343.20	4.5 (−3)	19.2	−0.51	2.3 (−3)	−1.1	340.21	1.6 (−3)	22.0			
2	345.52	6.0 (−3)	19.4	−1.22	2.2 (−3)	−1.7	341.12	6.7 (−3)	20.7			
3	348.68	5.3 (−3)	19.8	−2.01	2.0 (−3)	−0.6	342.83	1.2 (−2)	39.5			
4	352.67	1.3 (−3)	30.5	−3.43	2.0 (−3)	17.5	344.91	3.1 (−2)	18.3			
5							347.80	4.5 (−2)	16.4			
6							351.20	5.8 (−2)	14.2			
7							355.02	7.8 (−2)	11.2			
	k=3 v_R=8						k=2 v_R=7					
2							349.58	3.9 (−4)	8.3	0.01	4.1 (−4)	0.0
3	337.89	1.4 (−5)	12.2	0.00	1.4 (−5)	0.0	350.69	8.6 (−4)	7.8	0.04	9.5 (−4)	0.0
4	339.78	5.7 (−5)	11.6	0.00	5.8 (−5)	0.0	352.10	1.3 (−3)	9.5	0.13	1.5 (−3)	5.7
5	342.06	1.4 (−4)	10.9	0.00	1.5 (−4)	0.0	353.67	1.8 (−3)	6.4	0.23	2.1 (−3)	−0.2
6	344.70	2.8 (−4)	10.1	0.00	3.9 (−4)	0.0	355.40	1.7 (−3)	4.8	0.39	2.1 (−3)	0.1
7	347.64	1.9 (−4)	11.9	0.00	3.1 (−4)	0.1						
8	350.72	8.7 (−4)	7.9	0.01	7.1 (−4)	0.0						
9	353.91	5.9 (−2)	6.6	0.02	9.5 (−4)	0.0						
	k=1 v_R=6						k=0 v_R=5					
0							355.65	4.6 (−5)	5.6			
1	354.81	1.3 (−3)	5.3	0.57	6.3 (−4)	−0.5	356.57	1.2 (−4)	4.6			
2	355.03	3.5 (−3)	5.0	1.18	2.3 (−4)	−1.2	357.73	6.3 (−2)	2.3			
3	355.61	5.2 (−3)	4.3	1.62	6.3 (−4)	−1.2						
4	356.53	5.2 (−3)	4.2	1.82	1.6 (−1)	−2.4						
	k=3 v_R=9						k=2 v_R=8					
2							356.07	9.4 (−5)	2.8	−0.04	4.7 (−4)	0.3
3	349.68	1.6 (−5)	6.7	0.00	1.6 (−5)	0.0						
4	350.91	5.9 (−5)	6.3	0.00	5.8 (−5)	−0.1						
5	352.39	1.4 (−4)	5.6	0.00	1.2 (−4)	0.0						
6	354.03	2.7 (−4)	4.9	0.01	2.3 (−4)	0.0						
7	355.75	4.9 (−4)	4.0	0.02	3.5 (−4)	0.0						
	k=3 v_R=10											
3	355.65	3.8 (−4)	2.9	0.00	1.4 (−5)	−0.1						
4	356.28	1.8 (−4)	2.3	0.01	4.9 (−5)	0.0						
5	356.93	2.8 (−4)	1.7	0.03	9.4 (−5)	−0.1						

TABLE VII: He^+-para-D_2. Energies (E, in cm^{-1}), dissociative widths (Γ, in cm^{-1}), and radiative widths (Γ^{rad}, in 10^{-6} cm^{-1}) of rotational states associated with the v=0 j=5 threshold (b=5) in the range $59.745 - 357$ cm^{-1}.

	b=5 k v_R J p											
	p=1			p=−1			p=1			p=−1		
J	E	Γ	Γ^{rad}	ΔE (f-e)	Γ	$\Delta\Gamma^{rad}$ (f-e)	E	Γ	Γ^{rad}	ΔE (f-e)	Γ	$\Delta\Gamma^{rad}$ (f-e)
	k=5 v_R=0											
12	67.35	5 (−10)	241.5	0.00	1.2 (−7)	0.0						
13	99.53	1.1 (−6)	237.4	0.00	2.9 (−7)	0.1						
14	133.98	7.0 (−6)	233.2	0.00	4.2 (−6)	0.0						
15	170.65	35.3 (−6)	228.5	0.00	22.7 (−6)	0.0						
16	209.48	151.9 (−6)	223.5	0.00	100.8 (−6)	0.0						
17	250.38	808.3 (−6)	217.7	0.00	610.2 (−6)	0.0						
18	293.57	126.2 (−5)	206.4	0.05	284.3 (−5)	−5.0						
19	338.42	151.4 (−5)	205.5	−0.04	424.5 (−6)	0.2						
	k=5 v_R=1						k=4 v_R=0					
4							76.27	2.3 (−9)	243.7	0.00	2.8 (−9)	0.0
5	159.88	4.2 (−8)	206.5	0.00	1.3 (−8)	0.1	88.48	4 (−10)	242.1	0.00	1.3 (−9)	0.0
6	173.69	425.4 (−6)	204.1	0.00	5.0 (−6)	0.7	103.09	7.9 (−8)	240.2	0.00	1.8 (−8)	0.0
7	189.74	78.9 (−6)	202.7	0.00	3.1 (−6)	0.0	120.09	1.1 (−6)	238.0	0.00	3.5 (−7)	0.0
8	208.02	128.5 (−6)	199.9	0.00	5.2 (−7)	0.4	139.44	6.9 (−6)	235.3	0.00	2.4 (−6)	0.2
9	228.48	23.4 (−6)	197.7	0.00	11.8 (−6)	0.0	161.12	32.1 (−6)	232.6	0.00	11.0 (−6)	0.0
10	251.10	9.8 (−6)	194.7	0.00	8.4 (−7)	0.0	185.09	125.3 (−6)	229.3	0.00	42.3 (−6)	0.0
11	275.84	8.8 (−6)	191.4	0.00	3.4 (−6)	0.0	211.31	461.4 (−6)	225.5	0.01	167.9 (−6)	0.0
12	302.59	573.6 (−6)	182.3	0.00	544.3 (−6)	0.3	239.59	385.2 (−5)	208.7	0.02	276.4 (−5)	0.4
13	331.53	58.9 (−6)	183.6	0.00	10.3 (−6)	0.0	270.33	319.6 (−5)	211.3	0.08	592.6 (−6)	5.0
14							302.89	86.0 (−3)	204.3	0.94	23.8 (−3)	−43.9
15							338.09	818.9 (−5)	193.0	−0.03	51.4 (−6)	13.0
	k=3 v_R=0											
3	220.14	10.7 (−6)	225.1	0.00	5.9 (−6)	0.0						
4	229.53	34.2 (−6)	195.6	0.00	2.1 (−6)	0.2						
5	240.92	271.8 (−6)	216.0	0.01	65.3 (−6)	6.3						
6	254.65	113.9 (−5)	219.6	0.03	336.4 (−6)	0.1						
7	270.41	220.0 (−4)	200.5	−0.11	907.3 (−5)	−25.0						
8	288.99	595.2 (−6)	208.7	0.08	9.2 (−6)	3.6						
9	308.98	513.3 (−5)	199.4	0.10	148.0 (−5)	−15.1						
10	332.11	97.7 (−6)	187.2	0.27	9.7 (−6)	16.5						
11	355.90	26.5 (−3)	193.2	1.27	142.6 (−6)	4.0						
	k=4 v_R=1						k=2 v_R=0					
2							335.74	261.8 (−6)	199.6	0.06	1.1 (−8)	0.4
3							341.71	555.9 (−5)	184.1	0.40	110.9 (−6)	18.6
4	306.77	37.7 (−6)	187.9	0.00	1.0 (−4)	−1.5	349.70	306.0 (−5)	182.4	1.38	1.2 (−6)	−19.7
5	317.70	28.5 (−6)	187.0	0.00	3.4 (−9)	0.1						
6	330.80	1.1 (−6)	184.6	0.00	9.7 (−6)	−0.4						
7	345.94	153.6 (−4)	178.8	0.00	1.1 (−4)	0.5						

TABLE VIII: $He^+-para\text{-}D_2$. Energies (E, in cm^{-1}), dissociative widths (Γ, in cm^{-1}), and radiative widths (Γ^{rad}, in 10^{-6} cm^{-1}) of shape resonances b=1 $k\, v_R\, J\, p$.

		k=1						k=0				
		p=1			p=−1							
v_R	J	E	Γ	Γ^{rad}	ΔE (f-e)	Γ	$\Delta\Gamma^{rad}$ (f-e)	v_R	J	E	Γ	Γ^{rad}
0	27	57.87	0	127.5	22.10	6 (−26)	−6.7	0	23	100.54	1.5 (−7)	112.5
	28	117.39	4 (−14)	116.4	22.76	1 (−10)	−7.3		24	152.09	455.4 (−5)	117.0
	29	177.36	4.4 (−7)	104.3	23.18	23.8 (−6)	−8.1		25	203.85	221.3 (−4)	105.4
	30	237.30	15.9 (−4)	90.5	23.22	19.0 (−3)	−9.6		26	255.94	48.7 (−3)	89.2
	31	296.34	20.8 (−2)	73.6	22.48	93.9 (−2)	−11.4		27	308.01	94.1 (−2)	86.5
1	25	87.29	8 (−16)	91.6	15.98	2 (−11)	−5.6		28	363.16	2.1	106.8
	26	134.42	1.9 (−6)	80.3	16.15	93.1 (−6)	−6.4		29	421.87	2.1	90.9
	27	180.96	11.8 (−3)	66.4	15.80	98.5 (−3)	−7.7	1	20	91.80	3.6 (−5)	100.3
	28	225.43	1.0	48.7	14.63	3.0	−10.0		21	130.52	13.8 (−2)	88.3
2	22	66.27	∼0	70.5	10.59	1 (−14)	−4.2		22	169.23	14.1 (−2)	73.8
	23	102.52	1.5 (−6)	76.1	10.20	88.4 (−6)	−20.4		23	206.72	1.1	55.5
	24	137.18	33.8 (−3)	48.5	9.94	20.1 (−2)	−6.3	2	17	88.11	12.4 (−2)	64.6
	25	168.68	2.0	32.8	9.19	4.2	−1.0		18	115.02	89.5 (−3)	52.2
3	20	78.11	2.1 (−8)	45.6	6.89	4.5 (−6)	−3.7		19	140.90	81.7 (−2)	40.3
	21	103.36	27.4 (−3)	30.1	6.44	15.9 (−2)	−0.6	3	13	66.01	10.5 (−4)	44.3
	22	125.98	2.2	21.5	5.72	4.2	−2.4		14	83.29	35.4 (−3)	38.0
4	17	62.59	2 (−16)	32.7	4.12	6 (−11)	−2.0		15	100.59	55.0 (−2)	44.4
	18	80.20	34.8 (−4)	24.4	3.92	30.9 (−3)	−3.0		16	116.77	329.5 (−3)	118.7
	19	95.69	1.5	14.6	3.41	2.7	−1.5	4	10	67.43	25.2 (−3)	25.4
5	15	65.48	7.9 (−7)	19.6	2.27	26.6 (−6)	−2.8		11	76.77	40.2 (−2)	17.8
	16	75.97	3.1 (−1)	9.9	1.95	6.9 (−1)	−1.4	5	6	62.60	54.2 (−3)	10.5
6	13	64.50	54.4 (−5)	10.5	1.28	29.7 (−4)	−2.6		7	66.38	1.0	55.5
	14	70.28	8.2 (−1)	4.6	1.05	1.1	−0.2					
7	11	62.94	3.5 (−5)	4.7	0.68	2.0 (−2)	−0.4					
	12	66.16	9.3 (−1)	2.5	0.67	1.1	−0.1					
8	8	59.74	0	4.3	0.37	1.8 (−7)	−0.1					
	9	61.89	1.2 (−1)	2.3	0.41	1.4 (−1)	−0.1					
9	6	60.26	3.5 (−2)	1.6	0.21	3.9 (−2)	0.3					

TABLE IX: Rate constants $k(T)$ (in 10^{-15} $s^{-1}cm^3$) for radiative quenching of $^4He^+$ ions from gas mixtures with equilibrium and normal[a] deuterium at selected temperature values in the range $10^{-5}-100$ K compared to rate constants for quenching from mixtures with equilibrium and normal[a] hydrogen.

	$He^+ + D_2$		$He^+ + H_2$		$\frac{He^+ + D_2}{He^+ + H_2}$			$He^+ + D_2$		$He^+ + H_2$		$\frac{He^+ + D_2}{He^+ + H_2}$	
T	equi	nrm	equi	nrm	equi	nrm	T	equi	nrm	equi	nrm	equi	nrm
10^{-5}	0.39	0.41	0.46	0.71	0.86	0.57	4	46.1	41.6	89.6	40.2	0.51	1.04
0.0005	0.40	0.47	0.47	2.7	0.87	0.17	5	45.9	41.9	79.3	39.1	0.58	1.07
0.001	0.41	0.53	0.47	6.2	0.87	0.09	6	46.1	42.1	71.3	38.1	0.65	1.10
0.002	0.44	0.65	0.49	22.8	0.89	0.03	7	46.5	42.3	65.3	37.3	0.71	1.13
0.005	0.50	0.90	0.54	74.5	0.92	0.01	10	47.9	42.9	54.4	35.5	0.88	1.21
0.007	0.54	1.0	0.58	81.9	0.93	0.01	13	49.0	43.5	49.0	34.2	1.00	1.27
0.01	0.61	1.1	0.63	78.8	0.97	0.01	15	49.4	43.7	46.7	33.5	1.06	1.31
0.02	1.7	2.0	0.78	55.6	2.18	0.04	19	49.7	43.9	43.8	32.4	1.13	1.36
0.03	5.4	4.5	0.93	41.2	5.79	0.11	20	49.7	43.9	43.3	32.1	1.15	1.37
0.05	13.5	10.1	1.2	27.5	11.12	0.37	25	49.3	43.9	41.2	31.0	1.20	1.41
0.10	20.9	15.2	2.9	17.7	7.20	0.86	30	48.5	43.7	39.5	30.1	1.24	1.45
0.20	24.9	18.4	6.8	15.8	3.69	1.16	35	47.5	43.4	38.0	29.3	1.25	1.48
0.30	25.4	19.1	9.8	15.5	2.60	1.23	40	46.5	43.1	36.5	28.6	1.27	1.50
0.40	24.8	18.9	16.7	16.2	1.49	1.17	45	45.4	42.6	35.1	28.0	1.29	1.52
0.50	25.2	19.2	28.4	18.3	0.89	1.05	50	44.3	42.1	33.6	27.4	1.32	1.53
0.70	29.3	22.2	57.1	25.1	0.51	0.88	60	42.1	40.8	31.1	26.5	1.35	1.54
1.00	37.3	28.1	90.0	33.9	0.41	0.83	70	39.9	39.1	29.1	25.7	1.37	1.52
2.00	46.9	38.4	113.2	41.6	0.41	0.92	80	37.7	37.3	27.5	25.0	1.37	1.49
2.50	47.0	38.4	108.6	41.7	0.43	0.96	90	35.6	35.4	26.1	24.3	1.36	1.46
3.00	46.7	40.9	102.3	41.3	0.46	0.99	100	33.6	33.5	25.0	23.7	1.35	1.41

[a]Fixed ortho:para concentration, 2:1 and 3:1 for D_2 and H_2, respectively.

* Electronic address: felicja@fizyka.umk.pl

[1] F. Mrugała, V. Špirko, and W.P. Kraemer, J. Chem. Phys. **118**, 10547 (2003).
[2] F. Mrugała and W.P. Kraemer, J. Chem. Phys. **122**, 224321 (2005).
[3] F. Mrugała and W. P. Kraemer, J. Chem. Phys. **138**, 104315 (2013).
[4] R. D. Levine, *Quantum Mechanics of Molecular Rate Processes* (Clarendon, Oxford, 1969).
[5] W. P. Kraemer, V. Špirko, and O. Bludsky, Chem. Phys. **276**, 225 (2002).
[6] M. Šindelka, V. Špirko, and W. P. Kraemer, Theor. Chem. Acc. **110**, 170 (2003).
[7] S. Kassi, A. Campargue, K. Pachucki, and J. Komasa, J. Chem. Phys. **136**, 184309 (2012).
[8] R. T. Pack, J. Chem. Phys. **60**, 633 (1974).
[9] G. G. Balint-Kurti and M. Shapiro, Chem. Phys. **61**, 137 (1981).
[10] F. H. Mies, J. Chem. Phys. **51**, 787 (1969).
[11] R. E. Roberts, R. B. Bernstein, and C. F. Curtiss, J. Chem. Phys. **50**, 5163 (1969).
[12] R. A. Bain and Bardsley, J. Phys. **B5**, 277 (1972).
[13] O. I. Tolstikhin, S. Watanabe, and M. Matsuzawa, J. Phys. **B29**, L389 (1996).
[14] F. D. Colavecchia, F. Mrugała, G. A. Parker, and R. T Pack, J. Chem. Phys. **118**, 10387 (2003).
[15] F. T. Smith, Phys. Rev. **118**, 349 (1960).
[16] F. Mrugała and R. Moszynski, J. Chem. Phys. **109**, 10823 (1998).
[17] B. R. Johnson, J. Comput. Phys. **13**, 445 (1973).
[18] F. Mrugała, Int. Rev. Phys. Chem. **12**, 1 (1993).
[19] K. Hino, A. Igarashi, and J. M. Macek, Phys. Rev. **A 56**, 1038 (1997).
[20] Apart from calculations of the collision life-time and **S** matrices within the distorded-wave approximation, this algorithm has been also exploited in calculations of resonance structures in cross-sections for collision-induced absorption, see Refs. 16,21.
[21] Felicja Mrugała, J. Chem. Phys. **115**, 3155-72 (2001).
[22] R. D. Levine and R. B. Bernstein, *Molecular Reaction Dynamics and Chemical Reactivity* (Oxford University Press, New York, 1987), chap. 2.
[23] E. R. Sayfutyarova, A. A. Buchachenko, S. A. Yakovleva, and A. K. Belyaev, Phys. Rev. **A 87**, 052717 (2013); B. M. McLaughlin, H. D. L. Lamb, I. C. Lane, and J. F. McCann, J. Phys. **B47**, 145201 (2014); H. da Silva Jr, M. Raoult, M. Aymer, and O. Dulieu, New J. Phys. **17**, 045015 (2015).
[24] A. Harter and J. Hecker Denschlag, Contemporary Physics **55**, 33 (2014).

Appendix 2: Energy dependent rate constants

$K_{vj}(e)$ — a quantity of dimension (length)^3(time)$^{-1}$ can be defined as function of relative translational energy in the vj-channel, $e{=}E{-}\varepsilon_{vj}$, using the yield function $p^{\rm trad}_{vj}(E)$, cf. Eqs. (8) and (5), expressed as $\Theta(E{-}\varepsilon_{vj})\,p^{\rm trad}_{vj}(e)$. Namely,

$$K_{vj}(e) = \frac{1}{2j{+}1}\,\frac{\hbar^2\pi}{\sqrt{2\mu^3}}\,\frac{1}{\sqrt{e}}\,p^{\rm trad}_{vj}(e)\,. \tag{56}$$

Correspondingly to the background-resonance resolution of Eq. (6),

$$K_{vj}(e) \;\approx\; K^{\rm bck}_{vj}(e) + K^{\rm res}_{vj}(e) \tag{57}$$

$$\text{with}\qquad K^{\rm res}_{vj}(e) \;=\; \frac{1}{2j{+}1}\,\frac{\hbar^2\pi}{\sqrt{2\mu^3}}\,\frac{1}{\sqrt{e}}\,\sum_n (2J_n{+}1)\,\frac{\Gamma^{\rm trad}_n\,\Gamma_{n,vj}}{(e{-}e^{\rm res}_{n,vj})^2{+}(\Gamma^{\rm trad}_n{+}\Gamma_n)^2/4}\,. \tag{58}$$

Here n enumerates resonances lying above the vj-channel threshold, $e^{\rm res}_{n,vj}$ denotes position of n-th resonance relative to this threshold, $e^{\rm res}_{n,vj}{=}E^{\rm res}_n{-}\varepsilon_{vj}$, and $\Gamma_{n,vj}$ denotes the partial dissociative width which accounts for decay of the resonance into the vj-channel only.

If the translational motion is in thermal equilibrium, as assumed here, the following averages — functions of temperature, can be defined

$$K_{vj}(T) \;=\; \int_0^\infty de\,P_{\rm trn}(e,T)\,K_{vj}(e) \tag{59}$$

$$\text{with}\qquad P_{\rm trn}(e,T) \;=\; \frac{2}{\sqrt{\pi(k_{\rm B}T)^3}}\,\sqrt{e}\,\exp\Big(-\frac{e}{k_{\rm B}T}\Big)\,.$$

From these functions, the rate constants $k^{\rm c}(T)$, ${}_{\rm c}k(T)$, or $k^{\rm c}_{\rm nrm}(T)$ are obtained upon an additional averaging over the population of vj states. For example, the rate constant ${}_{\rm c}k(T)$ is obtained as

$${}_{\rm c}k(T) \;=\; \sum_v\sum_{j(c)} {}_{\rm c}P_{vj}(T)\,K_{vj}(T) = \sum_v\sum_{j(c)} {}_{\rm c}k_{vj}(T) \tag{60}$$

$$\text{with}\qquad {}_{\rm c}P_{vj}(T) = \frac{2j{+}1}{Z_{\rm c}(T)}\,\exp\Big(-\frac{\varepsilon_{vj}}{k_{\rm B}T}\Big)\,.$$

At ultra-cold collision energies, the functions $K_{0j}(e)$ with $j{=}0$ and $j{=}1$ that describe the 'trad' reactions of the He^+ ions with the o-D_2(p-H_2) and the p-D_2(-H_2) molecules, respectively, are constant and the constants coincide with the values of the respective functions ${}_{\rm c}k_{0j}(T)$ at $T{=}0$. This obviously is a consequence of the $\sqrt{e}$-dependence of the yield functions in the near-threshold regions, $p^{\rm trad}_{0j}(e){\approx}(2j{+}1)\,\mathcal{C}^{\rm trad}_{0(j,j)}\sqrt{e}$, cf. Eqs. (45) and (54). In the subthermal range, a $\sqrt{e}$-dependence, reflecting the validity of the capture model in the $\frac{-1}{R^4}$ -like potential, is revealed by the background parts of the yield functions, $p^{\rm trad(bck)}_{0j}(e){\approx}\xi(2j{+}1)\sqrt{e}$, cf. Eq. (51). Therefore one finds a similar coincidence between values of the background parts of the energy and temperature dependent rate functions,

$$K^{\rm bck}_{0j}(Tk_B) \approx {}_{\rm c}k_{\rm bck}(T) \approx k^{\rm trad}_{\rm cpt}\,,$$

which should hold true at least for $Tk_B{\ll}\varepsilon_{0\,j+2}{-}\varepsilon_{0j}$.

Thus, the collision-energy-dependent rates would provide practically the same information on the studied reaction as the thermally averaged rates if the resonance involvement were small. Just the opposite is true, however, in the considered systems. Not the nearly constant backgrounds but the highly peaked resonance parts of the functions $K_{vj}(e)$ decide on the overall reaction rates. For comparing between the systems, a smoothing-averaging of these functions is requisite. The proper way of the averaging here is, of course, that of Eq. (59). An illustration is provided in Fig. C8 where the functions $K_{00}(e)$ and $K_{01}(e)$ are plotted in two intervals of the energy e together with the functions $K_{00}(T)$ and $K_{01}(T)$ in the equivalent temperature intervals and all the four functions are compared between the $He^+{+}D_2$ and $He^+{+}H_2$ systems.

Fig. C8. $K_{0j_c}(T)^{(*)}$ versus energy dependent rate constants $K_{0j_c}(e)$

$e{=}E{-}\varepsilon_{0j_c}$, $j_c{=}0\,(1)$ for o (p)-D_2 and p (o)-H_2

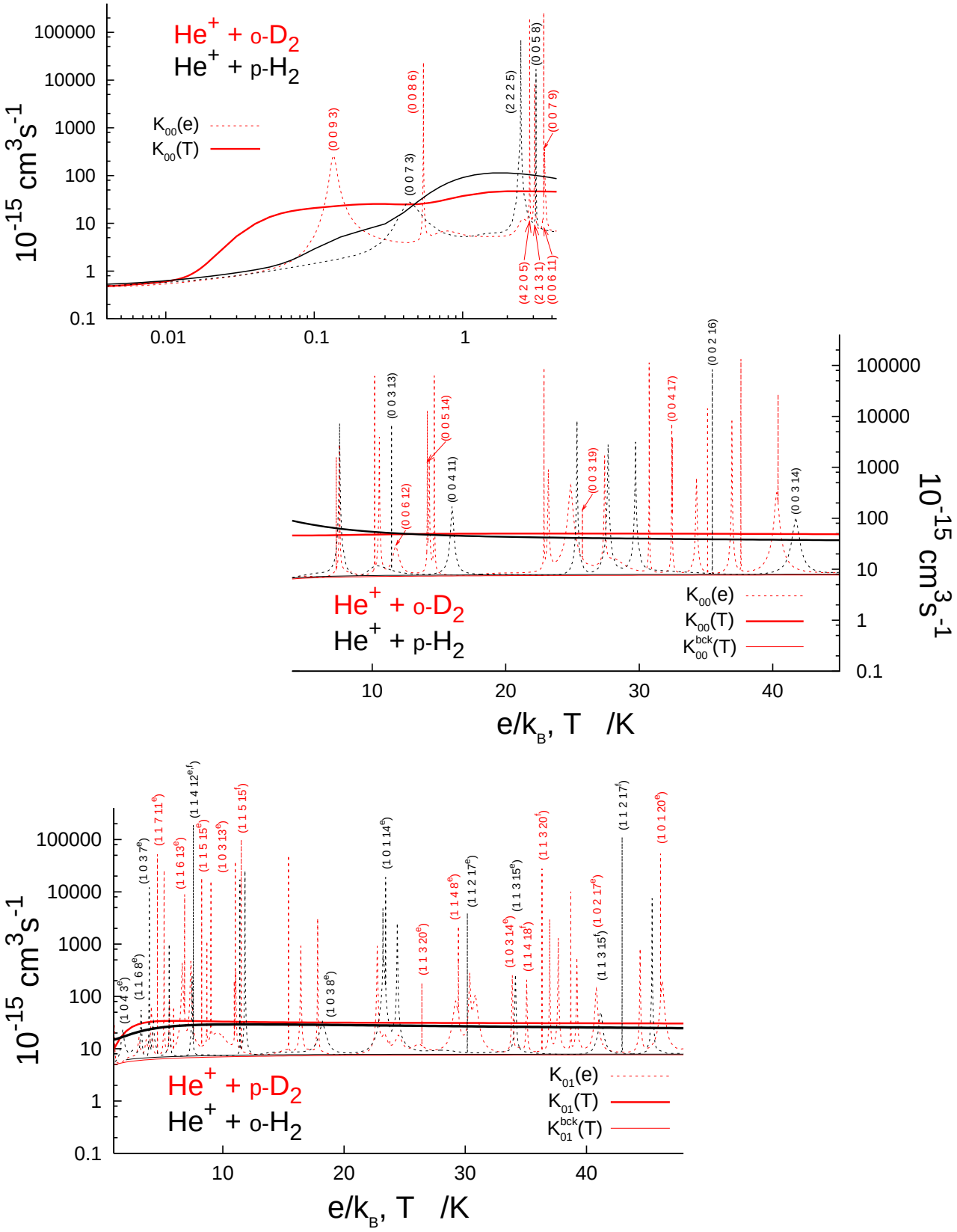

(*) In the T-range shown, the values of the functions $K_{0j_c}(T)$ constitute no less than 98% of the values of the respective functions ${}_ck(T)$, cf. Eq. (60).

The vertical labels of the resonance peaks in the functions $K_{0j_c}(e)$ are the quantum numbers $(b\,k\,v_R\,J)$. Except for the three $b{=}2,4$ cases near 2–3 K, only shape resonances are given label here.

Fig. C9. ${}_{\rm c}k(T)$ versus energy dependent rate constants $K_{0j_c}(e)$ and their averages $\langle K_{0j_c}(e)\rangle_{[e_1,e_2]} := \frac{1}{e_2-e_1}\int_{e_1}^{e_2} K^{\rm res}_{0j_c}(e)\,de + {}_{\rm c}k_{\rm bck}(ek_{\rm B}^{-1})$

j_c=0 (1) for o (p)-D_2 and p (o)-H_2.

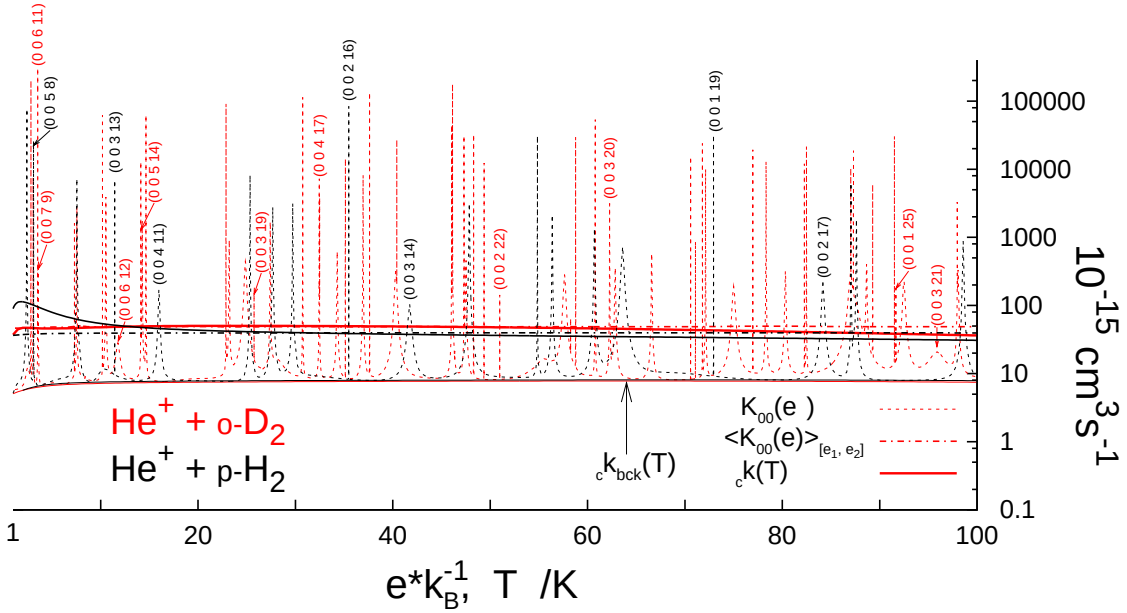

The function $K_{00}(e)$ for He^++o-D_2 exhibits 59 resonance peaks in the range shown. 10 peaks are due to shape resonances (b=0). In the function for He^++p-H_2, 20 resonance peaks occur of which 7 peaks are due to shape resonances. These resonances are accounted for by the averages $\langle K_{00}(e)\rangle_{[e_1,e_2]}$ plotted with the dash-dotted lines: red – for He^++o-D_2 and black — for He^++p-H_2. The respective functions ${}_{\rm o}k(T)$ and ${}_{\rm p}k(T)$ (solid lines) account, of course, for more resonances. At Ts above ∼80 K, they account for resonances from the energy range at least two times larger than shown here.

Enlarged view of the averages $\langle K_{00}(e)\rangle_{[e_1,e_2]}$ in the interval of $[e_1/k_B, e_2/k_B]$=[1, 100] K (dash-dot lines) and of their relations to the functions ${}_{\rm c}k(T)$ (solid lines).
Upper: all resonance and background contributions included in the quantities compared.
Middle: only shape-resonance contributions added to the backgrounds.
Bottom: a demonstration of how the functions ${}_{c}k_{\rm bck}(T)$ and $K_{00}^{\rm bck}(e)$ fit together. The wavy shapes of the latter are due to broad resonances left in the backgrounds.

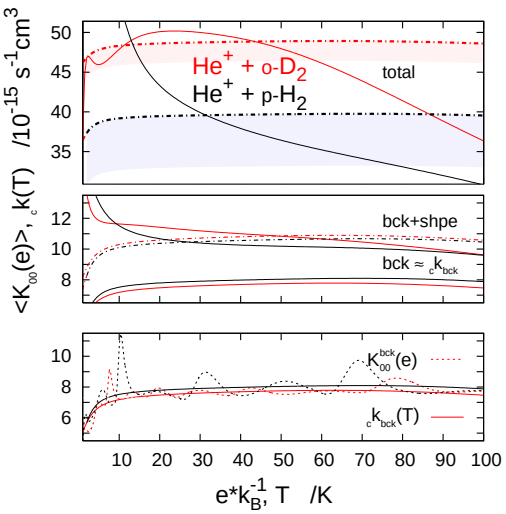

The lower borders of the shadowed strips show the averages $\langle K_{00}(e)\rangle_{[e_1,e_2]}$ in the interval $[e_1/k_B, e_2/k_B]$=[1, 257] K, i.e. ε_{00}+e_2 is close to the ε_{02} threshold in the He^++D_2 system.

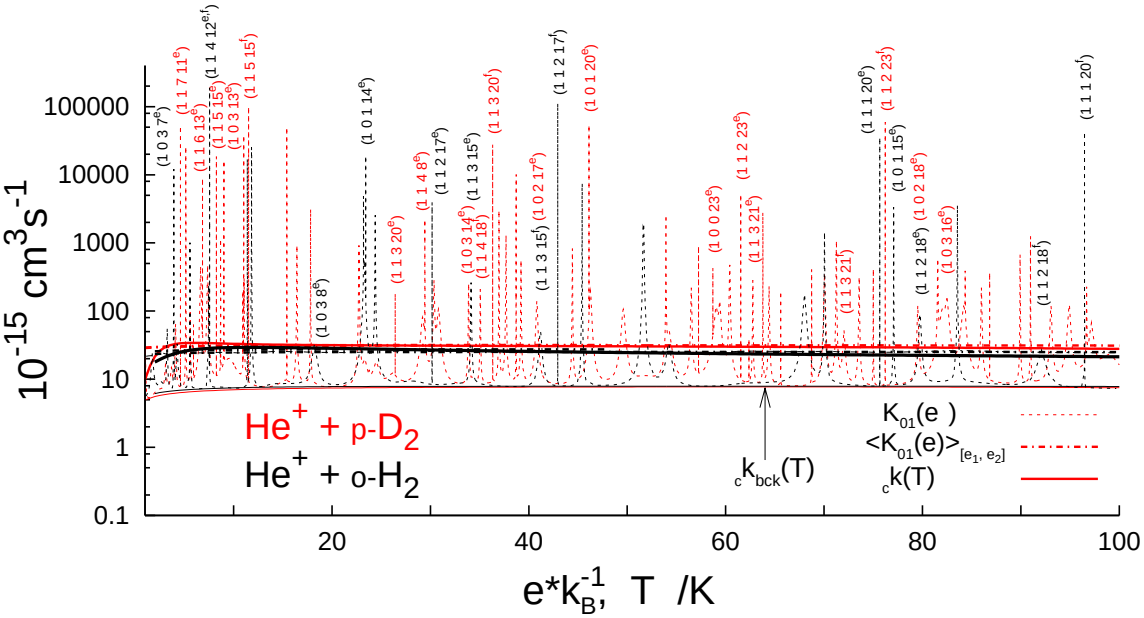

The function $K_{01}(e)$ for He^++o-D_2 exhibits 86 resonance peaks in the range shown. 29 peaks are due to shape resonances (b=1). In the function for He^++p-H_2, 34 resonance peaks occur of which 16 are due to shape resonances. For the sake of clarity, only the most pronounced shape resonance peaks are given label here.

Enlarged view of the averages $\langle K_{01}(e)\rangle_{[e_1,e_2]}$ in the interval $[e_1/k_B, e_2/k_B]$=[1, 100] K and of the respective functions ${}_ck(T)$ for He^+D_2 and He^+H_2. The lower borders of the shadowed strips show the averages $\langle K_{01}(e)\rangle_{[e_1,e_2]}$ for $[e_1/k_B, e_2/k_B]$=[1, 257] K.

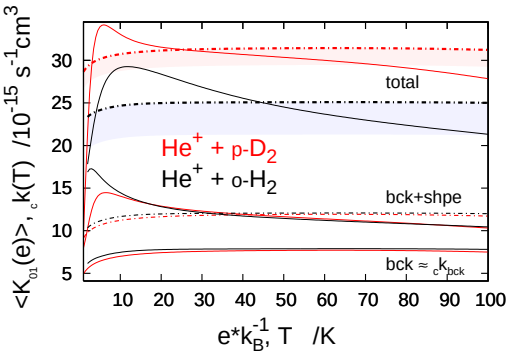

The averages $\langle K_{0j}(e)\rangle_{[e_1,e_2]}$ are counterparts of the mean values of the quasi-rate coefficients which are used in recent calculations[23] on radiative decay processes in cold atom-ion collisions, in particular in those referring to the experiment[24] with trapped Yb ions and Rb atoms. Though no physical argument can be given to justify the use of the averages $\langle K_{0j}(e)\rangle_{[e_1,e_2]}$ in the present context, it still seems interesting to see what picture of the resonance role in the 'trad' reaction these quantities would provide, and how much this picture would differ from that provided by the Boltzmann-averaged characteristics. Qualitatively, the pictures appear the same: both kinds of averages tell practically the same on the role of the shape resonances, both indicate that the rotational Feshbach resonances make several times larger contribution and that their role increases upon the H→D substitution. However, the contents of the small panels of Fig. C9 indicate also that the averages $\langle K_{0j}(e)\rangle_{[e_1,e_2]}$ are not generally suitable for quantitative considerations since they may depend on the choice of the interval $[e_1, e_2]$. Certainly, the latter comment applies to situations like in the He^++$H_2(D_2)$ systems where strong Feshbach resonances (with relatively large $\Gamma^{\rm trad}$ but not exceedingly larger than Γ) occur at low collision energies and because of them the Boltzmann-averaged rate constant functions are far from being constant functions.